THE UNIVERSITY OF MANITOBA

THE EFFECT OF ARTIFICIALLY THICKENING OXIDE LAYER ON THE CORROSION PROPERTIES OF TYPE 316L STAINLESS STEELS

By

WENYAN SHEN

A thesis
Submitted to the faculty of graduate studies
in partial fulfillment of the
requirements for the degree of
Master of Science

DEPARTMENT OF MECHANCIAL AND INDUSTRIAL ENGINEERING
WINNIPEG, MANITOBA
MAY 2001

THE UNIVERSITY OF MANITOBA

FACULTY OF GRADUATE STUDIES

*****

COPYRIGHT PERMISSION

THE EFFECT OF ARTIFICIALLY THICKENING OXIDE LAYER ON THE CORROSION PROPERTIES OF TYPE 316L STAINLESS STEELS

BY

WENYAN SHEN

A Thesis/Practicum submitted to the Faculty of Graduate Studies of The University of Manitoba in partial fulfillment of the requirement of the degree

of

MASTER OF SCIENCE

ACKNOLEDGEMENTS

I take this opportunity to thank Dr. Cahoon J. R. for his guidance and encouragement throughout the course and research of this work.

I would also like to acknowledge the technical assistance of Mr. John Van Dorp and Mr. Mike Boskwick at various stage of this work.

In addition, I would like to thank Dr. D. Polyzois and Dr. N. L. Richards for their helpful suggestions on my thesis.

My special thanks to my fellow students and post doctoral research associates, Uttara, Douglas, Dr. Chen, Dr. Gou, for their help and support during the two years. Last but not the least, I would like to thank all my family members, especially my husband, Mr. Ge Yu for his constant support and encouragement.

ABSTRACT

By using thermal vacuum annealing treatment, an oxide film is formed on the surface of 316L stainless steel. The characteristics of the oxide films are governed by vacuum heat-treatment systems, wherein temperature, time and oxygen pressure are the three primary factors.

The pressure of the vacuum system was nearly 5×10^{-6} torr. Seven types of samples were used to investigate the effect of surface treatment, annealing temperature and time on the corrosion resistance of the oxide film. The range of the annealing temperature was from 200°C to 600°C. Time in these experiments were 30 min, 90 min and 150 min.

Furthermore, Electrochemical polarization technique was used to evaluate the corrosion resistance of the oxide film. Through polarization curve, critical potential, E_c, protection potential, E_p, rest potential, E_{rest} , passive current density, i_{pass} and corrosion rate can be obtained. The differences between E_c and E_{rest} and E_c and E_p were used to evaluate the pitting resistance and crevice corrosion resistance of the oxide film. The larger the difference of Ec and Erest, the higher the pitting resistance of the specimen while the smaller difference of E_c and E_p, the higher crevice corrosion resistance of the specimen. Moreover, Secondary Ion Mass Spectroscopy(SIMS) is a major tool in the experiment for analyzing the distribution of the elements through the depth of the oxide film.

It is found that the oxide film formed at 200°C and 400°C showed increased Cr contents and decreased Fe contents in the oxide film compared to the bulk material. A region of essentially constant Cr/O ration and Si/O ratio in the oxide films formed at

room temperature, 200°C and 400°C were attained. The constant ratio indicates the presence of stoichmetric chromium oxide and silicon oxide. No region of constant Fe/O ration was observed. Moreover, mechanical polishing the surface of the specimens to 0.25μm significantly improved the pitting resistance of the oxide film compared to sanding the surface to 600 grit paper. As temperature increased from 200°C to 400°C, the thickness of the oxide film increased twice while the corrosion resistance decreased. Film formed at 500°C and 600°C offered no corrosion resistance to the stainless steel. In addition, oxide formation times at 400°C in excess of 90 min were detrimental to corrosion resistance of the specimens.

TABLE OF CONTNETS

ACKNOWLEDGEMENTS i

ABSTRACT ii

TABLE OF CONTENTS iv

LIST OF FIGURES vi

LIST OF TABLES x

I. **INTRODUCTION** 1

II. **LITERATURE REVIEW** 3

A. **Stainless Steel** 3

B. **Electrochemistry of Corrosion** 10

B.1 Thermodynamic Basis of Corrosion 10

B.2 Kinetics of Electrodes 14

B.3 Pitting 26

B.4 Crevice Corrosion 33

C. **Oxide Film** 36

C.1 Thermodynamics and Kinetics of Oxidation 36

C.2 Oxidation of Stainless Steels 43

D. **Measurement Techniques and Experimental Methods** 58

D.1 Electrochemical Technique 58

D.2 Secondary Ion Mass Spectrometry (SIMS) 63

III. **EXPERMIENT** 66

A. Material and Preparation of Specimen 66

B. Experimental Techniques 67

B.1 Secondary Ion Mass Spectrometry (SIMS) Analysis 67

B.2 Electrochemical Testing 68

IV. **EXPERIMENTAL RESULTS AND DISCUSSION** 70

A. **SIMS Results** 70

A.1 The Relationship of Concentration with Distance from the Metal Surface 70

B. **Electrochemical Polarization Test Results** 95

B.1 Effect of Surface Preparation on the Electrochemical Behavior of the Oxide Film Formed on 316L Stainless Steels 95

B.2 Effect of Oxide Formation Temperature on Electrochemical Behavior of 316L Stainless Steel 98

B.3 Effect of Vacuum Annealing Time at 400°C on the Electrochemical Behavior of 316L Stainless Steel 114

V. **SUMMARY CONCLUSION & RECOMMENDATIONS** 117

REFERENCES 120

LIST OF FIGURES

Fig. 1 Scanning electron micrograph showing a higher-magnification view of the crack on the failed implant. It indicates that the cracks were associated with the pits. 6

Fig. 2 Resistance of austenitic stainless steels containing 2.1 to 4.4% Mo to localized corrosion..... 7

Fig. 3 Schematic energy profile for equilibrium at an electrode. ΔG^* of the activation Gibbs free energy..... 11

Fig. 4 Schematic energy profile for activation polarization at an electrode: ΔG^* = activation Gibbs free energy, η/V = anodic overpotential. 17

Fig. 5 Schematic cathodic and anodic polarization curve. 19

Fig. 6 Logarithmic plot of current density, I, overvoltage, η, for a polarized electrode, showing limiting current density due to concentration polarization 21

Fig. 7 Schematic anodic polarization characteristics for a stainless steel in an acidic aqueous medium. 22

Fig. 8 Schematic representation of the anodic polarization of an active-passive metal in the presence of an oxidizer..... 24

Fig. 9 Autocatalytic processes occurring in a corrosion pit. 30

Fig. 10 Morphology of oxide layers formed on iron-chromium alloys in air. 44

Fig. 11 Chromium profiles of an Fe-10%Cr alloy after various surface treatments. ... 50

Fig. 12(a) Cr enrichment at the surface of alloy 430 during oxygen exposure at a partial pressure of 1.33×10^{-5}Pa at different temperatures. 53

Fig. 12(b) Cr enrichment at the surface of alloy 304 during oxygen exposure at different temperature. 53

Fig. 13(a) Depth profile showing Cr distribution after oxidation of alloy 430. 54

Fig. 13(b) Depth profile showing Cr distribution after oxidation of alloy 340. 54

Fig. 14 Potentiostatic test set-up. 59

Fig. 15 Simplified potentiostat. 60

Fig. 16 Schematic representation of anodic polarization curves for a metal immersed in solution containing aggressive ions. Potentialstatic measurements conducted (a) forward (b) backward. 62

Fig. 17 Galvanostatic polarization 63

Fig. 18 Schematic representation of the principles of SIMS analysis. 64

Fig. 19 SIMS result for oxide layer formed on type 316L stainless steel at room temperature. 72

Fig. 20 SIMS result for oxide Layer formed on type 316L stainless steel after vacuum annealing at 200°C, 90 min. 73

Fig. 21 SIMS result for oxide layer formed on type 316L stainless steel after vacuum annealing at 400°C, 90 min. 74

Fig. 22 The relationship of oxygen content with distance from the metal surface. 76

Fig. 23 The relationship of silicon content with distance from the metal surface. 80

Fig. 24 The relationship of Cr content with distance from the metal surface. 82

Fig. 25 The relationship of iron content with distance from the metal surface. 85

Fig. 26 The relationship of nickel content with distance from the metal surface..... 86

Fig. 27 The changing of Mo content with distance from the metal surface. 87

Fig. 28 The ratios of Cr/O with distance from the metal surface. 89

Fig. 29 The ratios of Si/O with distance from the metal surface. 90

Fig. 30 The ratios of Fe/O with distance from the metal surface. 91

Fig. 31 The ratios of Cr/Fe with distance from the metal surface. 92

Fig. 32 Electrochemical polarization curves for type 316L stainless steel after different surface finishes. 97

Fig. 33 Electrochemical polarization curves for specimens with oxide films formed at room temperature and vacuum annealing at 200°C for 90 min. 99

Fig. 34 Electrochemical polarization curves for specimens with oxide films formed during vacuum annealing at temperature from 300°C to 600°C. 101

Fig. 35 Effects of temperature of oxide formation and surface preparation on the corrosion rates of 316L stainless steel. 105

Fig. 36 Effects of temperature of oxide formation and surface preparation on the corrosion potential, E_{corr}, of 316L stainless steel. 106

Fig. 37 Effects of temperature of oxide formation and surface preparation on the critical potential, E_{crit}, of 316L stainless steel. 107

Fig. 38 Effects of temperature of oxide formation and surface preparation on the protection potential, E_p, of 316L stainless steel. 108

Fig. 39 Effect of temperature of oxide formation on the difference between the critical potential and corrosion potential, E_{cr}-E_{corr}, of 316L stainless steel. 112

Fig. 40 Effect of surface preparation and temperature of oxide formation on the difference between the critical potential and the protection potential, E_{cr}-E_p, of 316L stainless steel. 113

Fig. 41 Electrochemical polarization curves of 316L stainless steel with oxide films formed for different times during vacuum annealing at temperature at 400°C. 115

Fig. 42 Effect of time on the corrosion rate of 316L stainless steel with oxide films formed during vacuum annealing at temperature at 400°C. 116

LIST OF TABLES

Table 1 Terminology for characteristic potentials. 31

Table 2 Thickness of oxide film at Fe/Cr composition in the surface layer after oxidation at different temperature and oxygen partial pressure. 56

Table 3 The content of elements in the 316L stainless steel 66

Table 4 Vacuum Annealing Treatment (5×10^{-6} torr) 67

Table 5 Electrochemical Testing Results for oxide films formed in vacuum system 109

I. INTRODUCTION

Austenitic stainless steels are widely used in applications requiring resistance to corrosion and high temperature oxidation. However, for applications in chloride solutions, such as surgical implants, austenitic stainless steels are subject to localized crevice and pitting corrosion. This deficiency detracts from the performance of austenitic stainless steels and improving the localized corrosion resistance would greatly increase their utility.

Passivation treatments involving nitric acid are often used to modify the oxide film and enhance the corrosion resistance of austenitic stainless steels. Surgical implants receive a passivation treatment but essentially all multi-component, stainless steel implants suffer from localized crevice and pitting corrosion at locations between screws and plates or wherever two surfaces contact.

The oxide film on stainless steel can be thickened by heat treatment in air at elevated temperatures. However, such films are porous and non-coherent and do not increase the corrosion resistance of the stainless steel. There is a possibility that oxide films formed in vacuum at elevated temperature may be less porous and retain coherency.

The objective of our experiments is to cease the corrosion of type 316L stainless steel by artificially increasing the thickness of the oxide film which was formed at elevated temperature in a vacuum of about 5×10^{-6} torr. The thickness of the film was varied by varying the temperature between 200°C and 600°C. The composition and thickness of the oxide film were determined using secondary ion mass spectroscopy (SIMS). The electrochemical behavior was established using the cyclic dynamic polarization technique where the corrosion behavior is characterized by the parameters of corrosion potential

(E_{corr}), critical pitting potential (E_c), protection potential (E_p), and the passive current density (I_p).

II. LITERATURE REVIEW

A. Stainless steels

Stainless steel refers to an iron alloy with a chromium content of not less than 10%. Stainless steel possesses characteristics of corrosion resistance due to a thin, protective chromium oxide film forming on the surface when the alloy is exposed to the corrosive environment. The film is essentially insoluble, self-healing and nonporous. Generally, to obtain adequate corrosion protection, the content of chromium in the film is required to be more than 12%, and chromium contents of 18% or more are utilized for protection in severe environments. Most stainless steels can be used in marine environment, fresh water, and oxidizing atmospheres at elevated temperature. Some are also resistant to salt water and oxidizing chemicals [1].

There are five kinds of stainless steels: ferritic, austenitic, martensitic, precipitation hardening and duplex stainless steels. Type 316 stainless steel belongs to the austenitic stainless steel class. Austenitic stainless steel, because of the addition of nickel which is an austenite-stabilizing element, maintains the austenitic, face centered cubic (FCC) structure, at room temperature. It has excellent ductility, formability, and low-temperature impact properties and corrosion resistance[1]. Its strength is obtained by extensive solid solution strengthening.

Type 316 stainless steel contains 16-18% chromium, 10-14% nickel, and 2-3% Mo. Type 316L stainless steel, which is the low-carbon version for welding applications, has more corrosion resistance than other austenitic stainless steel, such as Type 302 or Type 304 alloys. The corrosion resistance of type 316 and 316L stainless steel is primarily affected by alloying elements, heat treatment, surface condition, and impurities in the

steel. Alloying elements play a significant role in influencing the corrosion resistance of stainless steels.

Chromium is the most important element in stainless steel for it provides both corrosion resistance and strength. The corrosion resistance is obtained by a protective oxide layer on the surface of the alloy. The film is first observed to form at Cr contents of about 10.5% Cr[2], but this affords only mild atmospheric protection. Increasing the chromium content of the stainless steel to 12-18%Cr greatly increases the stability of the film. Chromium content in excess of about 20% may adversely affect the mechanical properties, fabricability and weldability of the alloy.

Molybdenum, combined with chromium, is very effective in stabilizing the passive film in the presence of chloride ion. It may effectively increase the resistance to the initiation of pitting and crevice corrosion, and has a modifying influence on the corrosion processes over a wide range of potential, including crevice corrosion at lower potentials and chloride-induced pitting at higher potential [8].

Nickel is an austenite (FCC structure) former and tends to eliminate ferrite, the body centered cubic (BCC) structure. It also enhances mechanical properties and fabrication characteristics such as formability and weldability. Ni also promotes formation of the passive oxide film in a reducing environment.

Nitrogen is beneficial to austenitic stainless steels in enhancing pitting resistance because it retards the formation of the detrimental chromium-molybdenum σ phase and increases the corrosion resistance of the austenitic phase.

Manganese has detrimental influences on the corrosion resistance, especially the pitting resistance of the alloy. It interacts with sulfur to form manganese sulfides which may become the initiation sites for pitting corrosion.

Carbon is an element used for hardening alloys. However, it is detrimental to corrosion resistance in austenitic stainless steel due to its reaction with Cr to form $Cr_{23}C_6$ at grain boundaries which leads to the intergrular corrosion of stainless steels.

Since type 316 and type 316L stainless steels have generally good corrosion resistance, they are widely used in various fields of industry. For example, in the food and beverage industry, type 316 and type 316L stainless steels are applied as piping and tubing in breweries and machine parts for beverage-dispensing equipment; in the oil and gas industry as lining and tray components, tower piping and heat-exchanger tubes; in the pulp and paper industry as containers.

In addition, in the past 50 years, type 316L stainless steel has found another important application as a surgical implant material. According to strict medical standards, the metals used in the human body must be compatible with the body, must not introduce toxic species, and must not bring about poisonous reactions with body fluids. The widespread application of type 316L stainless steel as an orthopedic implant material further confirms its corrosive resistance.

However, with long-time exposure to corrosive environments that contain chloride ions, failures still occur with type 316 and type 316L stainless steels. Investigations verified that the main reasons for failures were pitting, crevice corrosion and corrosion fatigue, with pitting being the most common form of corrosion for type 316L stainless steel.

After examining a failed type 316L stainless steel Austein fernormal head prosthesis by scanning electron microscopy, Sivakumar and Kamachi [5] found that in spite of the recent innovative metallurgical and technological advances in the design of implants to improve the life of the implants, failures of implants did occur due to microcracks which originated from pits on the prosthesis as Fig. 1 shows.

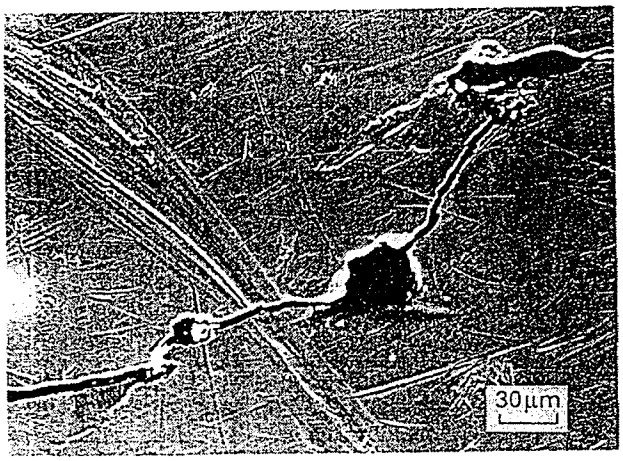

Fig.1 Scanning electron micrograph showing a higher-magnification view of the crack on the failed implant. It indicates that the cracks were associated with the pits[5].

Likewise, Magrin et al[6] concluded from the fractures of some osteosythesis type 316L plates applied during orthopedic surgery, that the fracture was a consequence of mechanical and chemical interaction with the biological environment and pits were usually the origin of the cracks.

Sivakumar et al[7] studied the cracking that occurred in a type 316L stainless steel, Kuntscher clover-leaf intramedullary rod which had been implanted in the right femur of 27 year old man. SEM and microprobe analysis showed that a high inclusion content and a low Mo content decreased the pitting resistance of the implant which resulted in failure. A potentiodynamic anodic polarization technique was used to confirm this conclusion.

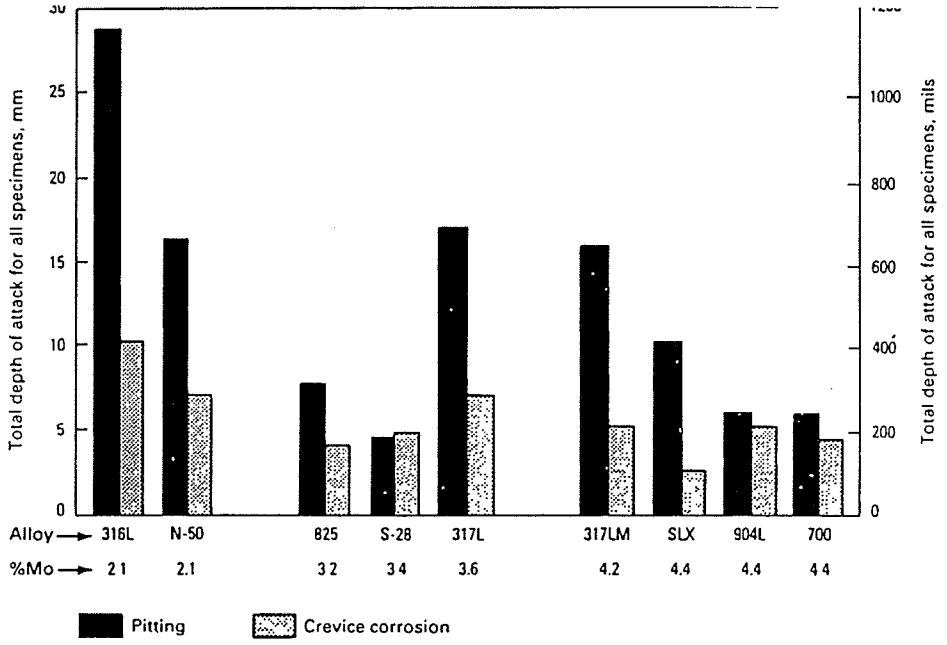

Fig.2 Resistance of austenitic stainless steels containing 2.1 to 4.4%Mo to localized corrosion[2].

Fig. 2[2] shows the resistance to localized corrosion of austenitic stainless steels in a paper mill bleach plant environment. In general, pits are deepest in the alloys containing the least Mo which confirms the beneficial effect of higher Mo concentrations.

The corrosion of liner plates [3] made of AISI type 316L stainless steel in the flash chambers of a multistage flash desalination plant located on the Arabian Gulf coast was investigated. These liner plates incurred severe corrosion during only six years of operation. The results showed that commercial grade type 316L stainless steel was susceptible to pitting, crevice and grain boundary corrosion under the operation conditions in the desalination plant.

Furthermore, some investigations [4] have shown that stress corrosion cracking which occurred around the weld zone of SUS 316L stainless steel in a waste water purification

plant using active carbon originated from pitting sites, and the active carbon promoted the occurrence of pitting corrosion.

Some techniques have been developed to improve the pitting corrosion resistance of type 316 and type 316L stainless steels. Metallic/organic coatings and oxide films are two useful methods to protect alloys against pitting. Coatings can be divided into metallic coatings and organic coatings. A metallic coating is a protection layer consisting of an anti-corrosion metal such as cadmium, copper, gold, etc., on the surface of the substrate metal. The protective function of an organic coating depends on the fact that organic chemicals generally do not corrode in basic, acid or salt solutions. However, metallic/organic coatings may also create some problems. Firstly, organic chemicals may pollute the environment. Secondly, the difference of the potentials existing between a metallic coating and the substrate metal may cause galvanic corrosion if the coating is damaged. If the substrate metal is anodic and the metallic coating is cathodic, galvanic corrosion leads to the damage of the substrate metal.

The presence of an oxide film is another protective method for some metals and alloys. It can be utilized only for the alloys containing elements which can be oxidized, such as chromium, aluminum. These elements can react with oxygen to form a continuously coherent oxide layer on the surface of the substrate metal which acts as a barrier to isolate the metal from the environment. Compared to coatings, oxide films have unique advantages. Firstly, the oxides pose little threat to the environment or the human body. Secondly, if the oxide film is damaged, it will not promote the corrosion of the substrate metal and is self-healing if oxygen is present in the environment. Thirdly, the thickness of oxide film is usually less than 100nm in thickness so that it will not

significantly change the size of the products. Therefore, in recent years, the formation of an oxide film has become the primary protective method for surgical implants of type 316L stainless steel.

ASTM specification F86-91 "Standard Practice for Surface Preparation and Marking of Metallic Surgical Implants" provides details for enhancing the oxide film on surgical stainless steel implants.

B. Electrochemistry of Corrosion

B.1 Thermodynamic Basis of Corrosion

Corrosion is the deterioration of metals due to reaction with the environment surrounding them. In general, a corroding system consists of two spontaneous coupled reactions: an anodic/oxidation reaction and a cathodic/reduction reaction, which both take place at the interface of the metal and an aqueous environment[9]. The reaction in which electrons are removed from the metal by chemical species from the aqueous environment is called oxidation or the anodic reaction. Reduction or the cathodic reaction is characterized by the consumption of electrons on the cathodic surfaces. As a result, the exchange of electrons between the two reactions produces an electric current and electric potential on the metal surface. Furthermore, the supply and consumption of electrons in the two coupled reactions is balanced. For example, oxidation of iron occurs while iron is immersed in an oxidizing solution, which leads to the transformation of Fe into Fe^{2+}, as shown in equation (1) [9].

$$Fe \rightarrow Fe^{2+} + 2e \cdots\cdots(1)$$

Meanwhile, this reaction is balanced by a reduction reaction involving the gain of electrons. If the solution is acidic, a possible cathodic reaction is the evolution of hydrogen:

$$2H^{+} + 2e \rightarrow H_2 \text{ (acid solutions)} \cdots\cdots(2)$$

Or :

$$O_2 + 4H^{+} + 4e \rightarrow 2H_2O \text{ (acid solution)} \cdots\cdots(3)$$

If the solution is neutral or basic (such as water or seawater exposed to the atmosphere), the hydrogen content in the solution is far lower than that in acidic solution,

and the cathodic reaction involves the absorption of dissolved oxygen instead of the evolution of hydrogen. Its reactive formula becomes:

$$O_2 + 2H_2O + 4e \rightarrow 4OH^- \cdots\cdots(4)$$

The overall reaction is:

$$2Fe + 2H_2O + O_2 \rightarrow 2Fe^{2+} + 4OH^- \rightarrow 2Fe(OH)_2 \cdots\cdots(5)$$

In the reaction, ferrous hydroxide precipitates from the solution and Fe is oxidized to the ferric salt:

$$4Fe(OH)_2 + 2H_2O + O_2 \rightarrow 4Fe(OH)_3 \cdots\cdots(6)$$

For an isolated electrode reaction such as equation (1), a dynamic equilibrium will be established on the electrode surface when the accumulation of electrons on the metal creates a characteristic potential relative to the solution.

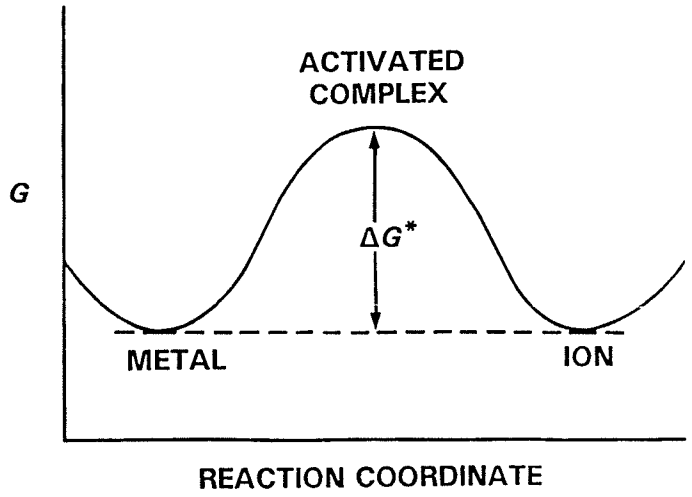

Fig.3 Schematic energy profile for equilibrium at an electrode.
ΔG* is the activation Gibbs free energy[10].

As Fig.3[10] shows, if the metal undergoes an oxidation reaction and metal atoms are converted into ions, there is a energy barrier which the atoms or ions must overcome. The energy that must be acquired to overcome the energy barrier is called the activation

energy, ΔG^* . At a given constant temperature, the activation energy is derived from a form of the Van't Hoff reaction isotherm[10]:

$$\Delta G = \Delta G° + RT\ln J \cdots\cdots(7)$$

where R is the gas constant, 8.314 J/mol, T is the absolute temperature, J is the activity quotient corresponding to a free energy change ΔG:

$$J = \frac{\alpha_{product1} \times \alpha_{product2} \times \cdots etc.}{\alpha_{reactant1} \times \alpha_{reactant2} \times \cdots etc.}$$

$\Delta G°$ is the standard Gibbs energy change for all reactants in their standard state. If the concentrations of metal ions are maintained at unit activity, each solution contains approximately 1 gram-atomic weight of metal ion per liter.

Since the system always has a tendency to transform to its lowest energy state (if ΔG is negative), this indicates a loss in Gibbs energy and no external forces are needed to act on the system. If ΔG is positive, this means that the transition represents an increase in Gibbs energy and requires that additional energy be added to the system. Thus, the direction of a reaction is reflected by this parameter.

In an electrode reaction, ΔG is balanced by the potential that the electrode acquires. The expression is [9]

$$\Delta G = -ZFE \cdots\cdots(8.a)$$

and

$$\Delta G° = -ZFE° \cdots\cdots(8.b)$$

where Z is the number of electrons involved in the reaction,

F is the Faraday constant, 96,487 coulombs $equiv^{-1}$,

E equals the cell potential,

E° is the standard electrode potential, corresponding to ΔG°, which is related to the inherent nature of the reactants.

From equation (8a) and (8b), we can see that, in fact, the electrode potential is a representation of the energy change in the reaction, which is the principal factor in determining what the reaction will be. For example, as the potential of Fe in neutral aerated water is increased, the favored reaction for iron is the dissolution or corrosion of iron into the soluble ions, Fe^{2+}, which continuously diffuse into the solution. If the potential is raised to an appropriate value, the ions of Fe^{2+} acquire electrons and deposit on the metal surface as solid iron, and this reaction becomes the primary reaction in the solution.

The free-energy change associated with an electrochemical reaction can be studied in an electrochemical cell containing anodic and cathodic electrodes in equilibrium with their ions but separated by a porous membrane. The concentration of metallic ions is maintained at unit activity and the dissolution and deposition of the metal must be equilibrated. These equilibratory electrodes are called half-cells. If the concentrations of all reactants are at unit activity, they are termed standard half-cells.

An electrode's potential cannot be measured in absolute terms, but can be indirectly obtained by comparing with a reference electrode, such as a standard saturated calomel electrode (SCE) or standard hydrogen electrode (SHE), as equation (9) shows.

$$E_{metal} = E_{measure} - E_{reference} \quad \cdots\cdots(9)$$

Therefore, the corrosion potential can be obtained by calculating the difference of potentials between the cathode and anode. The formula is written as:

$$E_{corr} = E_{cath} - E_{anode} \cdots\cdots (10)$$

If the reactants are not at unit activity, the Nernst equation[10] as indicated in equation (11) should be applied:

$$E = E^{\circ} + \frac{RT}{ZF} \ln \frac{\alpha_{oxide}}{\alpha_{red}} \cdots\cdots (11)$$

where α_{oxid} is the activities (concentrations) of oxidized species, and α_{red} is the activities (concentrations) of reduced species.

Thus, the potential of any reaction is not only determined by the concentration of the reactants, but also by temperature, the number of electrons participating in the reaction and the inherent nature of the reactants as well.

In any electrochemical reaction, most of the negative or active electrodes tend to give rise to an oxidation reaction, whereas the positive or noble electrode tends to produce a reduction reaction.

B.2 Kinetics of Electrodes

The direction of a reaction may be determined by the change of Gibbs free energy,ΔG^{*}, but the velocity of the reaction can not be predicted by this parameter. In fact, in electrode reactions, the kinetics or the rate of the corrosion is of more interest. The reaction rate, r, which is the fraction of substances transforming in a small time span, depends on the value of the activation energy and temperature. Their relationship can be formulated by the Arrhenius equation[110] as follows.

$$r = A\exp\frac{-\Delta G^{*}}{RT} \cdots\cdots (12)$$

where r is the corrosion rate (number of moles dissolving per second).

In equation (12), A is given by:

$$A = f\alpha\left(\frac{N_s}{N_0}\right)\rho$$

where f is the vibration frequency of the atom in the corroding solid ($\approx 10^{12}$/s). N_s = number of atom per unit area on the solid surface, N_0 is Avogadro's number, α is the probability that an atom on the surface where processes. The energy ΔG is vibrating in the right direction to leave the solid ($\alpha \approx 10^{-3}$) and ρ is the probability that an atom ready to leave the surface can be accommodated in the corroding solution ($\rho \approx 1$).

The electrode reaction is the process whereby ions are transported between the electrodes to exchange electric charges. Thus, the reaction rate, r, can be further characterized by the electric current, i, as indicated in equation (13)[10].

$$i = k\exp\frac{-\Delta G^*}{RT} = K\exp\frac{zFE^*}{RT} \cdots\cdots (13)$$

where ΔG^* is the activation energy, K and k are constants depending on the process and on the ion activity and which are related to A, given by previously.

Equation (13) is very important in predicting the rate of corrosion since E can be measured easily during the reaction.

B.2.1 Kinetics of Equilibrium on an Electrode

The equilibrium on an electrode is dynamic and ions are produced and discharged simultaneously at the electrode surface.

$$M^{n+} + ne \rightarrow M \quad \text{and} \quad M - ne \rightarrow M^{n+}$$

The metal atoms dissolve into the solution and become ions by losing electrons while the metallic ions gain electrons and then deposit on the electrode surface as solid metal. The rates at which the metal dissolves and ions deposit on the metal surface are equal,

since the electrodes are in equilibrium. Thus, there is no change in Gibbs energy, ΔG, in both processes. The rate of anodic reaction is the same as the rate of the cathodic reaction and the relationship can be represented by:

$$i_a = i_c = i_0 = k\exp\frac{-\Delta G^*}{RT} = K\exp\frac{ZFE^*}{RT} \cdots\cdots(14)$$

where i_a is the current density for the anodic reaction,

i_c is the current density for the cathodic reaction,

i_o is called the exchange current density which represents the rate of transformation of the substances at the interface.

B.2.2 Polarization

When a net oxidation or reduction process occurs at the electrode interface, the electrodes will no longer be at their equilibrium potential. The displacement of electrode potential from the equilibrium potential resulting from a net current is called polarization, the magnitude of which is frequently measured in terms of the overvoltage, usually abbreviated as η.

$$\eta = E_i - E^0 \cdots\cdots(15)$$

where E_i is the potential of the metal at the applied current density i ,

E^0 is the equilibrium potential of the metal also called the reversable potential.

This polarization may be either anodic or cathodic. Electrochemical polarization is divided into two main types, activation and concentration polarization.

B.2.2.1 Activation Polarization

Activation polarization refers to control of an electrochemical reaction by a slow step reaction at the metal-electrolyte interface. The slow step can be the electron-transfer process or the formation of corrosion products[9]. Moreover, when the equilibrium is disturbed it is always associated with changes of the activation energies of dissolution and deposition. The free energy profile of an electrode process dominated by activation polarization is shown in Fig. 4[10], where the electrode is assumed to be anodically polarized with an overpotential of voltage, η.

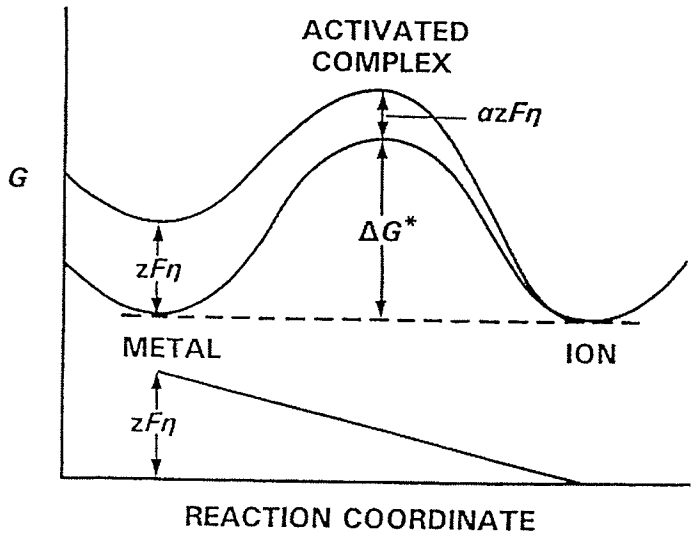

Fig.4 Schematic energy profile for activation polarization at an electrode:
ΔG^* = activation Gibbs free energy, η/V= anodic overpotential

At the equilibrium condition, the activation energies for anodic and cathodic reaction are both equal to the activation energy ΔG^*. However, when polarization occurs, the energy of the metal increases by $ZF\eta$ and the activation energy of the anodic reaction decreases by $(1-\alpha)ZF\eta$, where α is the symmetry factor defining the position of the point of the maximum in Fig.4. Hence, from equation (13)[10], the anodic current, i_a, can be obtained:

$$i_a = k\exp\frac{-[\Delta G^{*} - (1-\alpha)ZF\eta]}{RT} \cdots\cdots (16)$$

For the cathodic reaction, the activation energy is increased $\alpha ZF\eta$ by the polarization. Similarly, the cathodic current, i_c, is obtained from equation (13),

$$i_c = k\exp\frac{-(\Delta G^{*} + \alpha ZF\eta)}{RT} \cdots\cdots (17)$$

The net corrosion current is the difference of the two partial currents, as follows:

$$i_{net} = i_0[e^{\frac{\alpha ZF\eta}{RT}} - e^{\frac{-(1-\alpha)ZF\eta}{RT}}] \cdots\cdots (18)$$

Equation (18) is called the Butler-Volmer equation(BVE) [12]. If the polarization is anodic and $\eta > 0.1V$, the value of i_c can be neglected, or $i_{corr} \approx i_a$. If the polarization is cathodic and $\eta < -0.1V$, the value of i_a can be neglected, or $i_{corr} \approx i_c$. Then η is represented by[11]:

$$\eta = \beta \log i_0 \pm \beta \log i \cdots\cdots (19)$$

where η is overvoltage, i is the rate of oxidation or reduction in terms of current density and β is a Tafel constant, which is related with the characteristics of the solution.

Equation (19) is called the Tafel equation which is used to construct the E-log$|i|$ diagram for polarization studies.

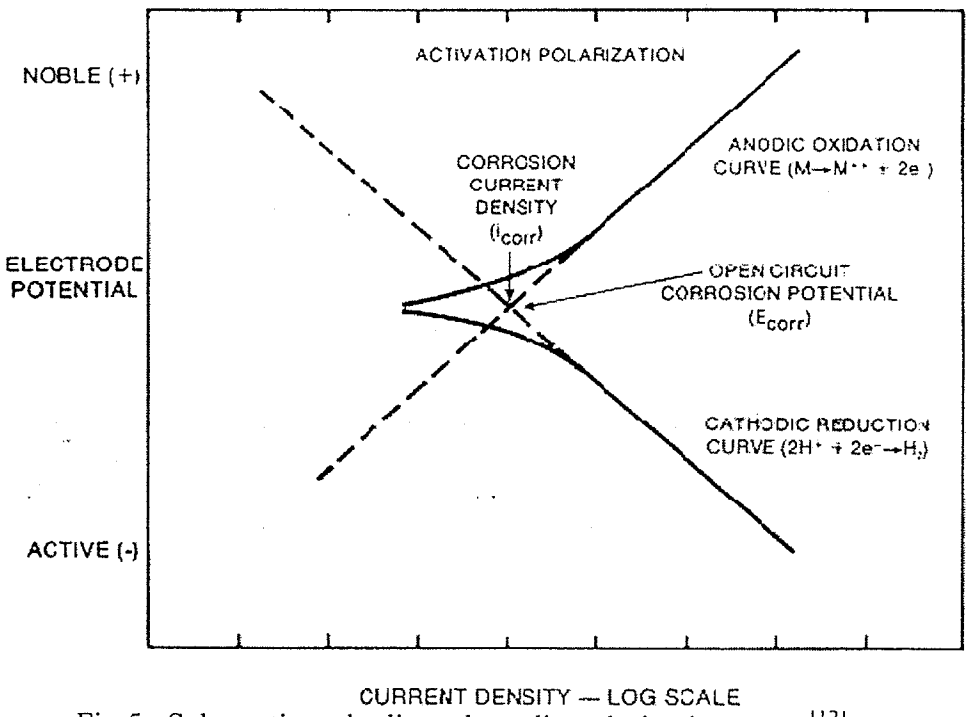

Fig.5 Schematic cathodic and anodic polarization curve[12]

As Fig.5 shows, when a logarithmic current coordination is used, the relationship between overvoltage (or potential) and current density is a linear function. Experimentally, β can be obtained from the slope of the anodic/cathodic polarization curve as shown in equation(19)[10]:

$$\beta = \frac{2.303RT}{(1-\alpha)ZF} \cdots\cdots (20)$$

Furthermore, in the E-log|i|diagram, all potentials are more negative than the reversible potential when a net reduction occurs, and all potentials are more positive than the reversible potential when a net oxidation occurs. At the reversible potential, there is no net oxidation or reduction because both reaction rates are equal at this intersection point.

If α=0.5, equation (18) becomes[10]:

$$i = i_0[e^{\frac{\alpha ZF\eta}{RT}} - e^{\frac{-(1-\alpha)ZF\eta}{RT}}] = 2i_0 \sinh \frac{ZF\eta}{2RT} \cdots\cdots (21)$$

If η is very small, <10mv, equation (21) becomes:

$$i = 2i_0 \sinh \frac{ZF\eta}{2RT} \approx \frac{i_0 ZF\eta}{RT} \cdots\cdots (22)$$

Thus the relationship between i and η is linear.

B.2.2.2 Concentration Polarization

Concentration polarization actually is an electrochemical reaction, the rate of which is controlled by diffusion in the electrolyte. As Fig. 6 shows[10] $\eta \rightarrow \infty$ indicates a limiting diffusion current density, i_L, which represents the maximum rate of reduction for a given system. Because there exists a limiting rate at which ions can carry charges through the solution to/from the electrode,

$$i_L = \frac{DZFC_B}{X} \cdots\cdots (23)$$

where D is the diffusion coefficient of the reacting ions,

C_B is the concentration of the reacting ions in the bulk solution,

X is the thickness of the diffusion layer.

Thus, the rate of corrosion may be changed by increasing the concentration of the reacting ions, and decreasing the thickness of the diffusion layer by stirring the solution.

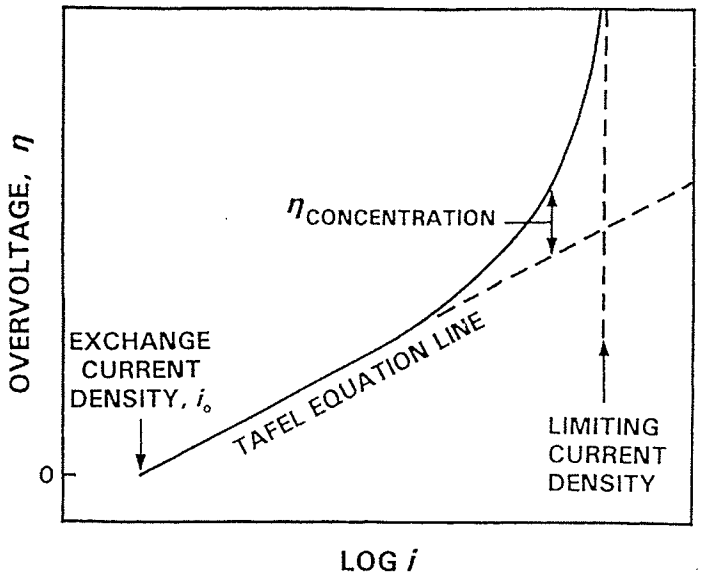

Fig.6 Logarithmic plot of current density, i, overvoltage,η, for a polarized electrode, showing limiting current density due to concentration polarization[10].

The relationship between reaction rate and overvoltage for concentration polarization is[9] :

$$\eta = \frac{RT}{ZF}\ln(1-\frac{i}{i_L})\cdots\cdots(24)$$

In fact, both activation and concentration polarization usually occur at an electrode. At low reaction rates, activation polarization usually dominates the reaction pace, whereas at higher reaction rates, concentration polarization will control the reaction process. The total polarization of an electrode is the sum of the contributions of activation polarization and concentration polarization, which is formulated by equation (25) [10].

$$\eta_T = \eta_a + \eta_c \cdots\cdots(25)$$

where η_T is total overvoltage,

η_a is the overvoltage of activation polarization,

η_c is the overvoltage of concentration polarization.

B.2.3 Passivation

B.2.3.1 Basic Principle of Passivation

Usually, passivation refers to the loss of chemical reactivity under certain condition. Faraday [10] suggested that passivation was caused by an invisible oxide film or an oxidative state of the metal surface, which was able to prevent contact between the metal and the solution. However, not all the oxides or hydroxides have a protective function. To be protective, an oxide film must be coherent and adherent to the metal surface and must be impervious to the solution.

The passivation of a specific metal or alloy is governed by anodic polarization characteristics, i. e., the current at the surface of a metal or alloy is a function of the potential applied to it.

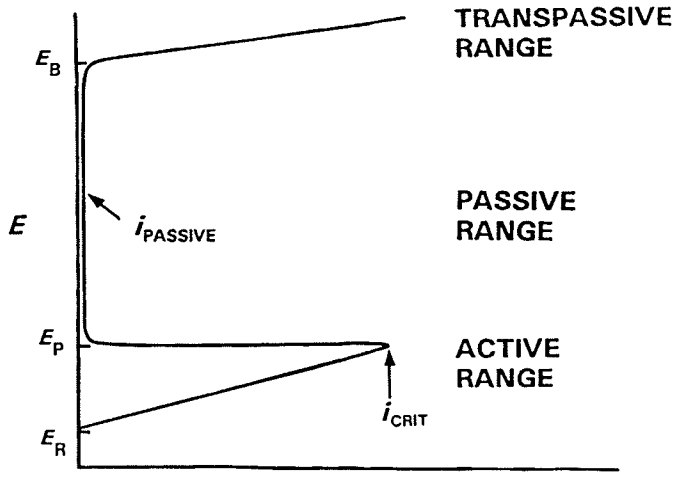

Fig.7[10] Schematic anodic polarization characteristics for a stainless steel in an acidic aqueous medium.

Fig.7 illustrates the typical behavior of passivation of a metal. The electrochemical characteristics of the passive metal can be divided into three regions: active, passive and transpassive. In the active region, the current density or the rate of dissolution of the metal increases with the increase of anodic potential. After the current density reaches its maximum, I_{crit}, it becomes independent of the potential and passivation of the metal occurs in the solution. When the metal is in the passive region, the critical anodic current is symbolized by i_{pass}. Normally, i_{pass} is smaller than i_{crit}. At high anodic potentials, the current density will increase rapidly and this region in the anodic polarization curve is called the transpassive region. In this the transpassive region, the rate of metal corrosion will increase greatly with small increases in potential. The potential at the transition from the passive region to the transpassive region is called the breakdown potential E_B, which indicates the breakdown of the oxide film and the appearance of pitting on the metal surface.

From the anodic polarization area, it is possible to determine the region of passive potential, the rate of passive corrosion and the conditions necessary for achieving passivity.

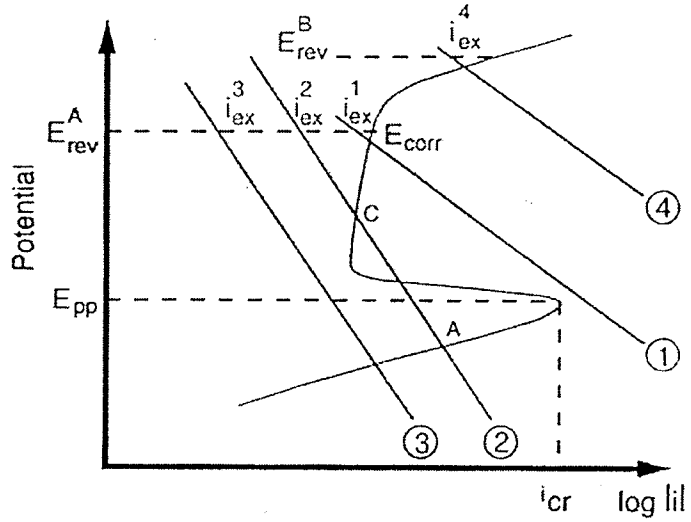

Fig. 8 Schematic representation of the anodic polarization of an active-passive metal in the presence of an oxidizer[12]

Fig.8[12] shows four different conditions whereby cathodic polarization curves intersect the anodic polarization curve. Cathodic line(1) meets the anodic curve in the passive region and because the line has no intersections with the active dissolution curve, the rate of corrosion in this condition is very small. For this case the metal incurs passivation. For line(2), the cathodic curve intersects the anodic curve in points A and C, which represent corrosion potentials. Point A corresponds to a bare surface undergoing active dissolution, which results in pitting. Otherwise, point C infers the passivation of the metal. Line (3) represents active dissolution of the metal, because the cathodic and anodic curves meet in the active region. For line (4), the cathodic curve crosses the transpassive region of the anodic polarization curve. At this intersection there is a large current density and extensive pitting corrosion will result.

B.2.3.2 Factors influencing the polarization characteristics

The breakdown of the oxide film in a solution can be caused by cathodic reduction, chemical dissolution or attack on the underlying metal at a film imperfection. Two

environmental factors that influence the polarization characteristics of stainless steel are pH and the presence or absence of Cl^- or Br^- ions.

In acid media, there are active, passive and transpassive ranges with the potentials rising in the cathodic polarization curve of stainless steel, but there is no active range for steel in neutral media. The steel is either immune or passive below the breakdown potential under this condition. However, when chloride or bromide ions are introduced into the solution, the anodic polarization is quite different. The passive range is terminated by the intervention of a current at a potential E_{pp}, which is called the pitting potential. The value of E_{pp} in solutions containing Cl^- ion is much lower than that in a solution without Cl^- ion. With the concentration of chloride ions increasing, the pitting potential moves to a progressively lower value and is less positive than the breakdown potential.

The compositions of alloys also can effect the passivation characterizations[12].

(i) Increasing the chromium content may lower passivating potentials and higher breakdown pitting potentials, reduced passive current densities, critical current densities. These benefit the corrosion resistance of the alloys.

(ii) Addition of nickel decreases the critical current density without affecting the passivation potential.

(iii) Addition of molybdenum leads to lower critical current densities and increased pitting potentials.

B. 3 Pitting

B.3.1 Initiation of pitting

Pitting is a form of localized corrosion that results in the metal dissolving preferentially from vulnerable areas on the surface. In practice, the surface of the metal or alloy has some chemical inhomogeneties or physical defects that are more susceptible to attack in aggressive environments compared with the remaining surface. This susceptibility will increase with the number of local imperfections in the passive film on the surface. When the passive film breaks down at small isolated sites scattered over the metal surface, local active/passive cells are created and pitting occurs. Some nonmetallic inclusions, e.g. sulfides and sulfide-oxide inclusions and second phase precipitates, are able to nucleate pits in a variety of iron and nickel-based alloys[16-23]. Therefore, the chemical composition of the passive film, its structure, chemical and physical properties, coherence, and thickness are of paramount significance in the nucleation and propagation of localized corrosion.

Usually, pitting corrosion leads to the formation of cavities in passivated metals or alloys exposed to nearly neutral solutions containing aggressive anions, especially chloride. There are two general forms of the pitting caused by the breakdown of the passive film on a metal or alloy: low potential pitting and high potential pitting. The former follows cathodic or self-activation and is generally characterized by etching[24]; the latter follows anodic action in the presence of the factors leading to film breakdown, and occurs in the form of hemispherical pits[15].

It is generally acknowledged that inhomogeneities in the chemical composition of the surface will affect the protective properties of a passive film more strongly than physical

defects. The following features are thought to induce the formation of weak spots in the passive film[1]:

(i) Breakdown between the metal matrix and nonmetallic inclusions where differences of thermal expansion coefficients exist.

(ii) Inclusions having greater chemical reactivity than that of the metal or alloy itself.

(iii) Grain boundaries at which some impurities segregate.

(iv) Flaws or various kinds of mechanical damage.

(v) Dislocations.

The role of sulfide inclusions as favored pit nucleation sites on stainless steel was recognized some time ago[25]. The forms of sulfide inclusions in stainless steels include sulfide particles, sulfide inclusions such as (Cr, Mn)S, (Al, Cr,Mn)S, TiSx, and also mixed sulfide-silicate inclusions[26].

Kim et al.[27] examined the effect of S and Ni on the pitting resistance of 316L stainless steel in 3.5%NaCl +1N H_2SO_4 solution by anodic polarization. They found that increasing the content of S in the alloys led to increase the amount and distribution area of sulfide inclusion, therefore the result was the deterioration of corrosion resistance of alloys. In addition, the reduction in Ni content led to the decrease pitting resistance due to the increased amount of the inclusions.

Not all sulfide inclusions are effective nucleating sites for pitting corrosion. Both ferritic 13%Cr steels [31] and austenitic stainless steels [32] contain (Mn,Fe)S sulfides. In steels containing approximately 0.3 to 0.6% Mn, a portion of Mn segregates in the sulfides. As the Mn content increases, it replaces Cr in the sulfides. Chromium-rich

sulfides are resistant to salt spray (5%NaCl solution), while MnS is readily attacked by this medium. Further, the dissolution products may stimulate anodic corrosion of the stainless steel.

Azuma and Hirata [28] investigated two types of 316L stainless steel: a conventional steel and a purified, low Mn one, corroded by moist Cl_2 gas. Using secondary ion mass spectroscopy analysis, they found that Mn was enriched on the attack part of the surface oxide film. The preferential attack was considered to be caused by the deposition of Mn.

Jackson et al[29,30] substantiated the above results by experiments. They found that Mn had a strong detrimental effect on general and localized corrosion properties of stainless steel.

In Fe-Cr-Ni alloys and stainless steels as well as mild carbon steels and low alloy steels, manganese sulfide inclusions are the most susceptible sites for pit nucleation. By electron microprobe analysis, Smialowski et al [26] studied pit nucleation in a commercial 18 Cr-9Ni austenitic stainless steel in 0.5M NaCl solution with a constant potential of 0.5V SHE. It was established that pits nucleated at mixed manganese and iron sulfide inclusions . The form of the inclusions was either separate particles or shells surrounding the oxides.

The study of the corrosion behavior of 304 and 316 stainless steel in 0.5 $kmol/m^3$ NaCl solution by Nishimura et. al[34] showed that addition of Mo decreased the number and/or the activity of active sites such as MnS for dissolution and led to the formation of a uniform film with fewer defects. Therefore, the addition of Mo benefited the pitting resistance of the alloys[35-38].

B.3.2 Process of Pitting

Pitting is an autocatalytic process as illustrated in Fig.9 [9]. Because there are always some susceptible areas on the surface of the metal, pitting takes place when the metal is put into an aerated sodium chloride solution. Within the pits, the metal rapidly dissolves, while oxygen reduction takes place on adjacent surfaces. This process is called a self-stimulating or self-propagating process, because the dissolution of metal within the pit will gradual increase in the concentration of M^{z+} ions in the pits and produce an excess of positive charge in this area. In order to achieve electroneutrality, chloride ions migrate into the pits. OH^- ions also migrate into the pits, but in neutral or acidic saline solution, the concentration of Cl^- ions is very much greater than that of the OH^- ions. Therefore, the number of Cl^- ions entering the pit is much higher than the number of OH^- ions. Thus, there is a high concentration of MCl in the pits, and as the result of hydrolysis, a high concentration of hydrogen ions forms via the following equation:

$$Fe^{3+} + 3H_2O = Fe(OH)_3 + 3H^+ \quad \ldots\ldots (26)$$

Hydrogen ions and chloride ions form hydrochloric acid which stimulates the dissolution of metals and alloys. Since the concentration of oxygen is very low within the pits, there is little oxygen reduction reaction occurring in the pits. The cathodic oxygen reduction on the surfaces adjacent to pits tends to protect the rest of the metal surface.

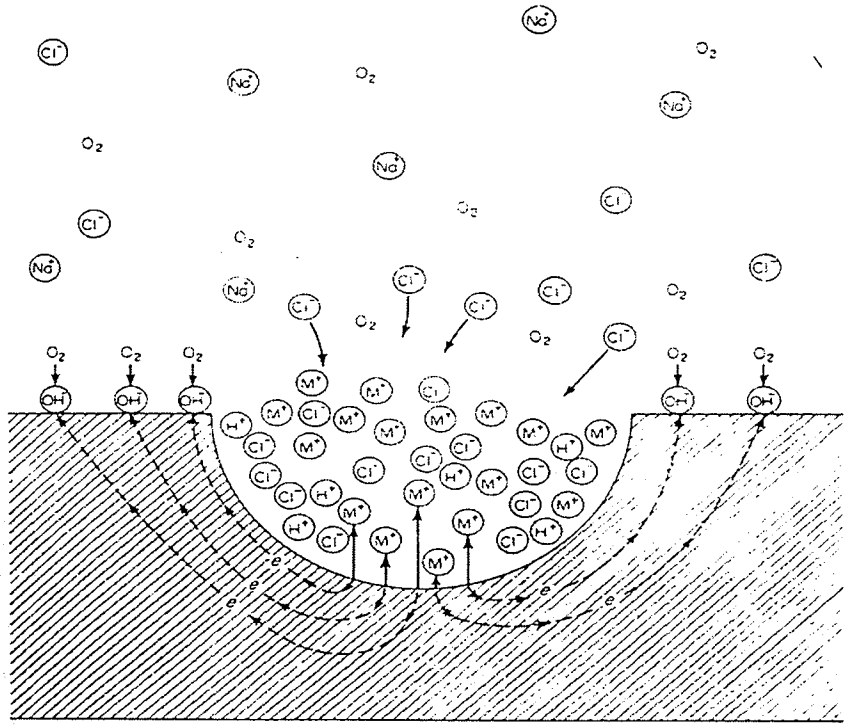

Fig. 9 Autocatalytic processes occurring in a corrosion pit.

Once pits have nucleated, some pits grow but others can repassivate. This is sometimes attributed to the changes of the microenvironment within the pits that influences the balance between dissolution and passivation. To arrest pit growth once it has started, the potential on the metal must be reduced to a value significantly below the pitting potential which is the so-called protection potential.

B.3.3 Measurement of the Susceptibility to Pitting

In 1934, Brennert [40]was the first to suggest the importance of the pitting potential in characterizing the susceptibility of metals and alloys to pitting corrosion. In 1963, Pourbaix [41] postulated two characteristic pitting potentials: the potential for pit initiation and the protection potential. The terminology for characteristic potentials is shown in Table.1[42-44,15].

Table 1 Terminology for Characteristic Potentials

Expressions	Symbols	Characteristics	Comment
Breakdown potential	E_b	Potential above which pits nucleate and grow	
Critical Pitting Potential	E_c		
Pitting Initiation	E_I		
Critical Potential for Pitting nucleation	E_{np}		
Protection Potential	E_{pp}	Potential below which no pitting occurs and above which pits already nucleated can grow	At potentials $E_{pp}<E<E_b$, pits already nucleated can grow.
Repassivation Potential	E_p		

The breakdown potential, E_b, according to the shape of the anodic polarization curve, is the potential value at which the current density begins to increase sharply at the end of the passive region. Aggressive anions (Cl^-, Br^-, etc) tend to lower the breakdown potential which characterizes the pitting resistance of a given metal or alloy in any given solution. The more positive the breakdown potential, the more pitting resistance the material possesses. By measuring the polarization curve from negative to positive potentials using potentiostatic methods, the breakdown potential can be determined. Measurements taken in the reserve direction during a cyclic polarization scan determine the protection potential or repassivation potential[41,44].

B.3.4 Factors Influencing Pitting

The effects of various alloying elements on the pitting susceptibility of steels have been investigated by many researchers. Usually, elements having beneficial effects on pitting resistance shift E_c or E_b to more positive values, while those having detrimental effects shift E_c or E_b to more negative values.

Horvath and Uhlig [45] invesitigated the influence of Cr, Ni and Mo on the E_{np} of different alloys (Cr-Ni, Cr-Fe, Cr-Fe-Ni, and Cr-Ni-Mo). They showed that the breakdown potential increase in the Cr content. For 15Cr-Fe-Ni alloys, E_{np} was shifted slightly in the noble direction when the Ni content increased.

Sugimoto and Sawada[46] suggested that even a small quantity of Mo added to Fe-Cr or Fe-Cr-Ni alloys significantly improves the pitting resistance. Without Mo in Fe-Cr alloys, the amount of Cr necessary to attain complete inhibition of pitting in 1N HCl was about twice that needed in the 20Cr-25Ni-5Mo alloy. Lizloves and Bond[47] studied high purity 17%Cr steels and austentic steels containing up to 3% Mo by potentiokinetic polarization curves and came to the same conclusion. Moreover, in the presence of Mo, not only did the E_{np} shift to more positive values, but the critical current density and primary passivation potential also decreased considerably.

Other researchers[49-53] found that Mo content was depleted in the external layers of the oxide film on Mo-containing stainless steels and Fe-Mo alloys and this element was detected only in the internal oxide layers close to the alloy surface.

Beddoes et al[54], suggested that the cold worked state exhibited an improved resistance to pitting corrosion for 316L stainless steel due to more Mo content in the cold worked materials than annealed materials. However, Mudali and Ningshen[55] found that an increase in cold work from 0% to 25% or an increase in grain size from 70 to 570 μm for 316L SS significantly decreased the pitting resistance.

Malik and Kutty[56] investigated the effect of chloride concentration, pH, dissolved oxygen and temperature on the pitting behavior of 316L SS in aqueous solutions by electrochemical polarization techniques. They found that as the Cl^- concentration

increased, the corrosion rate linearly increased and E_{pit} shifted to more negative potentials. Temperature had the same effects as the Cl^- concentration. pH had an opposite effect which the corrosion rate decreasing with increasing pH. Other researchers substantiated these results[57, 34, 58-61].

Salvago and Fumagalli[63] investigated the corrosion behavior of AISI 304 and 316 stainless steel in 0.1M HCl solution by potentiostatic and potentiodynamic tests. The results showed that the structure (γ, $\gamma+\alpha$ or $\gamma+\sigma$), the surface exposed (longitudinal or short transverse) and the Mo content all influenced the minimum breakdown potential value. Grain boundary precipitates, grain size and cold work affected the shape of the survivial probability vs potential curve.

B.4 Crevice Corrosion

Crevice corrosion[14] is a type of localized corrosion which occurs within narrow crevices that may be formed by the geometry of the structure, contact of the metal with non-metallic materials and deposits of sand, dirt on the metal surface. It can occur with a variety of metal and alloys, espcially for the metals and alloys that depend on passivity for their corrosion resistance. The environment in which metal occurred crevice corrosion can be any aggressive solution including natural waters, but solutions containing chloride ions are the most conductive to crevice corroison.

In general, the cathode reactant (e.g. dissolved oxygen) easily react with the metal surface outside the crevice, whereas access to the crevice is much more difficult since it only can be achieved by diffustion through the narrow mouth of the crevice. And the width of crevice is a very important factor to effect the crevice corrosion. The crevice

must be wide enough to permit the entry of solution, but sufficiently narrow to maintain a stagnant zone of solution with the crevice to keep the reaction rate of cathode reactant slow and the access of the reactants only by diffusion and migrantion.

Streicher[33] had studied various stainless steels, Inconels, Hastelloys and pure metals using an aartificial crevice. 10% $FeCl_3$ solution (pH = 1.6) at 50°C was used as solution and attack was found to occur within 24 h on all suspentible alloys while it could take up to 4 months without a crevice. Almost all the stainless steel used in the tests failed.

The process of crevice corrosion is similar to that of pitting corrosion. When the materials immersed in a solution containing oxygen, oxygen reduction will occur on both the surface that outside the crevice and the surface within the crevice. However, since the crevice is too narrow, oxygen is very difficult to diffusion into it. As time increased, all the oxygen in the crevice are consumed by oxygen reduction reactions and the oxygen concentration within the crevice become negligible. Therefore, oxygen reduction within the crevice will cease and the reactions in the crevice will be controlled by anodic dissolution of the metal. The excess of positive charges formed within the solution will result in the diffusion of Cl^- and OH^- from the bulk solution to maintain charge balance. Hydrolysis of the metal chloride (equation 26) will reduce the pH value and result in the presence of the high chloride concentration which prevents passivation and benefits anodic dissolution. This squence of events results in an autocatalytic process gradual increasing the anodic dissolution in the crevice.

For stainless steel, the rapid reduction of dissolved oxygen on the surface outside the crevice will become passive with a potential greater than E_{pp}, whereas the metal within the crevice will be active with a potential less than E_{pp}. Since the area of the surface

outside the crevice is much bigger than the surface inside the crevice, the rate of metal dissolution in the crevice will be accelerated.

C. Oxide Film

C.1 Thermodynamics and Kinetics of Oxidation

When some metals or alloys such as Al, Ti and stainless steel are exposed to air, a thin film of oxide 3-10 nm thick forms on the surface of the metal in a few minutes. The film is almost impenetrable at room temperature and can protect the metal from harmful environments. The growth of the oxide is driven by two electrochemical processes: an anodic reaction and a cathodic reaction. The anodic process converts the metal to cations and produces the electrons at the metal/oxide interface whereas the cathodic process converts oxygen to anions and consumes electrons at the oxide/atmosphere interface. When an anion collides with a cation, an oxide is formed. To produce a new oxide, the anion or cation must diffuse through atomic scale defects in the oxide structure. Therefore, oxide structures play a significant role in the formation of an oxide on a metal or alloy.

As the temperature rises, the diffusion rate of ions increases. If the relative volume of oxide can not be compatible with that of the metal, tensile or compressive stress will be produced at the metal/oxide interface which may cause cracks or buckles in the oxide film. Hence, this type of oxide film has no protection for metals or alloys. If the oxide film is continuous, coherent, and adherent to the metal substrate, the oxidation rate is controlled by the transport of the metal/oxygen through the film, which will act as a protective barrier for the metal or alloy.

The growth of oxide is sustained by two following processes, and is controlled by he slower of these two processes:

(i) Interface reaction at the metal/oxide or the oxide/atmosphere interface.

(ii) Diffusion of the reactants through the oxide film.

C.1.1 Thin Films

A thin film refers to an oxide layer whose thickness is 3-10 nm, corresponding to an oxide layer of 30-100 atoms of oxide. The film usually grows rapidly, in a few minutes, and when the thickness of the film reaches the above range of value, it will cease growing. Since the film forms very quickly, the thickness of the film is a function of time and may not be controlled by diffusion. The relationship of the thickness and time can be logarithmic, inverse logarithmic or cubic functions depending on the metal or alloy.

From a protection viewpoint, this film plays an important role, because it provides initial protection on all new surfaces of metals or alloys. The process for the oxide film can be describe as follow: before electronic equilibrium is established, oxygen atoms are adsorbed at the oxide/atmosphere interface by the oxide lattice and at the same time electrons from the metal pass through the thin film by thermionic emission or tunneling. Secondly, the oxygen atoms react with these electrons to become anions, O^{2-}. Therefore, the growth of the film is limited by availability of electrons.

C.1.2 Thick Films and the Wagner Theory

The Wagner theory[76,88] can be used to explain the formation of an oxide layer that is thick enough to attain local equilibrium at both the oxide/atmosphere and metal/oxide interfaces.

If x represents the distance from the metal surface, $n_c(x)$ and $n_p(x)$ are the concentrations of cation vacancies and positive holes, v_c and v_p are their mobilities and D_c and D_p is their diffusion coefficients. Therefore, the flux of cation vacancies (number crossing a unit area per second) will be expressed by[14]:

$$J_c = -D_c\, dn_c/dx - n_c v_c F \cdots\cdots (27)$$

where F(x) is the electrostatic field in the oxide. The flux of positive holes is

$$J_p = -D_p\, dn_p/dx - n_p v_p F \cdots\cdots (28)$$

If the system is at equilibrium, $J_c = J_p = 0$ and the field F will be negligible. If the oxide layer is thick enough, electrical neutrality in the oxide can be assumed. By using Einstein's relation, v/D =e/kT,

$$J = -2(kT/e)v_c\, dn/dx \cdots\cdots (29)$$

If X is the thickness of the oxide layer and Ω is the volume of the oxide per metal atom, the rate of growth, is given by:

$$dX/dt = k_2/X \text{ or } X^2 = 2K_2t \cdots\cdots (30)$$

$$K_2 = 2D_c\Omega(n_x - n_0) \cdots\cdots (31)$$

$$D_c = A\exp(-Q/kT) \cdots\cdots (32)$$

where Q is the activation energy for self-diffusion.

$$K_2 = B\exp(-Q/kT) \cdots\cdots (33)$$

This parabolic law is called the Wagner Theory. According to the theory, the oxide grows by two reactions. One is the ionization of oxygen into anions at the oxide/atmosphere interface and the other is the dissociation of the metal into cations and electrons at the metal/oxide interface. Since the concentration gradient of the reactants exists through the interfaces, the reactants such as electrons, vacancies and so on, will pass through the oxide layer by diffusion. Therefore, the growth of the oxide layer is controlled by the rate at which the reactants diffuse through the oxide lattice defects.

In order to minimize the energy of the system, the atoms in solids are closely packed. The arrangement in a given oxide is determined by the relative numbers of anions and

cations, the stoichiometric ratio, and cation/anion radius ratio. Since the material always tends to attain its lowest energy, a degree of disorder exists in the metal, which will lead to lattice defects in the structure. There are two types of lattice defects for a metallic oxide: lattice vacancies caused by ions missing from lattice positions, and interstitials which are generated by additional ions inserted between ions on their normal lattice sites.

C.1.3 Lattice Defects in Metal Oxides[14]

C.1.3.1 n-type oxides

If the oxide consists a metal such as zinc, the cation interstitial (n-type) oxide is created by inserting a metal atom into the lattice. The metal atom is transformed into an interstitial cation and interstitial electrons. Since there are excess cations, more electrons are required to balance them, and this kind of oxide is called n-type oxide due to negative charge carriers.

The process of forming n-type oxide includes two reactions. One is the oxygen reaction which occurs at the oxide/atmosphere interface where the oxygen is ionized as anions to provide electrons to react with the interstitials existing in the metals or alloys. For example:

$$\frac{1}{2} O_2 + Zn^{2+} \bullet + 2e \bullet = ZnO \cdots\cdots (34)$$

The other reaction occurring at the metal/oxide interface is metal atoms converting to cations and electrons, supplying the intersitial species and consuming the metal:

$$Zn(metal) = Zn^{2+} \bullet (\text{cation interstitial}) + 2e \bullet (\text{interstitial electrons}) \cdots\cdots (35)$$

The overall reaction is :

$$Zn + \frac{1}{2} O_2 = ZnO \cdots\cdots (36)$$

Since there is an equilibrium existing at the interfaces of the oxide layer, the equilibrium constant K is given by:

$$K = \frac{1}{[\alpha_{o_2}]^{\frac{1}{2}} \times \alpha_{(Zn^{2+}\bullet)} \times [\alpha_{(e\bullet)}]^2} \cdots\cdots(37)$$

Equation (37) shows that the equilibrium constant K is inversely proportional to $\alpha_{(Zn^{2+}\bullet)}$, $[\alpha_{(e\bullet)}]^2$ and $[\alpha_{O2}]^{1/2}$. Since the defect population is small, $\alpha_{(Zn^{2+}\bullet)} \propto n_{(Zn^{2+}\bullet)}$ and $\alpha_{(e\bullet)} \propto n_{(e\bullet)}$, where $n_{(Zn^{2+}\bullet)}$ and $n_{(e\bullet)}$ are the number of interstitial zinc ions and interstitial electrons. Assuming ZnO_2, $Zn^{2+}\bullet$ and $e\bullet$ are unit activity, and ideal behavior for oxygen gas, the equilibrium constant K is :

$$K = \frac{1}{[P_{o_2}]^{\frac{1}{2}} \times n_{(Zn^{2+}\bullet)} \times [n_{(e\bullet)}]^2} \cdots\cdots(38)$$

From stoichiometric considerations, $n_{(Zn^{2+}\bullet)} = 1/2\ n_{(e\bullet)} = n$. Substituting into equation (38), equation (39) is obtained as follows:

$$n = p^{\frac{-1}{6}} \cdot k^{\frac{-1}{3}} \cdots\cdots(39)$$

where k is a constant, which depends upon the equilibrium constant K and coefficients relating to $\alpha_{(Zn^{2+}\bullet)}$ and $\alpha_{(e\bullet)}$.

Equation (39) means that the number of the atoms at any interface is related to the pressure and the constant k. Likewise, from equation (39), the number of intersitials at the oxide/atmosphere interface, n_{atm} ,is given by

$$n_{atm} = p_{atm}^{\frac{-1}{6}} \cdot k^{\frac{-1}{3}} \cdots\cdots(40)$$

where P_{atm} is to the prevailing oxygen pressure.

The number of intersitials at the metal/oxide interface, n_0 ,is given by

$$n_0 = p_0^{-\frac{1}{6}} \cdot k^{-\frac{1}{3}} \cdots\cdots(41)$$

where P_0 is the dissociation pressure of the oxide.

From equations (40) and (41), the number of atoms at different interfaces can be used to infer the direction of the concentration gradient. If $P_{atm} > P_0$, then $n_{atm} < n_0$, and there is a concentration gradient from the metal/oxide interface to the oxide/ atmosphere interface and therefore cation interstitials diffuse from the metal/oxide interface to the oxide/atmosphere interface. If $P_{atm} < P_0$, the direction of the interstitial diffusion will be reversed.

C. 1.3.2 p-type Oxides

A cation vacancy is created by removing a metal atom from the lattice. For some metals, e.g., manganese, iron, cobalt, nickel, and copper, the energies of the d electrons are close to the energies of the valency electrons. As a consequence, sufficient electrons can be withdrawn to compensate for charge imbalance introduced by cation vacancies. For example in nickel oxide, Ni^{2+} is very easily converted to Ni^{3+} and at the same time electron holes are created in the d orbitals. The electron holes offer mobility for the electrons. Therefore, the predominant defects in the lower oxides of these metals are cation vacancies and the oxide is a positive charge carrier which is called a p-type oxide.

The process for forming p-type oxides is as follows: the oxide lattice absorbs the oxygen atoms and ionizes them into anions, O^{2-}. The cation is transferred from a lattice site to the vacancy of the existing local lattice. On the other hand, the electrons from the metal ion d shells ionize oxygen into anions, creating electron holes.

$$\tfrac{1}{2}\,O_2 = NiO + Ni^{2+}\ \text{(cation vacancy)} + 2e\ \text{(electron holes)} \cdots\cdots (42)$$

The complementarily partial reaction at the metal/oxide interface is that the atoms from the metal enter into the oxide, converting into cations and electrons, and consuming cation vacancies and electron holes in the oxide:

$$Ni + Ni^{2+} + 2e\ \text{(oxide)} = 0 \cdots\cdots (43)$$

The overall reaction is :

$$Ni + \tfrac{1}{2}\,O_2 = NiO \cdots\cdots (44)$$

The equilibrium constant, K, is given by:

$$K = \frac{\alpha_{(Ni^{2+})} \times [\alpha_{(e)}]^2}{[\alpha_{o_2}]^{1/2}} \cdots\cdots (45)$$

$n_{(Ni2+)} = 1/2_{(e)} = n$,

$$n = p^{1/6} \cdot k^{1/3} \cdots\cdots (46)$$

Equation (46) shows that the number of atoms at any interface is proportional to $P^{1/6}$ and $k^{1/3}$. If $P_{atm} > P_0$, the oxygen pressure in the environment exceeds the dissociaton pressure of the oxide, then $n_{atm} > n_0$. Thus, a concentration gradient exists between the oxide/atmosphere interface and the metal/oxide interface. As a consequence, the cation vacancies diffuse inwards from the oxide/atmosphere interface to the metal surface. And the nickel ions transport outwards from the metal through the oxide to the oxide/atmosphere interface.

C.2 Oxidation of Stainless Steels

Stainless steels will form a protective film on their surface by preferential oxidation of chromium. In 1938, Price and Thomas[65] found that selective oxidation of chromium occurred during low temperature annealing of the finished steel part in a vacuum with a certain residual pressure of oxygen. This kind of selective oxidation at reduced oxygen partial pressure has been extensively studied[66-68]. Since the free energies of formation of the Cr_2O_3 and Fe_2O_3 are 250.0 and 176.8 kcal/mole respectively[69], Cr_2O_3 is more stable than Fe_2O_3. Therefore, the selective oxidation of chromium will be favored by a higher driving force than the oxidation of iron. In the surface layer of the alloy, the amount of iron is reduced and the amount of chromium is enriched simultaneously[70-72]. The chromium surface enrichment is further promoted if a low partial pressure of oxygen is introduced into the vacuum[74].The very thin oxide film (<10nm) exhibits good corrosion resistance to normal tap water and sea-water[68,75].

Jensen and Mitchell et. al[76], invesigated the oxidation of Fe-26Cr alloy at 600°C in 5×10^{-3}, 5×10^{-2} and 5×10^{-1} torr oxygen. The results of the electron back-scattering Fe^{57} Mössbauer spectroscopy showed that the oxide film had two layers: an inner Cr-rich oxide (γ-Cr_2O_3) and an outer Fe-rich oxide (Fe_3O_4).

Transatti et.al[77], studied 304L stainless steel in a continuous air stream at temperatures in the range from 150°C to 300°C for 30 and 120 min. Using XPS analysis, they reported that the oxide film which was formed at room temperature on the surface of the stainless steel consisted of Fe and Cr mixed oxide, presumably $Fe(Fe,Cr)_2O_4$. As the temperature was increased, Fe oxides increased in percentage (mol%) to form a non-protective layer (FeO, FeOOH), whereas the amount of Cr oxide decreased. They

suggested higher mobility of iron ions was the reason for formation of the double structure of the oxide film. In addition, the rapid diffusion of iron ions through the oxide film produced a Fe concentration gradient at the metal/oxide interface.

There are five oxides in the iron-chromium-oxygen system: FeO, Fe_3O_4 (magnetite), Fe_2O_3 (hematite), Cr_2O_3 and $FeCr_2O_4$ (chromite). Chromium combined with Fe_2O_3 as the mixed oxide, $(Fe,Cr)_2O_3$ and in Fe_3O_4 as the mixed spinel. The relative stabilities of these oxides are a function of alloy composition but also depend on following factors[10]:

(i) Diffusion of anions and cations within the oxides

(ii) The progressive reduction of activity of chromium at metal surface by selective oxidation

(iii) The increased stress within and between the layers as the oxide layers thicken.

Fig. 10 shown the morphology of the oxide layers[10]

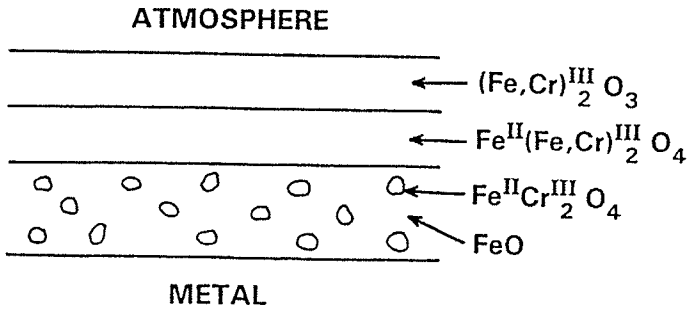

Fig.10 Morphology of oxide layers formed on iron-chromium alloys in air.

Olefjord's study [78] on the oxide film formed on austenitic stainless steel established that the composition of the film depended on reaction temperature and time. At high temperatures, the oxide was found to be enriched with the easily oxidizable elements, such as Cr and Mn. After oxidation at room temperature, and at an intermediate temperature (250°C), iron was found as the main component in the top layer of the oxide.

The investigations of the top layer after oxidation at 500°C for different times showed that chromium content increased with oxidation time.

After investigating the primary rate of duplex scale formation of 316 stainless steel annealed in vacuum at 600°C, Smith[79] suggested an oxygen pressure dependence, $Kp \propto Po_2^{0.135}$, and concluded that at 600°C the rate controlling process for oxidation during the initial stage of vacuum-annealing 316 stainless steel was the diffusion of Fe cation in the outer magnetite layer.

In another experiment[103], Smith used Fe and Mn tracers to study the diffusion of various elements in duplex scales on vacuum-annealed 316 stainless steel at temperatures of 655-1000°C. The Fe tracer concentration decreased with the increase of penetration at all temperatures. Diffusion coefficients in the oxide layers and the underlying alloy were evaluated using finite difference methods. The Cr and Mn tracer concentrations increased with their distance in the outer oxide layer over the whole temperature range.

Electron spectroscopy for chemical analysis (ESCA)[69] has been used to analyse the composition of oxide films formed on chromium steel with 6-10%Cr at room temperature in pure oxygen at 0.2atm annealed for 2 min to 46 h. It was demonstrated that the total chromium content in the oxide was proportional to the concentration in the metal, but it varied with depth inside the film. At the oxide/gas boundary, the chromium concentration was less than that in the metal, while chromium was enriched at the metal phase boundary. It was suggested that the oxide consisted of $(Fe,Cr)_2O_3$ in the outmost zone and $FeCr_2O_4$ at the inside at room temperature, because of low atomic mobility, it was possible to form a layer at the interface between the oxygen and the metal which contained iron and chromium. Thus at room temperature, oxygen pressure was a decisive

factor in determining the composition of the film. As the temperature was raised, chromium atoms moved preferentially into the film, substituting for iron which in turn diffused outwards and formed more oxide. Depletion of Cr in the metal next to the oxide interface will cause a decrease of Cr concentration in the outer zone of the oxide film. In this way, chromium content will decrease outwardly in the film, according to the classical theory of selective oxidation.

Hakiki and Montemor[80] investigated the oxide film formed on austenitic type AISI 304 stainless steel annealed in air for 2 hours temperatures ranging between 50 and 450°C. It was shown that the films had a typical duplex structure: an external iron oxide region and an inner mixed iron-chromium oxide region. The thickness of the oxide layer was increased by a factor greater than four when the temperature of formation of the films increased from 50 to 450°C. However, the largest change in thickness occurred essentially in the outer iron oxide region whereas the thickness of the chromium-rich region was not significantly affected. Further, as the temperature increased, the inner region gradually enriched in iron. Other experiments confirmed this result[81,82].

The microstructure of the oxide film formed on 316L stainless steel in air at 500°C for 5 min was characterized by an energy filtering transmission electron microscope equipped with an electron energy loss spectroscopy detector[83]. It was observed that the oxide film was composed of nanoscale γ-Fe_2O_3 grains of ~4nm, followed by a mixture of α-Fe_2O_3 and Fe_3O_4 phases of grain size from 20 to 75nm. There existed an alloying depletion of Cr and Mn in the oxide film and the O content in the oxide film decreased from the oxide surface toward the oxide/metal interface.

Montemor et.al[84] verified the results of the above experiment. They found that at 350°C, the Cr profile reached a maximum near the oxide/alloy interface. The oxide had a region of about 10 atomic layers enriched in chromium relative to the substrate. The study on 316 stainless steel showed that Mo was only found in the inner oxide layer and the presence of Mo increased the amount of Cr content in the oxide film but had no influence effect on the oxide thickness[85,86]. Mathieu et al[87] suggested that the Mo being present in the metal/oxide interface could decrease the activity of the metallic ion or act as a diffusion barrier for the Fe and Cr ions in the oxide.

It is generally accepted that Cr-rich oxides exhibit lower diffusion rates than Fe-rich oxides. Yoakam and Schumacher[89] studied the electrochemical behavior of as-received bright annealed samples of 316L stainless steel exposed in HCl solution. They established that enhanced Cr/Fe and CrO/FeO ratios on the surface of the stainless steel improved the corrosion resistance of this material.

It was demonstrated[90] that heating a specimen with a clean metallic surface in high vacuum of 10^{-8} torr resulted in a layer of chromium oxide on the surface. And the enrichment of Cr in the oxide film could enhance the corrosion resistance of steels[91,92].

Further investigation[93] on the effect of various oxidation conditions on metal dissolution for SUS304L stainless steels in deaerated pure water at 488K, verified that the key factors controlling the metal dissolution are the thickness, structure and compactness of the oxide film, together with its composition.

Yashiro[94] studied surface composition and structure changes of stainless steels under vacuum heat treatment and controlled heat treatment. Surface element segregation

was found, and low oxygen, controlled atmospheres were helpful in obtaining an oxide film which had good corrosion resistance.

Yen and Tsai[95] investigated the early oxidation ($t \leq 120$min) of AISI 430 stainless steel by thermal gravimetric analysis and Auger electron spectroscopy. Oxidation could be divided into two regions: one is a rapid growth rate for $t < 5$ min and the other is a parabolic or slower growth rate for $t > 5$ min. They found that there existed a critical temperature, T_c, above which a chromium-rich oxide film was formed. For this stainless steel, T_c was equal to 947K. When $T \geq T_c$, the corrosion resistance of the oxidized metal was enhanced.

Wood and Whittle[68] used the same treatment as Price and Thomas[65] on chromium-alloyed steels. They concluded that the protective abilities of the oxide film were related to not only a pure Cr_2O_3 layer with a thickness in the micron range, but also to the zone in the alloy next to the oxide layer. If the zone was depleted in chromium, the surface layer usually had a good resistance to high temperature oxidation but had less corrosion resistance in chloride solutions. Trasatti and Camona[77] confirmed this result, and pointed out that the Cr-depleted film increased the susceptibility of the alloy to pitting corrosion.

Hultquist and Leygraf[73] determined that the oxide film on chromium-alloyed stainless steel exhibited good corrosion resistance to normal tap water and seawater and attributed to this enrichment of chromium in the region next to the film. For a given stainless steel, the annealing temperature and the oxygen partial pressure were the two most important factors in the formation of the oxide layer. The precipitation of chromium carbides at grain boundaries and phase transformations established a limit for the

annealing temperature of chromium-alloyed steel, which was between 550 and 750 K. On the other hand, depending on alloy composition and surface pretreatment, the oxygen partial pressure should range from 10^{-8} to 10^{-5} Pa. Therefore, a very thin surface film was formed and usually its thickness was less than 10nm. The author attributed the corrosion resistance of the oxide film to chromium having a stronger tendency to form oxide compounds than iron and a low partial pressure being able to further promote the formation of a chromium-rich surface. Furthermore, some experiments confirmed the above results. For instance, at 800K below a critical oxygen partial pressure of about 10^{-5} Pa, the oxide layer consisted mainly of chromium oxide. However, above this oxygen partial pressure, the oxide layer consisted primarily of iron oxide. Therefore, at different temperatures, there exists a critical oxygen partial pressure which determines the composition of the oxide film. To obtain an oxide film high in chromium, it is necessary to anneal the chromium-alloyed steel in a dilute atmosphere with an oxygen partial pressure lower than the critical value.

Leygraf and Hultquist[97] suggested that in order to attain good resistance to localized corrosion of stainless steels in chloride-containing solution, the maximum thickness of the protective film formed by a vacuum annealing treatment was of the order of 100nm. In addition, it was important to avoid a surface enrichment of iron, since the iron- rich film was detrimental to the corrosion resistance. They investigated 25 different combinations of annealing temperature, annealing time, oxygen partial pressure and total pressure by analyzing the oxide film using AES. The profiles of the oxide films are shown in Fig.11[73].

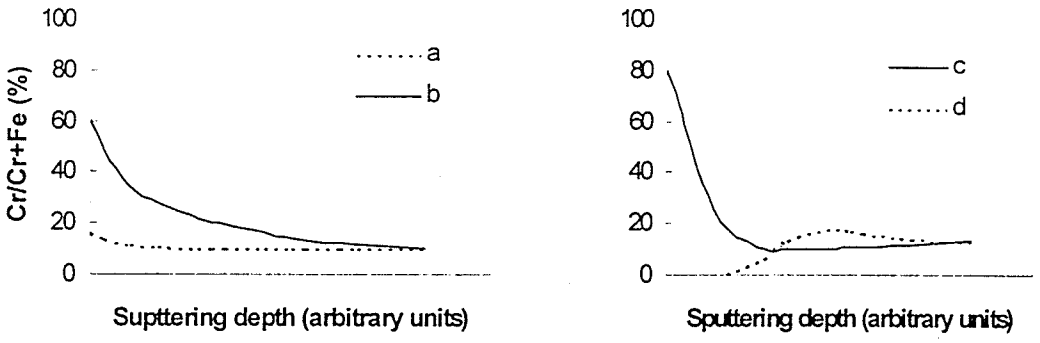

Fig.11 Chromium profiles of an Fe-10%Cr alloy after various surface treatments

In Fig.11, curve a is the chromium profile of a mechanically polished Fe-10Cr alloy, indicating a slight chromium enrichment in the film prior to surface treatment. Curve b shows the chromium profile of the same alloy after a successful surface treatment resulting in an increase in corrosion resistance. The surface treatment established a balance between annealing temperature and oxygen partial pressure and resulted in a marked surface enrichment of chromium with no measurable chromium depleted zone beneath the oxide film.

Curve c shows a high surface content of chromium after another surface treatment. There is no increase in corrosion resistance obtained because the growth of the oxide film was too fast, which resulted in a chromium depleted zone next to the oxide film due to the limited supply of chromium migrating from the interior of the alloy to the surface region.

Curve d is another example of unsuccessful surface treatments in the case there was an too high oxygen partial pressure for the annealing temperature, which led to an iron enrichment in front of the chromium-rich zone of the film.

In the thermal passivation of stainless steel, both the total and the partial oxygen pressure in the residual gas have to be matched to the annealing temperature and time. These process parameters should on their part accord to the composition of the alloy and surface pretreatment in order to modify the structure and composition of the existing surface layer of the steel into a more protective film exhibiting maximum corrosion resistance[73].

Hultquist and Leygraf pointed out[98] that the total oxide thickness should not be more than 100Å. The essential parameters determining the Cr enrichment in the surface region were the diffusion of alloy components from the bulk to the solid/gas interface and the flow of oxygen to this interface. Selective oxidation could be explained by different probabilities, γ_{Cr} and γ_{Fe}, for the oxidation of available chromium and iron. When the supply of chromium was equal to or less than the supply of oxygen, all the results of AES were consistent with γ_{Cr} =1 and with γ_{Fe} varying from 0-0.15, depending on the supply of oxygen. A formula which related the kinetic parameter to the observed AES results was given by:

$$\left(\frac{Cr}{Cr+Fe}\right)_{AES} = \left(\frac{Cr_{ox}}{Cr_{ox}+Fe_{ox}}\right)\left(1-e^{-D/\lambda}\right)+\left(\frac{Cr}{Cr+Fe}\right)_{bulk} \cdot e^{-D/\lambda} \quad \cdots\cdots(47)$$

where $\left(\frac{Cr}{Cr+Fe}\right)_{AES}$ is the ratio measured by AES,

D=total oxide thickness,

λ=mean free path of Auger electrons = 14 Å

$\left(\frac{Cr}{Cr+Fe}\right)_{bulk}$ is the ratio in the steel matrix,

$\left(\frac{Cr_{ox}}{Cr_{ox} + Fe_{ox}}\right)$ is the ratio of what in the oxide.

However, too high an enrichment of Cr in the oxide layer will result in a Cr depletion in the region beneath the oxide, which is caused by too limited a supply of Cr from the bulk and this has a marked detrimental effect on the corrosion resistance of the steel[99].

Greyling and Roux[100] studied the effect of temperature and oxygen partial pressure on the formation of oxide films on AISI 304 and 430 stainless steels. The temperature range was 450-600°C and the oxygen partial pressure range 6.7×10^{-7} to 1.33×10^{-5} Pa. Fig.12 gives the surface Cr content of alloys 304 and 430 as a function of oxygen exposure at different temperatures.

They proposed that at low temperature, Cr had a low mobility so that there existed a low supply of Cr at the surface. Therefore, oxygen prefered to combine with the more abundant Fe. As the temperature reached 600°C, Cr had sufficient mobility to segregate to the surface and to combine with oxygen so as to reduce the chemical potential gradient.

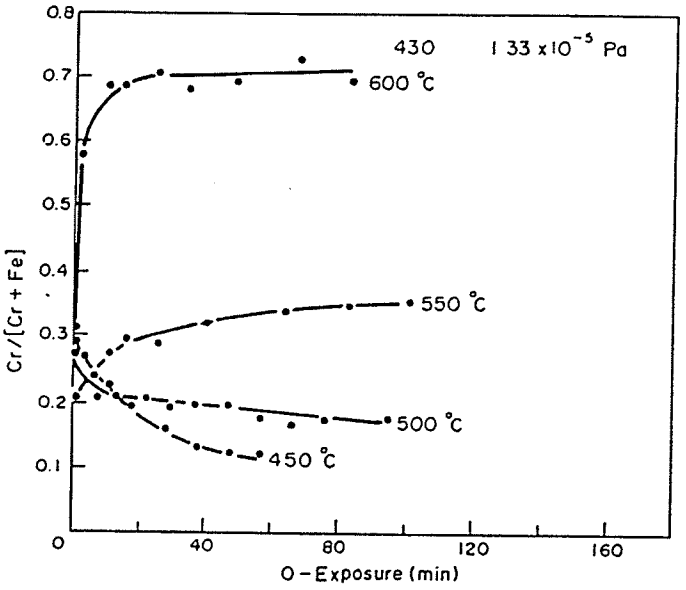

Fig.12 (a) Cr enrichment at the surface of alloy 430 during oxygen exposure at a partial pressure of 1.33×10^{-5}Pa at different temperatures

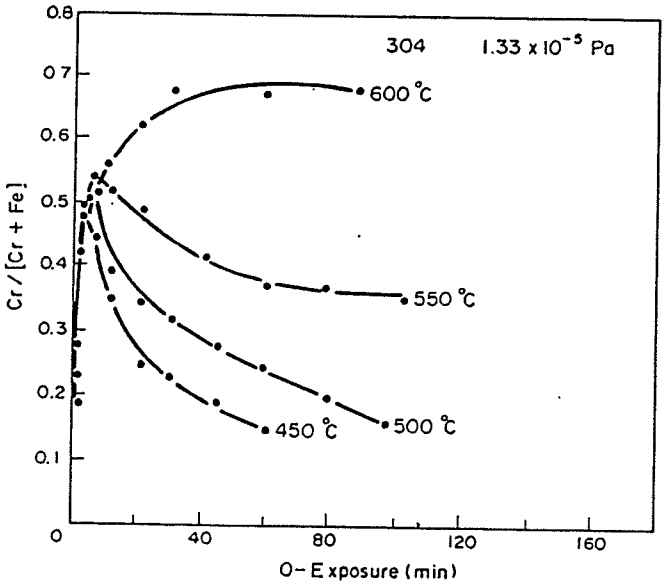

Fig. 12(b) Cr enrichment at the surface of alloy 304 during oxygen exposure at different temperature.

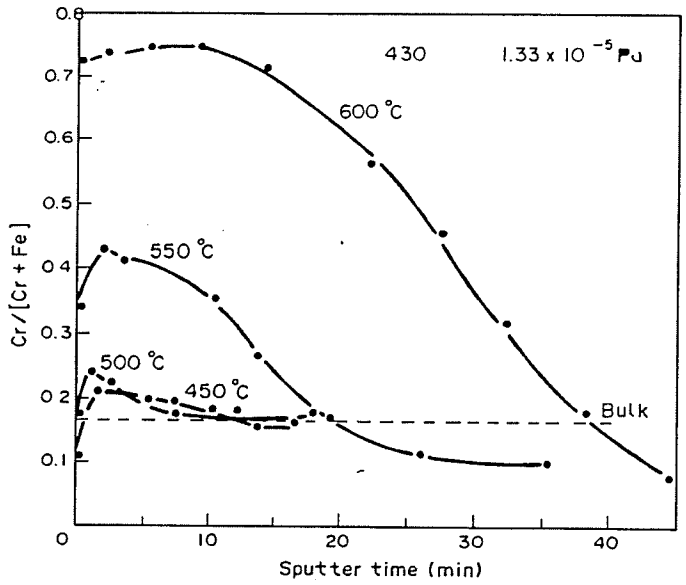

Fig.13 (a) Depth profile showing Cr distribution after oxidation of alloy 430

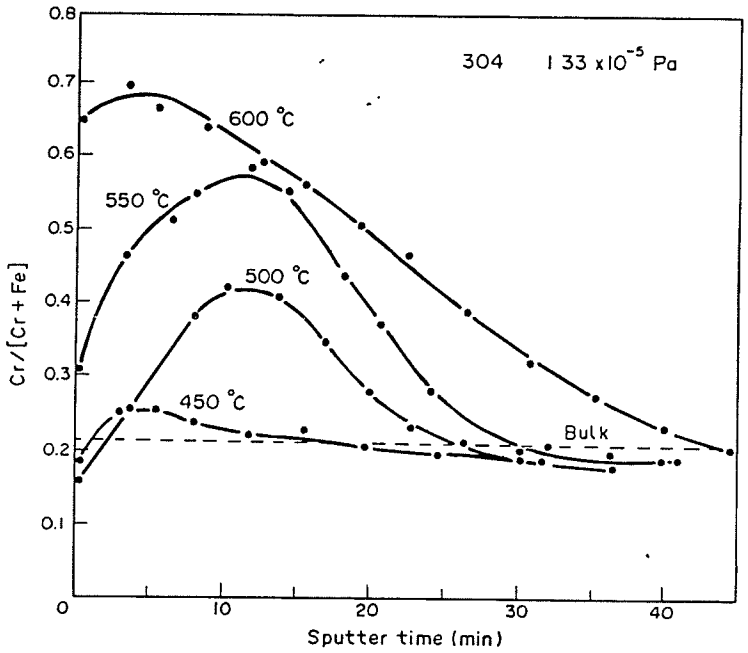

Fig.13(b) Depth profile showing Cr distribution after oxidation of alloy 304.

Comparing Fig. 12 with Fig. 13, it may be concluded that at a low oxygen pressure, Cr exhibited a greater affinity for oxygen than Fe. The main feature on the depth profiles taken after oxidation at 1.33×10^{-6} Pa was the larger depletion of Cr under the oxide layer in the case of the lower Cr content for type 430 stainless steel compared to type 304 stainless steel. Results of all the oxidations are summarized in Table 2.

From table 2, the optimum conditions obtained for oxide film were 600°C with an oxygen partial pressure of 1.33×10^{-5} Pa with an oxidation time of 90 min. Therefore, the thickness of the oxide film is 42nm and there is no depletion of Cr in the zone next to the oxide film.

Table 2 Thickness of Oxide Film and Fe/Cr Composition in The Surface Layer After Oxidation at Different Temperatures and Oxygen Partial Pressure

Temperature (°C)	Pressure (Pa)	Time (min)	Fe:Cr ratio		Thickness (nm)	
			430	304	430	304
400	1.33×10^{-5}	60	1:0.13	1:0.2	10.0	19.0
	1.33×10^{-6}	120	1:0.45	1:3.2	2.5	10.0
	6.7×10^{-7}	180	1:0.26	1:15	1.0	7.0
500	1.33×10^{-5}	100	1:0.21	1:0.2	22.0	27.0
	1.33×10^{-6}	130	1:1.5	1:1.1	7.0	10.0
	6.7×10^{-7}	210	1:1.7	1:1.8	4.0	7.0
550	1.33×10^{-5}	105	1:0.54	1:0.55	22.0	30.0
	1.33×10^{-6}	150	1:1.8	1:0.7	7.0	—
	6.7×10^{-7}	205	1:0.97	1:0.30	—	—
600	1.33×10^{-5}	90	1:2.7	1:2.1	43.0	42.0
	1.33×10^{-6}	135	1:0.97	1:0.2	—	—
570	6.7×10^{-6}	120	1:1.5	1:1.5	24.0	26.0
	6.7×10^{-6}	120	1:1.7	1:1.8	26.0	27.0
	6.7×10^{-6}	120	1:1.8	1:2.0	26.0	26.0

In an investigation of the oxide film formed on Fe and Fe-Cr alloys at elevated temperature (700-800 °C) and at low oxygen partial pressure (~10×10^{-3} Pa), Kuroda and Lubun[101] pointed out that at high temperature and at oxygen pressures of $\approx 10^{-5}$ Torr, $Fe_{1-x}O$ nucleated on pure iron. For Fe-3%Cr alloy, because of Cr suppressing the formation of $Fe_{1-x}O_x$, the nucleation of oxides occured by a surface precipitation process rather than a chemisorption and subsequent epitaxial process. Once oxide nuclei formed, oxygen diffused through the preexisting oxide film and reacted in a way that favored the growth of the original nuclei rather than the formation of new nuclei. Oxide nuclei grew outwardly until a limited thickness was reached, and after that the oxide continued to grow, mostly in lateral directions, until a roughly uniform scale was developed. For higher Cr-containing alloys, the nucleation of a spinel oxide $(Fe, Cr)_3O_4$ on the Fe-18% Cr alloy was observed. The pre-existng oxide film was amorphous or very fine-grained, which could be responsible for provideing rapid diffusion paths for oxygen. Rapid diffusion of oxygen along the phase boundary took place between the metal and the oxide. Therefore, the spinel oxide nucleated beneath the preexisting oxide film and grew inward towards the metal by the interface diffusion of oxygen.

Hulquist and Leygraf [102] investigated the electrochemcial behavior of 316L stainless steel after thermal passivation via vacuum annealing in the range 525-775K. The critical potential for crevice corrosion in a netural sodium chloride solution was at least 250mv. Due to selective oxidation of chromium and nickel during such thermal treatments, corrosion resistance results from a marked chromium film enrichment and a less marked nickel film enrichment.

D. Measurement Techniques and Experimental Methods

D.1 Electrochemical Technique

In 1903 Whitney proposed that corrosion of metals in a solution was an electrochemical reaction [105]. Therefore, electrochemistry can be applied to explain the basic theories of corrosion and to solve many engineering problems. The electrochemical technique possesses the unique characteristic that it is very clean in controlling the corrosion process. It can be used to increase the corrosion rate of a metal or alloy, or induce passivity of certain alloys without adding chemical oxidizing agents. It may also be used to measure the corrosion rates without moving or disturbing the specimen.

MacDowell and Ontiveros [106] studied the corrosion resistance of seventeen different materials via three methods: electrochemical corrosion testing, accelerated corrosion testing in a salt fog chamber, and a long term exposure at a beach corrosion testing site. Based on the results of these experiments, they found that the result of the electrochemical test was in a good agreement with the actual beach exposure test. This suggested that electrochemical testing is a good tool for optimizing the range of potential candidate alloys before conducting actual long term exposure tests thus saving both money and time. Also, Forsan and Aromaa [107] proved the validity of this suggestion by further experiments.

At present, many electrochemical techniques exist but most common in industry are the potentiostatic technique, the potentiodynamic polarization technique, the polarization resistance technique as well as the galvanostatic polarization technique.

D.1.1 Potentiostatic Technique

In general, the rates of anodic and cathodic reactions are a function of the potenial of the corroding system. The potential can be altered by applying an external current. Furthermore, by measuring the applied external current at potentials other than the corrosion potential, information about the anodic and cathodic reactions can be obtained. This is the basic principle of the potentiostatic testing or constant potential testing.

The set-up of a typical potentiostatic testing unit is illustrated in Fig.14[11].

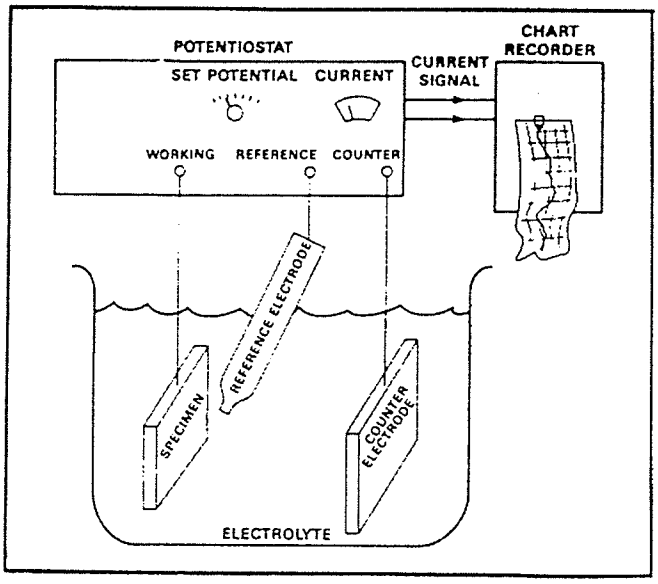

Fig.14 Potentiostatic test set-up

The system consists of a potentiostat, the specimen, a reference electrode and an inert counter electrode, the electrolyte, and a strip chart recorder or data acquisition unit which records the current and voltage output from the potentiostat.

- Potentiostat

By applying a variable current between the specimen and the counter electrode, the potentiostat is used to maintain a potential difference between the specimen and the reference electrode. The potentiostat measures the present potential difference then

modulates the applied current to attain the desired or "set" potential. The system is shown schematically in Fig.15[11].

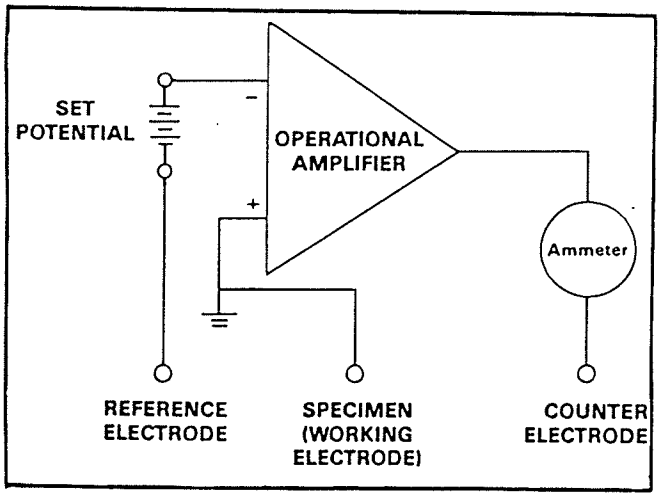

Fig.15 Simplified potentiostat

- Reference Electrode

Since a reference electrode usually maintains a stable potential, it can be used as a reference point for the measurement of other potentials. The corrosion potential is the difference between the measured potential and the reference electrode potential. The most common reference electrodes for aqueous room-temperature tests are: saturated calomel (Hg/HgCl in KCl), silver/silver chloride (in KCl) and copper/copper sulfate.

- Counter Electrode

A counter electrode, which is usually made of an inert material such as platinum or graphite, is the electrode used to supply current to the working electrode. For some materials, the expected corrosion morphology can be quickly assessed by anodic polarization, which can be used to artificially increase the corrosion rate. If the potential in potentiostatic anodic polarization is not too far anodic from the corrosion potential, the

morphology of the corrosion (uniform, pitting, dealloying) is frequently similar to that of a naturally corroding material.

To obtain the corrosion rate, the specimen is polarized either anodically or cathodically 5 to 10 mv away from its corrosion potential. Meanwhile, the applied current is monitored until a steady state is achieved. The corrosion rate is given by [11]:

$$\text{Corrosion Rate}(^{\mu m}/_{y}) = [\frac{\beta_a \beta_c}{2.3(\beta_a + \beta_c)}] \times \frac{\text{steady state current(mA)} \cdot \text{equiv wt}(^{g}/_{c})}{\text{potential offset(mv)} \cdot \text{area}(cm^2)} \times 3156(^{\mu m \cdot s}/_{cm-y})$$

D.1.2 Potentiodynamic Polarization Techniques

Potentiodynamic test uses a controlled potential which is varied, usually linearly, as a function of time. By simultaneously measuring the current and potential, a plot of the relationship of current changes resulting from potential changes can be obtained.

The process of sweeping a range of potentials in the anodic (more electropositive) direction of a potentiodynamic polarization curve at a high scan rate of about 60v/h is called the rapid-scan technique. If the scan rate is relatively slow, such as 1 v/h, the process is called the slow-scan technique.

- Rapid-Scan Technique

The feature of rapid-scan technique is to minimize the formation of an oxide film, so that the measured currents correspond to relatively film-free or thin-film conditions. In addition, the rapid-scan technique helps maintain a stable environment while changing the nature of the metal surface.

For rapid scan tests the specimen is first mechanically or chemically cleaned and immersed in the testing cell. Cathodic polarization scanning is then done at a sweep rate of 50-60v/h, which further cleans and activates the specimen and prevents it from

spontaneously passivating or returning to the equilibratory state with its environment. Finally, anodic polarization provides information concerning the anodic reaction under a variable potentiodynamical potential without the interference of any pre-existing passive or corrosion product film or scale.

- Slow-Scan Technique

For the slow-scan technique, the oxide film has enough time to form on the metal surface. If the scanning rate is zero, maximal stability of the metal surface will be obtained, but at high electropositive potentials, the environment could be affected or changed. Slow-scan polarization allows the specimen to attain equilibrium (open circuit corrosion potential, E_{corr}) in the solution before the potential scan is conducted. However, this technique precludes the study of how the metal reached the steady state condition.

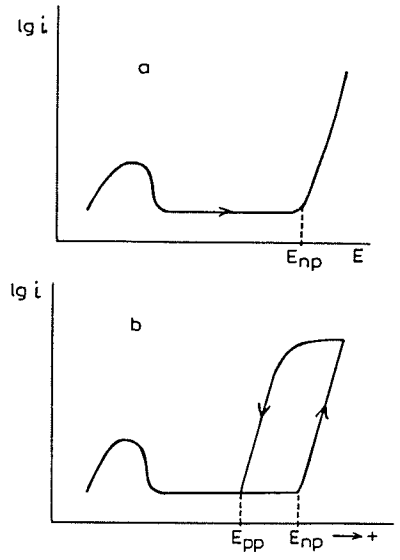

Fig.16 Schematic representation of anodic polarization curves for a metal immersed in solution containing aggressive ions. Potentiostatic measurements conducted (a) forward (b) backward[15].

For example, for 316L stainless steel [109], the process by which the passive film is formed at the corrosion potential is slow, and a slow scan rate allows the integral film to form. Therefore, a slow-scan rate is more suitable to study localized corrosion rather than the rapid-scan rate.

D.1.3 Galvanostatic method

In constant with the potentiostatic method, a fixed current is imposed on the electrochemical system and the change of the potentials is measured. Therefore, the current density is the independent factor and the steady-state potential is the dependent one. Fig.17[11] is the equipment required for galvanostatic measurement.

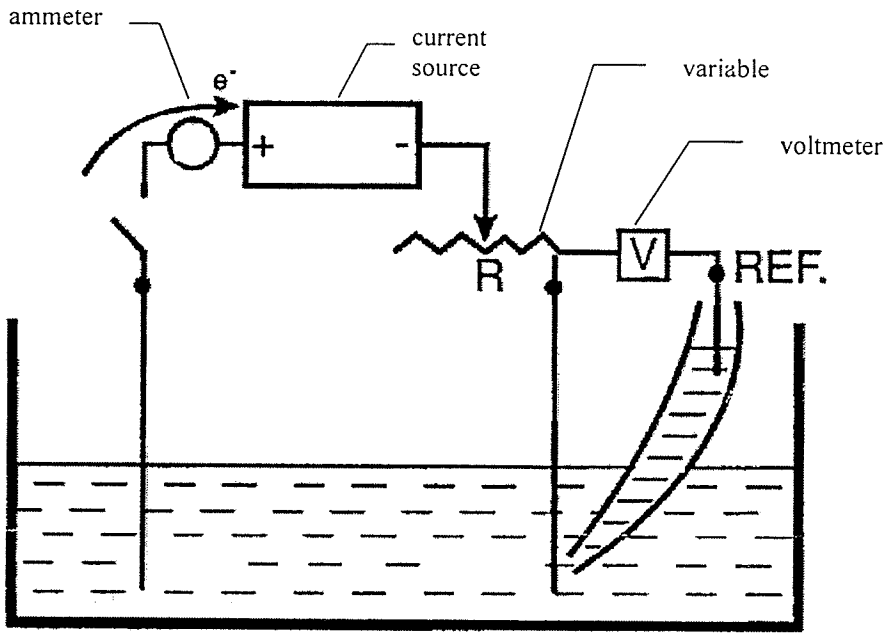

Fig.17 Galvanostatic polarization

D. 2 Secondary Ion Mass Spectrometry (SIMS)

The process for secondary ion mass spectrometry analysis is described as follows:

Under high vacuum, samples are bombarded by primary energetic particles, such as ions or neutral atoms, in the KeV range. As a result, most superficial layers of the sample are sputtered from the metal as secondary ions. The emitted secondary ions are filtered according to their mass charge ratios and are detected via spectrometers. The concentration of the ions is proportional to the intensity of the energy detected by the spectrometers. Fig. 18 shows the principles of SIMS analysis.

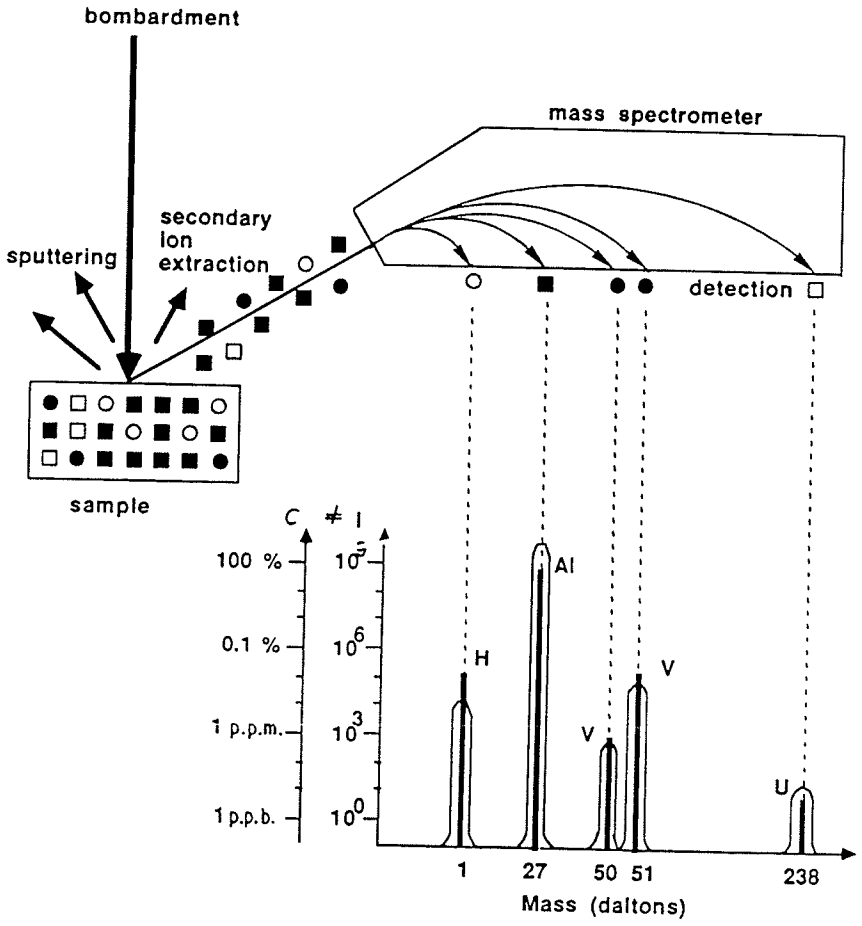

Fig. 18 Schematic representation of the principles of SIMS analysis

Through this method, information about the metal surface can be obtained. SIMS has extensive applications, i.e. qualitative analysis of metallurgical samples by mass spectra, qualitative microscopy by ion imaging, quantitative bulk analysis of metallurgical

samples, thin film and interface analysis by depth profiles, and use of isotopic tracers for mechanism studies.

In this experiment, SIMS was used to analyze the concentration of elements in the thin oxide film which should reflect the corrosion resistance of the oxide film. The change in ion intensity, I, with erosion time, t, reflects the actual depth profile; concentration, C, with depth, z.

III. EXPERIMENTAL

A. Material and Preparation of Specimen

The material used in the experiments was commercial 316L stainless steel, whose nominal composition is shown in Table.3[2].

Table 3 The content of elements in the 316L stainless steel

Element	Cr	Ni	Mo	Mn	C	S	P	Si
Composition (%At)	17-19	9-13	1.1-1.7	2.01	0.14	0.05	0.08	1.97
Content(wt %)	16-18	10-14	2.0-3.0	2.00	0.03	0.03	0.045	1.00

The specimens, of diameter 16mm and thickness ≈ 1mm, were cut from cold rolled bar.

For the experimental specimens, two types of surface treatments were used. For one type, the specimens were wet-ground gradually through a series of 120, 180, 240, 400 and 600 grit SiC paper. For the other, after wet grounding, the specimens were mechanically polished sequentially from 6 μm and 1 μm diamond paste to 0.25 μm Al_2O_3 colloid. After grounding or polishing, all the specimens were ultrasonically cleaned in ethanol and then dried using a warm air stream.

Then vacuum-annealing treatments were conducted at different temperatures and times in a dynamic vacuum $\approx 10^{-5}$ torr as shown in Table 4. The temperatures were measured using a chromel-alumel thermocouple.

Tabel 4 Vacuum Annealing Treatment (5×10^{-6} torr)

Surface Treatment	Temperature	Time
Sanded to 600 grit paper	Room Temperature	
Mechanical Polishing	Room Temperature	
	200°C	90 min
	300°C	90 min
	400°C	30 min
		90 min
		150 min
	500°C	90 min
	600°C	90 min

B. Experimental Techniques

B.1 Secondary Ion Mass Spectrometry (SIMS) Analysis

Three specimens were polished to 0.25μm and then annealed at 200°C to 400°C. The element distributions of the oxide film formed on samples at room temperature, 200°C and 400°C were analyzed at the Surface Science Center, University of Western Ontario, London, Ontario. A Cameca IMS-3f ion microprobe with a Cs^+ beam was used and the various secondary ions of interest were monitored. The Cameca instrument conditions are summarized as follows:

Primary:

Beam	Cesium
Polarity	positive
Accelerating Voltage	10KV
Primary Beam Raster	250×250 μm
Beam Current	1 nA

Secondary:

Polarity	negative
Accelerating Voltage	4500V
Transfer Optics	150 μm (imaged field)
Contrast Aperture	4 (largest)
Field Aperture	2 (60 μm diameter)
Energy Window	130 eV
Offset Voltage	200V, 100V on ^{98}Mo (low intensity)

Approximate depth scales for the profiles were obtained by measuring the SIMS craters with a Tencor P-10 surface profilometer.

B.2 Electrochemical Testing

The cell used in the experiments comprised a 500ml Erlenmeyer flask filled wih 450ml 3.5%NaCl solution at room temperature. The pH value was measured using a pH instrument, Rodiometer Copenhager type PHM71b. The potential of the specimen in solution was monitored using a saturated (with KCl) calomel electrode isolated from the sodium chloride solution with a ceramic porous plug tube filled with saturated KCl.

The cyclic potentiodynamic polarization technique was used to investigate the electrochemical behavior of the oxide film formed on type 316L stainless steels. The tests were conducted on a Model 350A Corrosion Measurement system made by Princeton Applied Research Company. The specimen was immersed in the 3.5% NaCl solution for 30 minutes before testing in order to reach a steady state. The exposed area of the specimen was 1cm^2. The specimen was slowly scanned (positively) at a rate of 1mv/second from 250mv below the open circuit corrosion potential to the point where the

corrosion current density reached 1×10^6 nA/cm^2. Then, the specimen was negatively polarized to about –0.4 V in order to obtain the protection potential of the oxide film. The polarization curve is a plot of potential versus log current density and can be divided into three regions: passive region, transpassive region and repassive region. The parameters of corrosion potential (E_{corr}), cirtical pitting potential (E_c), protection potential (E_p), and passive current density (I_p) characterize the polarization behavior. The corrosion current was obtained by extending the Tafel region of the cathodic portion of the polarization curves to the rest potential.

IV. EXPERMENTAL RESULTS AND DISCUSSION

A. SIMS Results

A.1 The Relationship of Concentration with Distance from the Metal Surface

The SIMS results for oxide layers formed at room temperature, 200°C and 400°C vacuum annealing treatments are shown in Fig 19, 20 and 21 respectively. The intensities in Fig. 19 ~ 21 generally represents concentrations in the specimens. Kerber and Tverberg[48] point out when a "clean" metallic sample is exposed to the atmosphere, an oxide film forms instantaneously. At the same time, it will absorb hydrocarbons and carbon oxides as well as water vapor on its surface. Therefore, the surface of the specimen typically shows 10~20% carbon and 30~50% oxygen. A freshly cleaned metallic surface is very reactive and adsorbs water vapor and atmospheric contaminants. Hence, the oxide layer formed on the metal surface in these experiments would comprise two parts: a hydroxygen and hydrocarbons layer and a metallic oxide layer. It is assumed that the actual oxide film surface exists at the position where the oxygen content reaches its maximum in the oxide film. Usually, according to the chemical composition of the specimens, the oxide layer on the surface of 316L stainless steel is composed of $(FeCr_2)_2O_3$. Therefore, the chemical compositions of the oxide film at different depths can be estimated from Fig. 19 ~ 21 assuming the bulk concentration is that given in Table 3.

For one series of polished specimens, the oxide layer on the surface of the metal was formed at room temperature. SIMS analysis shows that the maximum oxygen content in the specimen occurs at a depth of 20 Å. The oxygen content drops to the nearly same value as that of the bulk at a distance from the surface of the specimen of about 60 Å.

According to the suggestion of Kerber and Tverberg [48], it is assumed that the layer at less than 20 Å depth is a hydroxygen and hydrocarbon layer. The change of silicon and chromium with distance from the surface of the specimen shows the same trend as oxygen. In the oxide layer, the maximum contents of Cr and Si are about 36% and 2.2% respectively, and the content of iron is lower than that of the bulk. As the distance from the surface increases, the iron content increases, reaching its bulk value at about 50 Å. Nickel exhibits the same tendency as iron.

For the 200°C specimen, oxygen reaches its maximum value at 25 Å and reaches the bulk value at about 100 Å. Si and Cr exhibit the same tendency as oxygen. The maximum values for Cr and Si are 29% and 3% respectively at a depth of 25 Å. For the 400°C specimen, the oxygen reaches its maximum concentration at a depth of 25 Å, and reaches the bulk concentration at a depth of about 120 Å. The maximum value for Cr and Si are about 34% and 5% respectively.

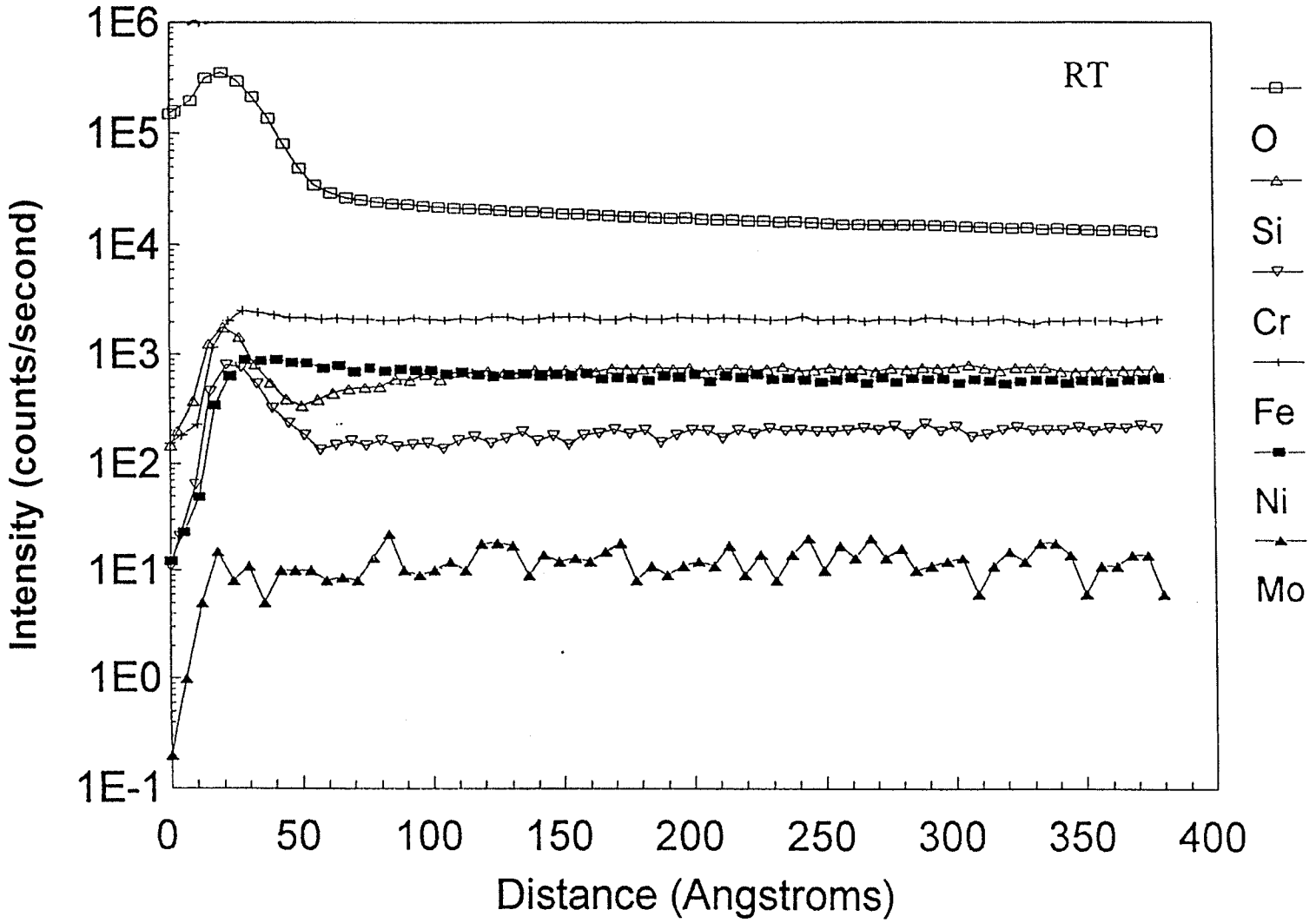

Fig. 19 SIMS Result for Oxide Layer Formed on Type 316L Stainless Steel at Room Temperature

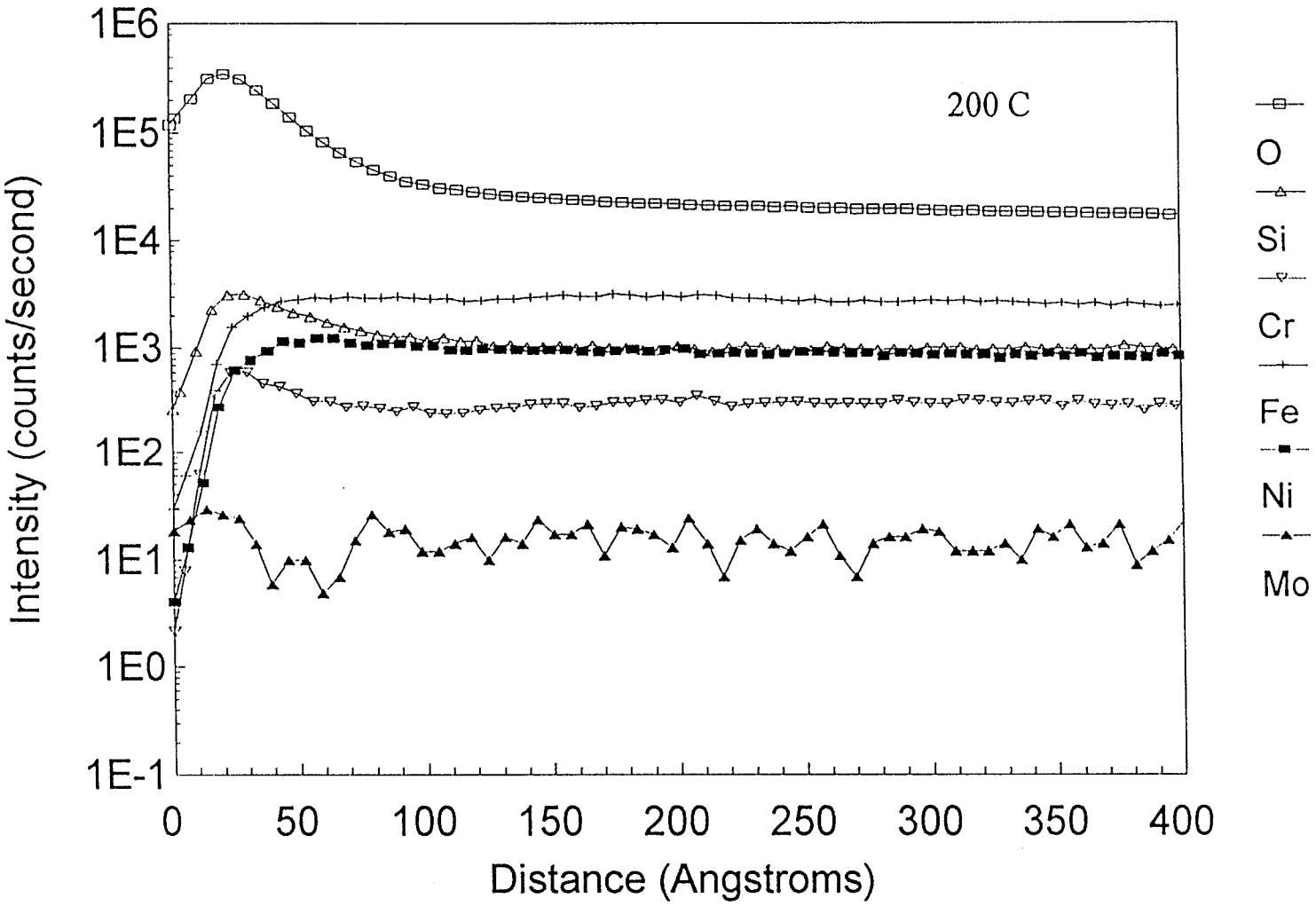

Fig. 20 SIMS Result for Oxide Layer Formed on Type 316L Stainless Steel at 200°C, Vacuum Annealing, 90min

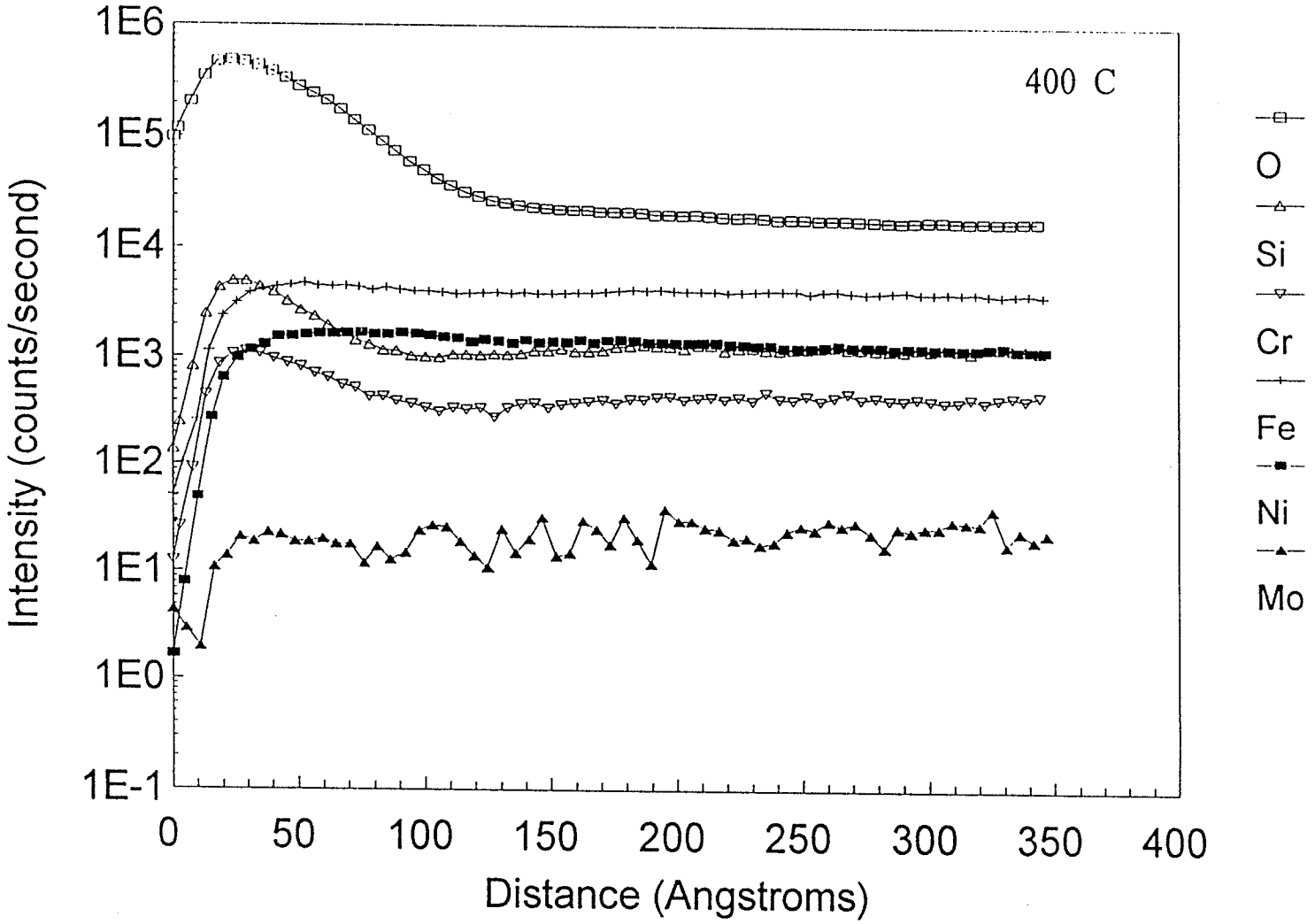

Fig. 21 SIMS Result for Oxide Layer Formed on Type 316L Stainless Steel at 400°C, Vacuum Annealing, 90min

A.1.1 The Relationship of Oxygen Concentration with Distance from the Surface of the Metal

Fig. 22 shows the relationship of oxygen content with distance from the metal surface. The results from Fig. 19 ~ 21 have been normalized to yield the same bulk intensities. As the temperature of oxide formation increases, the oxygen diffuses further into the specimen. For 400°C, the distance of the oxygen diffusion is 120 Å, for 200°C 80μm, and for room temperature 50 Å.

If x is the distance from the metal surface, a is the activity of the reactant, n is the concentration of reactants (cation vacancies and positive holes) in the oxide, ν is its mobility, and D the diffusion coefficient, then the flux of reactant (number crossing a unit area per second) can be expressed by:

$$J = -D\frac{da}{dx} - nF\nu \cdots\cdots (48)$$

where F is the electrostatic field in the oxide. Often, the concentration is used in this equation but since Fig. 19 ~ 21 clearly show "uphill" diffusion, the correct unit of activity must be used.

If the oxide layer is sufficiently thick, the whole oxide film can be assumed as electrically neutral except in narrow regions near the two interfaces. Therefore, the flux of reactant depends only on the activity gradient and the diffusion coefficient that are functions of the reaction temperature. Therefore, as the temperature increases, the flux of reactants will increase.

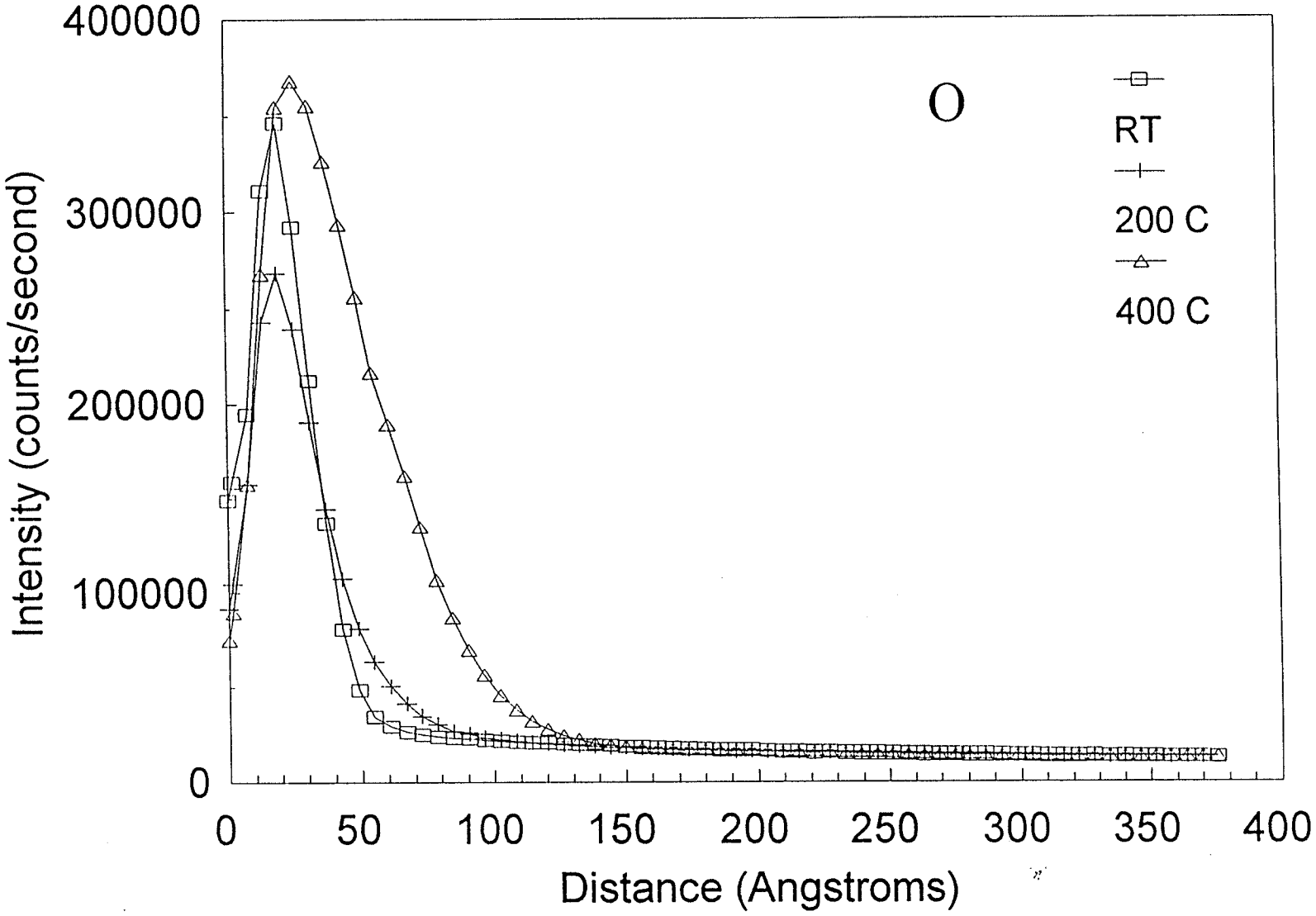

Fig. 22 The Relationship of Oxygen Content with Distance from the Metal Surface

For the specimen reacted at room temperature, the temperature is low, so the flux of reactants is limited. Therefore, just a thin oxide film is formed on the surface of the specimen. This film provides initial protection for the metal or alloy. However, this oxide layer is rather thin so that it may not offer optimum protection for the alloy. In order to increase the corrosion resistance of the specimen, a slightly thicker oxide film may be beneficial to form a barrier to keep the corrosive solution from diffusing to the metal/oxide interface.

When the specimen is annealed in the vacuum system above room temperature, the metal will dissociate into cations and electrons at the metal/oxide interface. Meanwhile, oxygen will be ionized into anions due to the electrons passing through it at the oxide/atmosphere interface. Between the metal/oxide interface and oxide/atmosphere interface, there exists the activity gradient of the reactants. According to equation (48), these reactants diffuse through the oxide layer and react with anions. Metal cations and electrons will diffuse outwardly to the oxide/atmosphere interface since the activity of these ions is higher at the oxide/metal interface than that at the oxide/atmosphere interface. Nevertheless, oxygen atoms and ions will diffuse inwardly since the activity of these reactants is lower at the oxide/metal interface than that at the oxide/atmosphere interface. When the oxygen anions and metal cations meet in the oxide growth zone, more oxide forms. In this way, the thickness of the oxide film increases, and the rate of growth is controlled by the diffusion of the reactants through the oxide lattice. SIMS analysis results show that the higher the temperature, the further the oxygen diffusion distance. Due to the radii of metal ions being smaller than that of oxygen ions, metal ions

have a higher mobility than oxygen atoms/ions during the process of diffusion through the oxide film. Therefore, the oxide growth occurs nearer the oxide/atmosphere interface than the metal/oxide interface.

A.1.2 The Relationship of Silicon Content with Distance from the Metal Surface

The correlation of silicon content with distance from the metal surface is indicated in Fig. 23 where the bulk intensities have again been normalized. As the temperature increases, the content of silicon increases in the oxide layer. For the room temperature specimen, when the distance is 50 Å, there exists a silicon depletion zone just beneath the surface of the oxide layer. The silicon from this zone has diffused towards the surface of the metal to form a higher concentration of silicon. However, for the 200°C and 400°C specimens, there are no obviously silicon depletion zones as shown in Fig. 23. The origin of the higher Si concentrations in the oxide films of the 200°C and 400°C specimens is not clear.

Szklarska[15] suggested that silicon and its compounds exert a detrimental effect on the pitting resistance of the materials if segregated at the grain boundaries or present in the form of inclusions in the materials. In addition, silicon and its compounds will damage the continuity of the oxide film formed on the surface of the materials. The higher the content of silicon in the oxide layer, the less the corrosion resistance of the oxide layer.

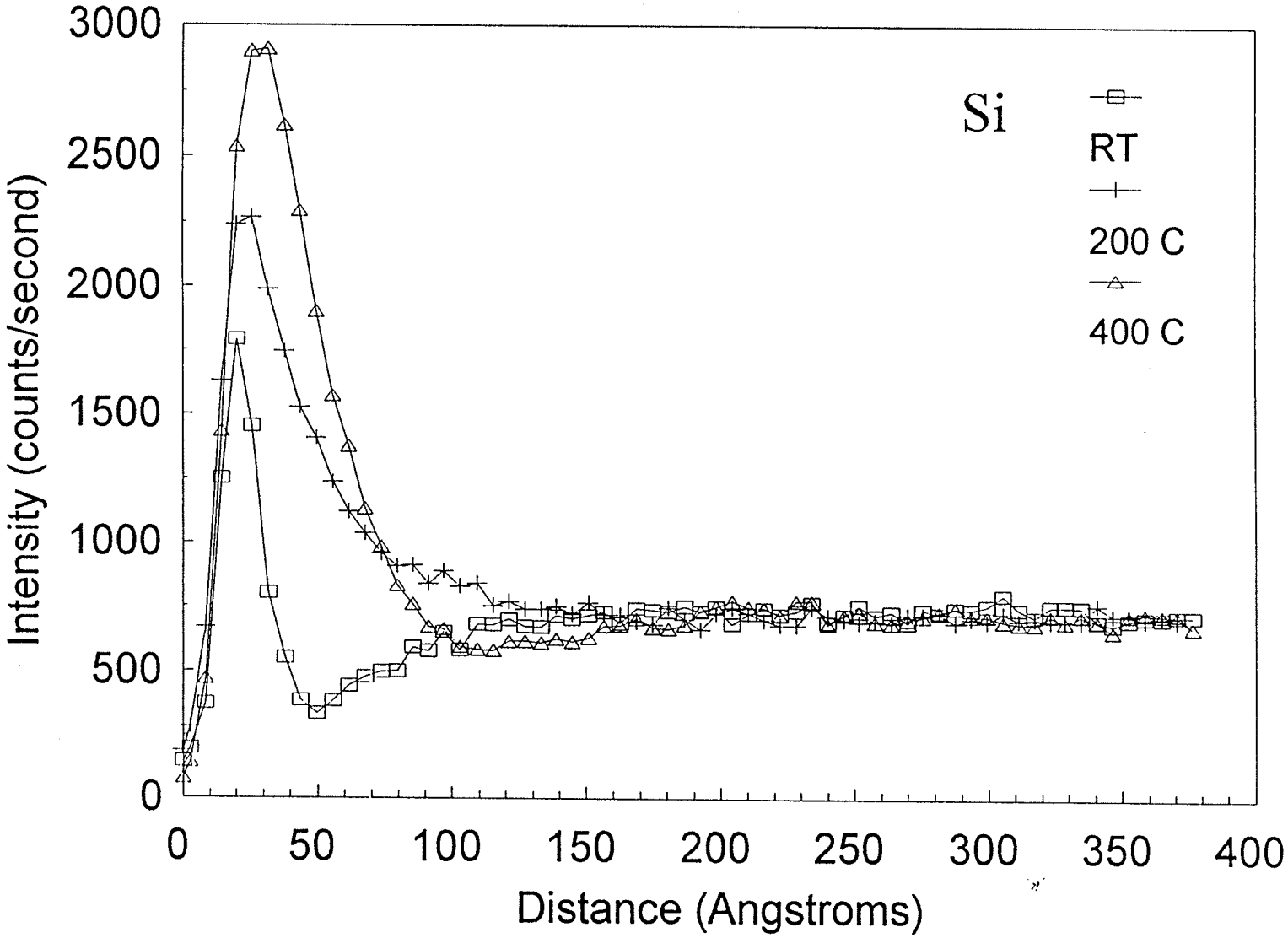

Fig. 23 The Relationship of Silicon Content with Distance from the Metal Surface

A.1.3 The Relationship of Chromium Content with Distance from the Metal Surface

Fig. 24 shows the relationship of Cr content with distance from the metal surface. Within the first 30 Å, Cr content of the room temperature specimen is higher than that of specimens vacuum annealed at 400°C and 200°C. Usually, the corrosion resistance of stainless steel is attributed to the Cr-rich oxide film formed on the surface. Therefore, a high content of chromium in the oxide film will improve the corrosion resistance of the oxide film. However, too high an enrichment of chromium in the oxide layer will result in a chromium depletion zone in the region beneath the oxide layer. Cr for the enriched layer comes from the zone immediately adjacent to the layer and at low temperature the diffusion rate of Cr from the bulk is not sufficient to replenish the depleted zone. The existence of a chromium depletion zone will decrease the corrosion resistance of the oxide layer. For the room temperature specimen, an obvious chromium depletion zone approximately 150 Å in length can be seen from Fig. 24, but for the 200°C and 400°C specimens a chromium depletion zone is not evident.

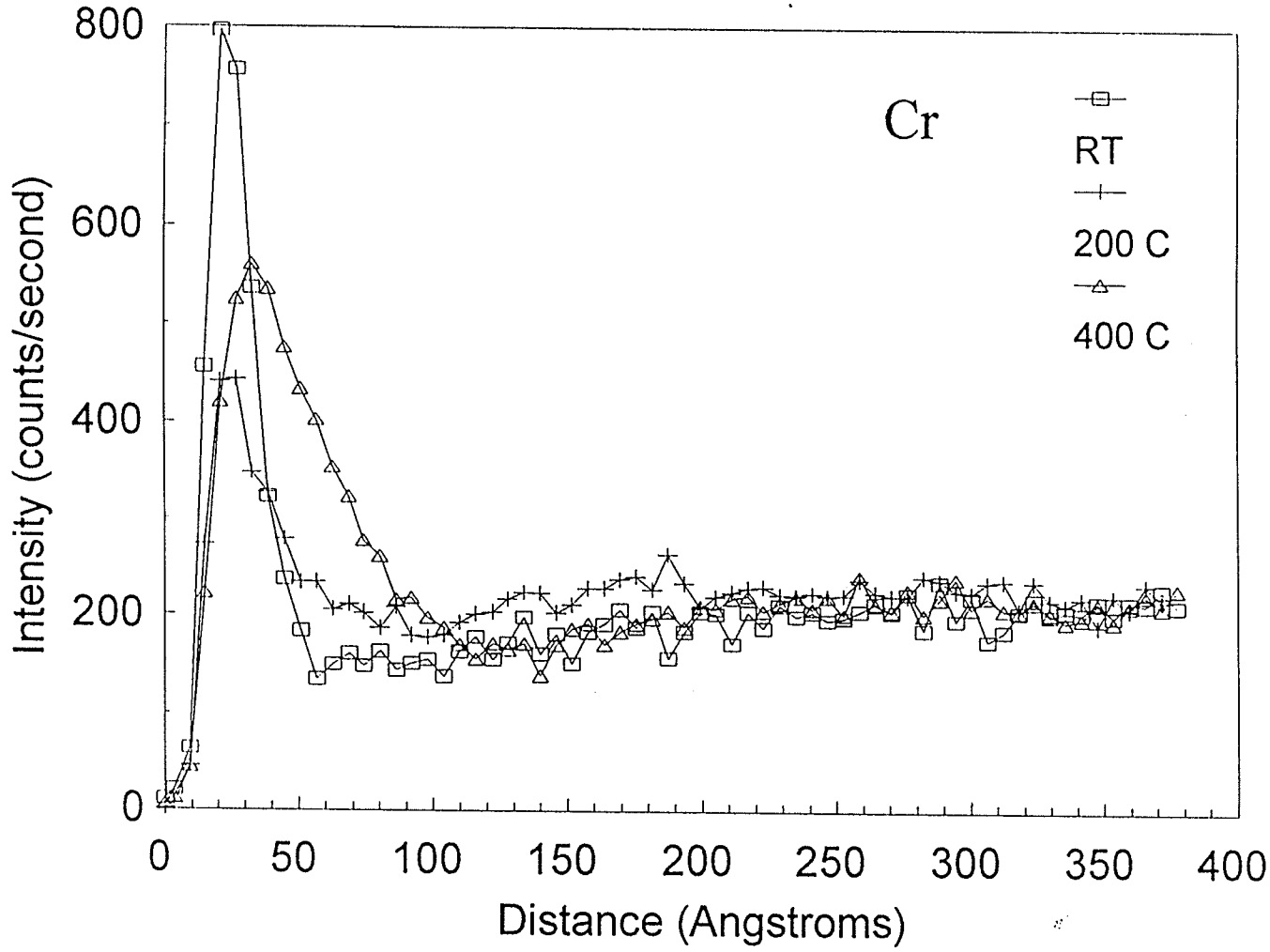

Fig. 24 The Relationship of Cr Content with Distance from the Metal Surface

A.1.4 The Relationship of Iron Content with Distance from the Metal Surface

The change of iron content with distance from the metal surface is given in Fig. 25. At the surface of the oxide layer, the iron content is very low compared to the bulk. However, as the distance increases, the iron content rises quickly essentially reaching its bulk value at depths of about 50 Å for all the specimens.

The concentration gradient of iron in the oxide film will likely cause the diffusion of iron from the bulk to the metal surface and this iron will react with oxygen to form oxides. Unfortunately, an oxide layer enriched in iron offer little corrosion resistance for the specimen.

A.1.5 The Relationship of Nickel Content and Molybdenum Content with Distance from the Metal Surface

The correlation of nickel content with distance is shown in Fig. 26. For distances less than 50 Å, the Ni content of the room temperature sample is the highest, followed by the 200°C sample with the 400°C sample being the lowest. At distances greater than 50 Å, the Ni contents of all three samples are similar.

Nickel promotes formation of the passive oxide film in a reducing environment. Some investigations[80,92] have shown that nickel is beneficial in extending the range of stable passivity and may improve the corrosion resistance of the material. However, Fig. 26 shows that the Ni content remains above the bulk value to a distance of about 300 Å, the Cr content remains below the bulk value up to about 300 Å as shown in Fig. 24. Since the increased Ni content near the metal surface results in a decreased Cr content, the corrosion resistance may not be improved by the increased Ni content.

The changing of Mo content with distance from the metal surface is shown in Fig. 27. For the room temperature and 400°C specimens, the Mo content is low while that of the 200°C specimen is considerably higher. While the presence of Mo is known to increase the pitting corrosion resistance of austenitic stainless steels, its influence on the character of the oxide film is unclear. Montemor et al[84] suggested that the presence of Mo increased the amount of Cr in the oxide film but had no influence effect on the oxide thickness. Mathieu et al[87] suggested that the presence of Mo in the metal/oxide interface could decrease the activity of the metallic ion or act as a diffusion barrier for the Fe and Cr ions in the oxide.

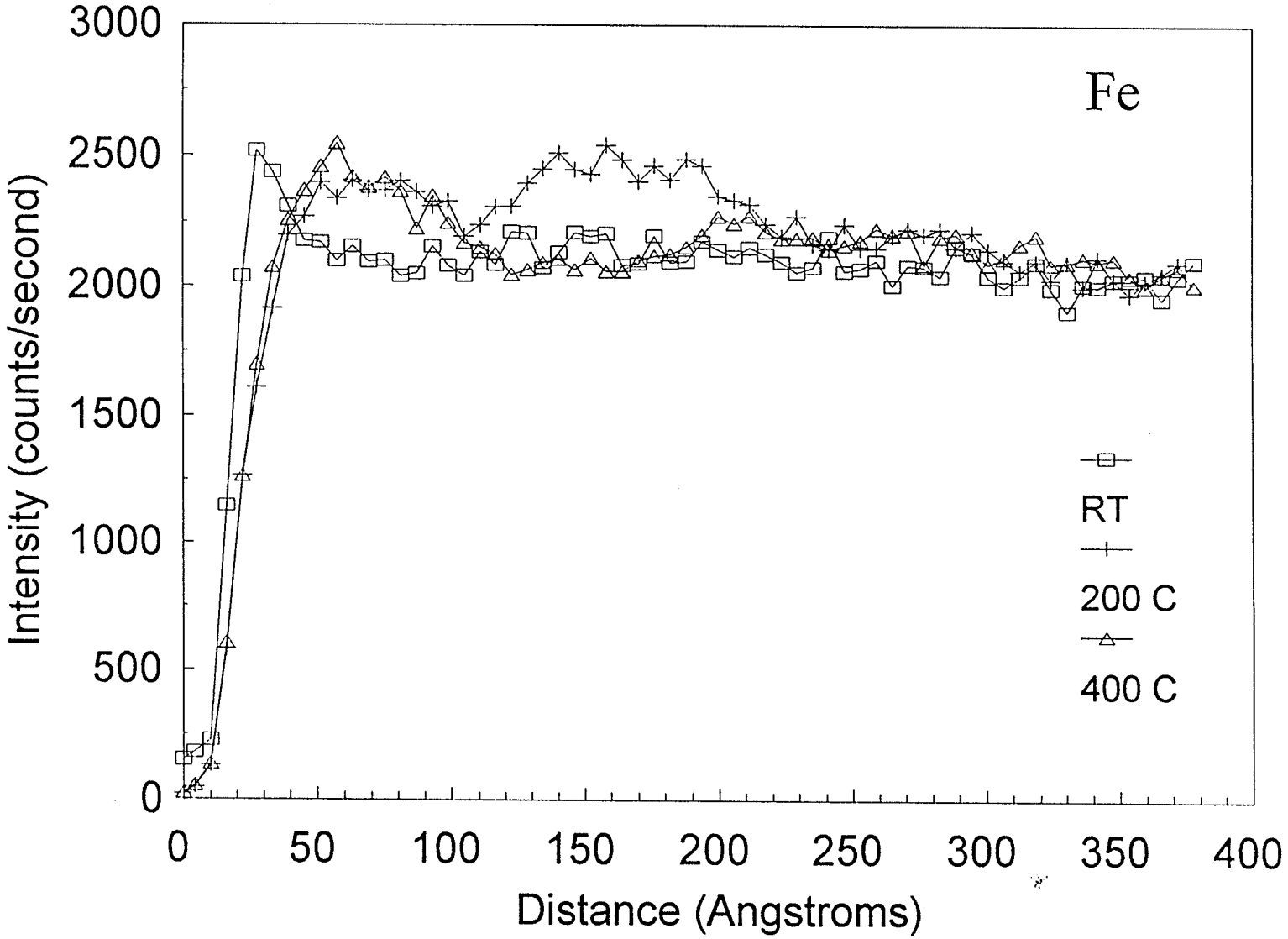

Fig. 25 **The Relationship of iron Content with Distance from the Metal Surface**

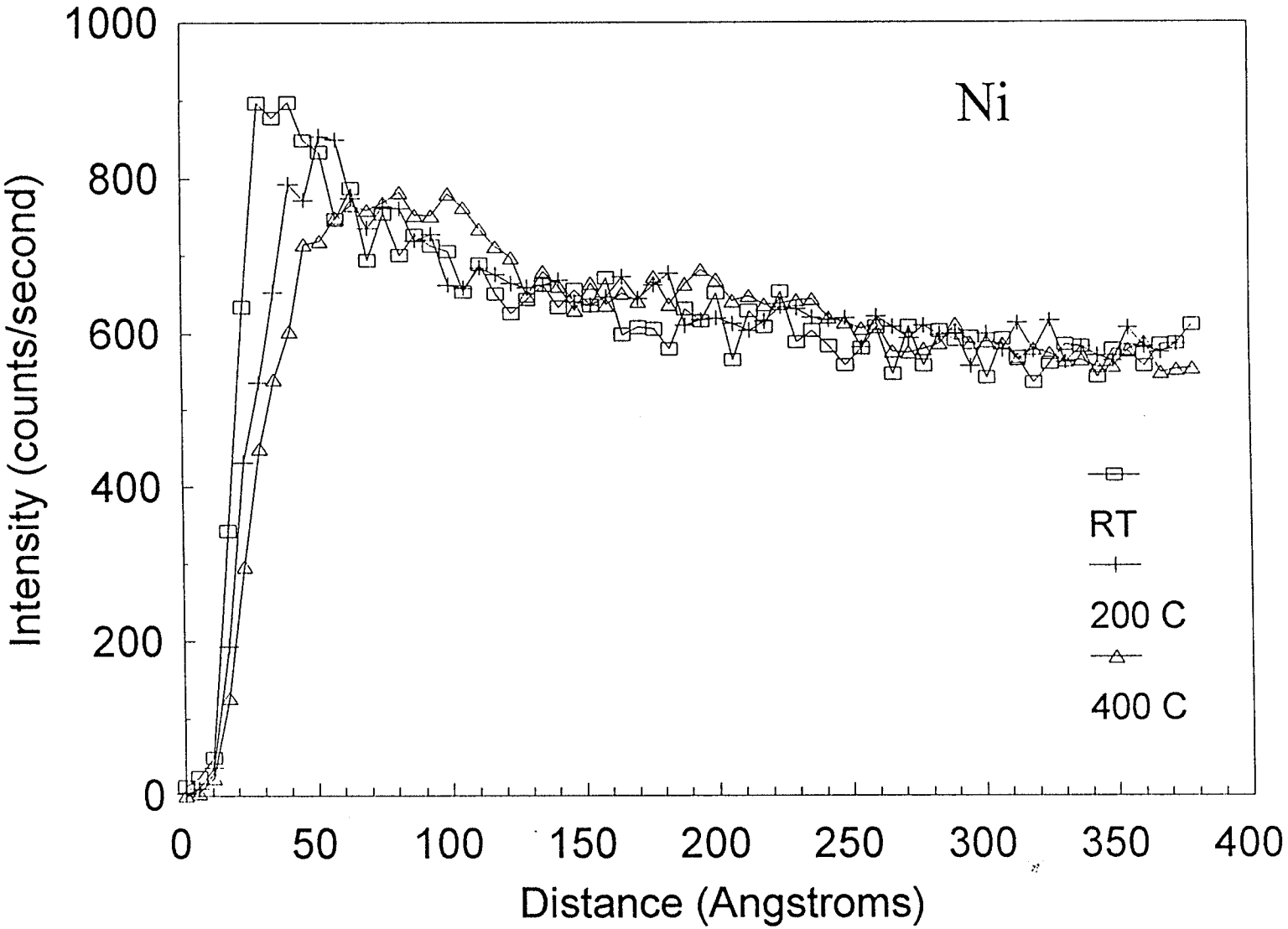

Fig. 26 **The Relationship of Nickel Content with Distance from the Metal Surface**

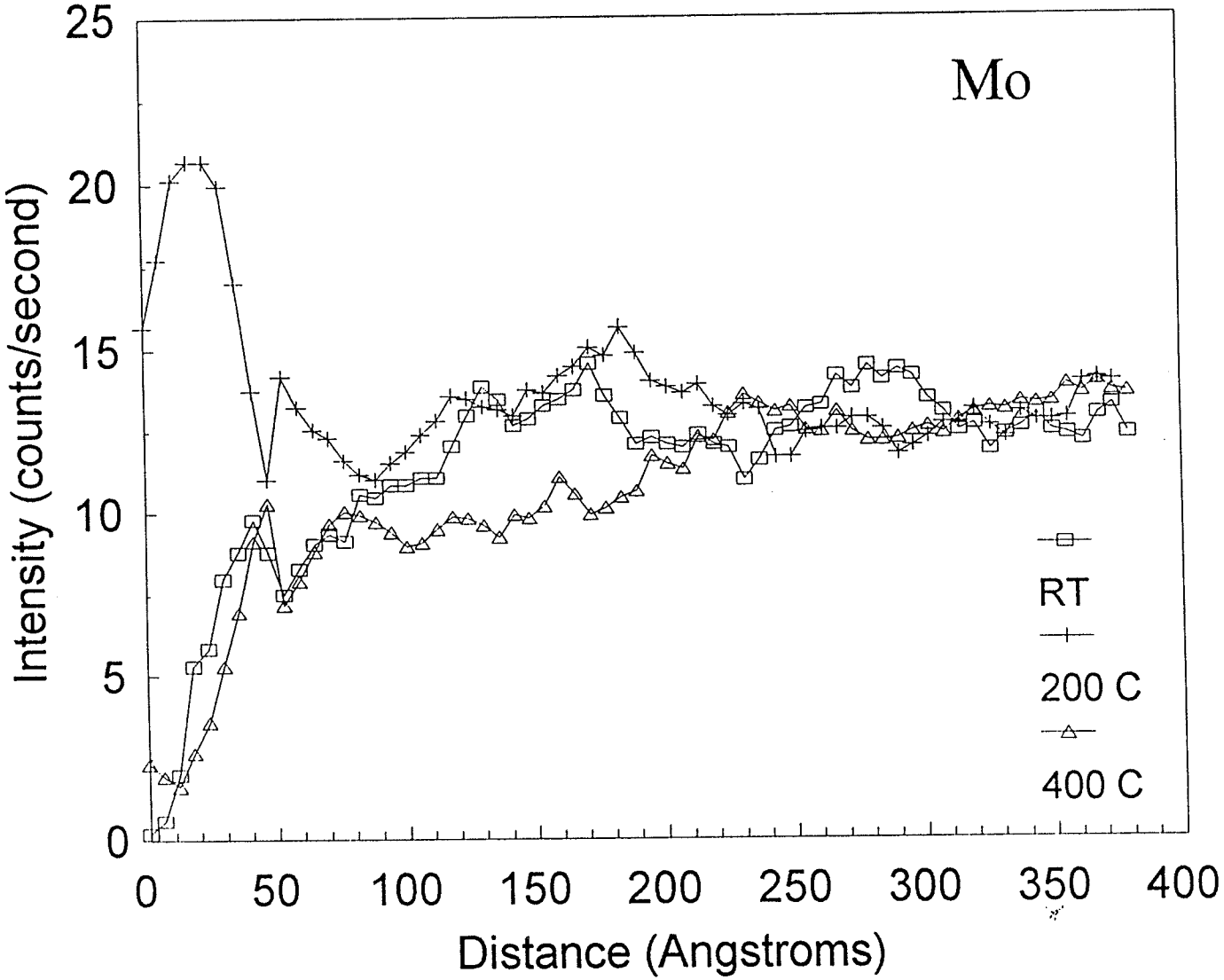

Fig. 27 The changing of Mo Content with Distance from the Metal Surface

A.1.6 The Variation of Me/O Ratio with Distance from the Metal Surface

The ratios of Cr/O, Si/O and Fe/O with distance from the metal surface are shown in Fig. 28 ~ 30. Fig. 28 shows that as the distance increases from the metal surface, the ratio of Cr/O increases. At a distance of 20 Å, the Cr/O ratio remains constant for a distance which represents the thickness of a stoichiometric oxide layer. For the room temperature and 200°C specimens, the thickness of the oxide layers is 5 ~ 10 μm, while the thickness of the oxide layer for the 400°C specimen is 50 Å. Equation (48) can explain this tendency. The diffusion of the reactants is controlled by temperature and the activity gradient in the oxide layer. For the room temperature and 200°C specimens, the temperature is low and comparatively a few chromium ions can diffuse from the bulk to the surface of the metal. Also, oxygen cannot diffuse long distances to meet metal ions as Fig. 22 shows. Therefore, just a thin oxide layer forms on the surface of the metal. As the temperature is increased to 400°C, the diffusion rates of the chromium and oxygen ions increase and a thicker oxide layer results.

The ratios of Si/O with distance are similar to those for Cr/O as shown in Fig. 29 with a stoichiometric oxide forming at a distance of about 20 Å from the surface. However, for the 200°C specimen, only a slight SiO_2 oxide forms. For the room temperature specimen, the thickness of SiO_2 is nearly 10 Å and for the 400°C specimen, 50 Å. The Fe/O ratio given in Fig. 30 shows that a stoichiometric Fe oxide does not form.

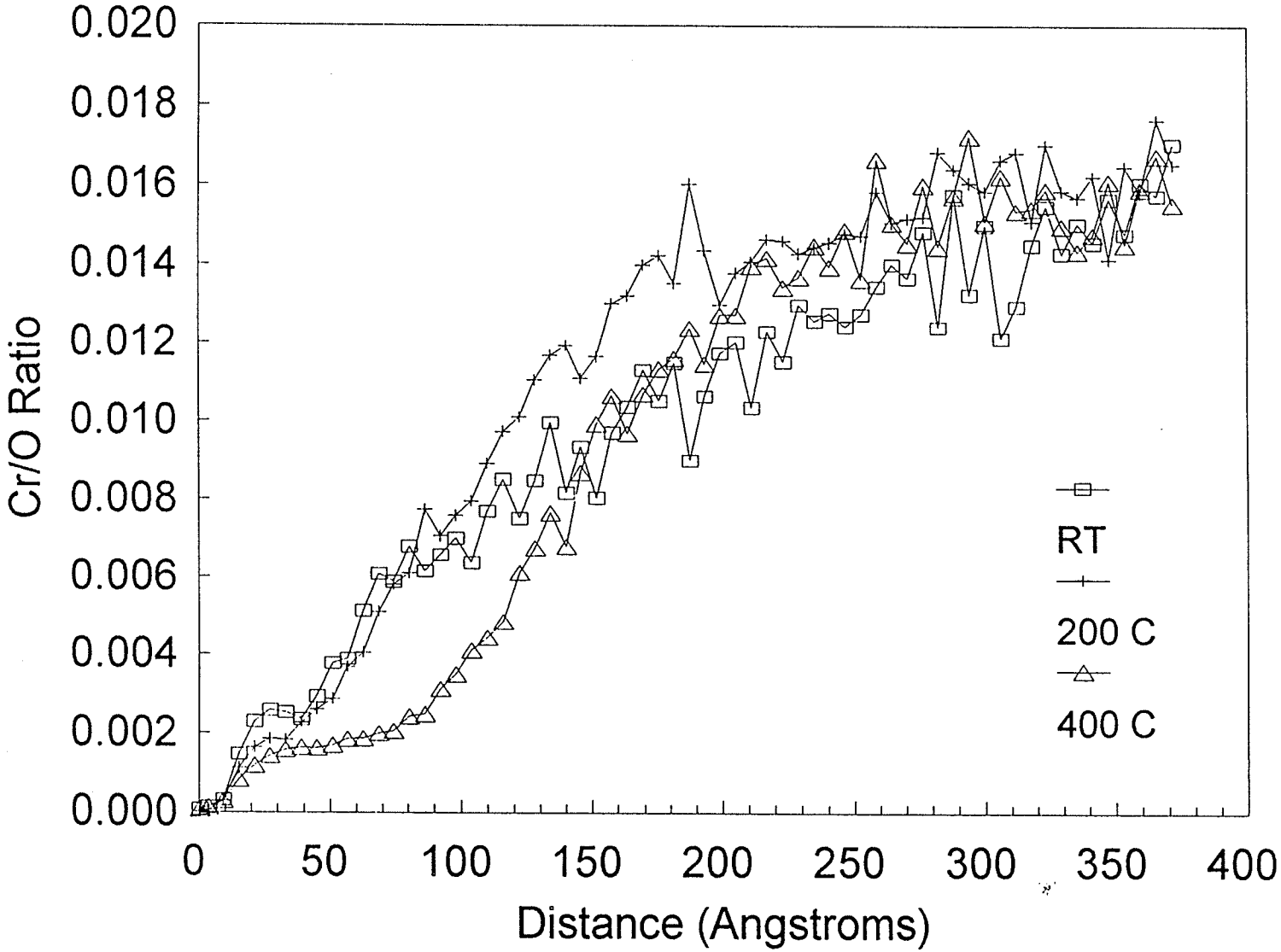

Fig. 28 The Ratio of Cr/O with Distance from the Metal Surface

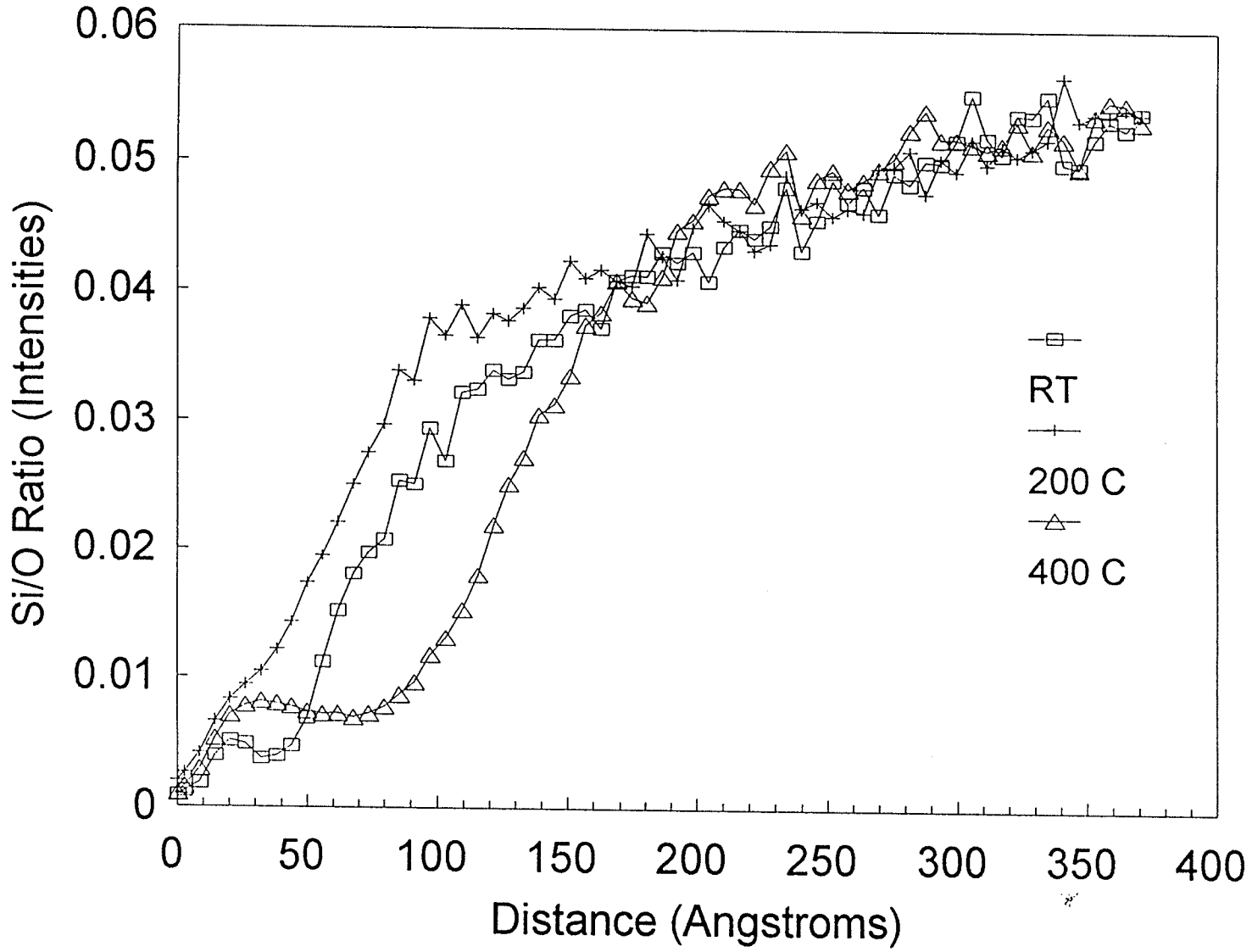

Fig. 29 The Ratio of Si/O with Distance from the Metal Surface

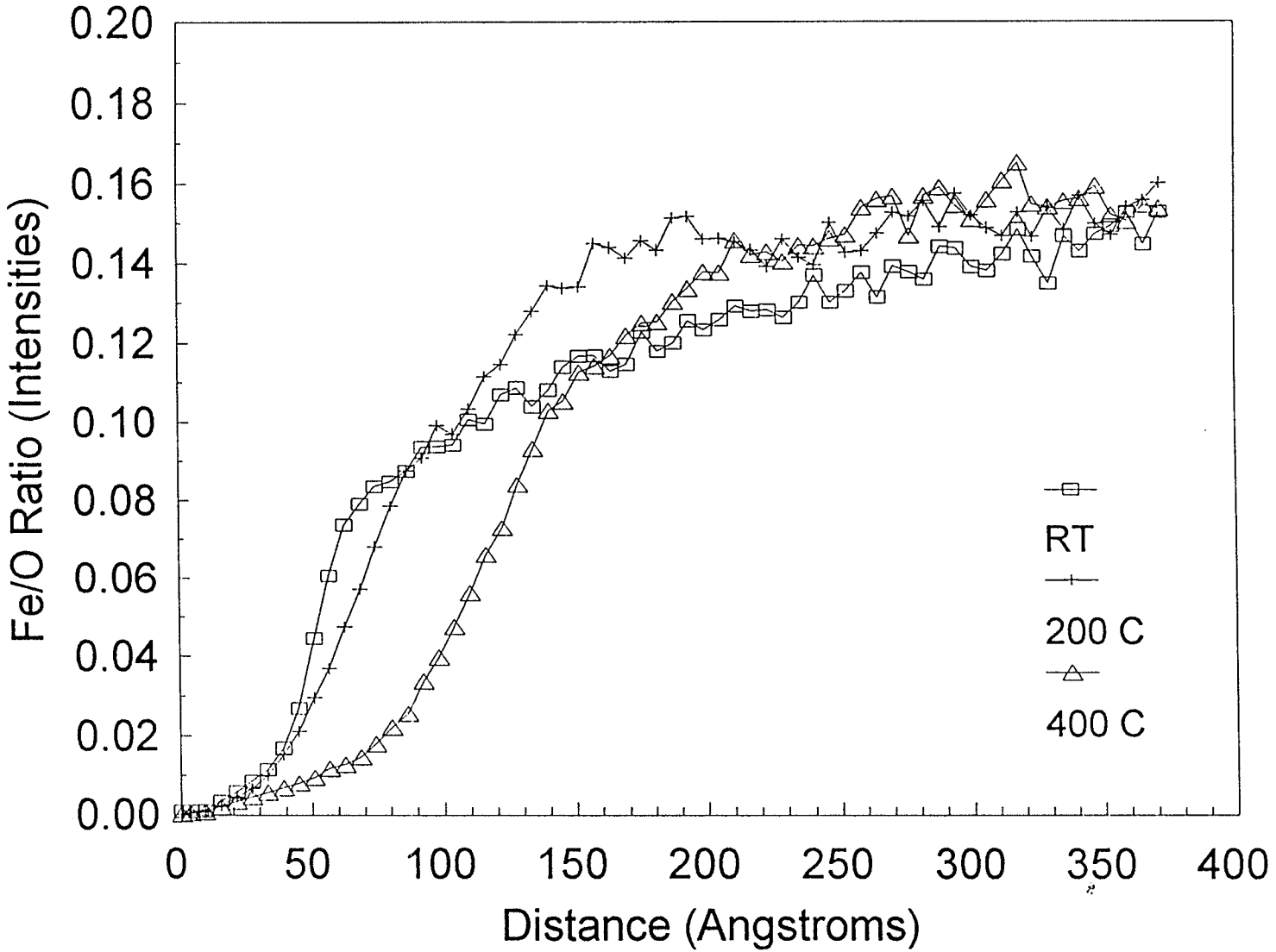

Fig. 30 The Ratio of Fe/O with Distance from the Metal Surface

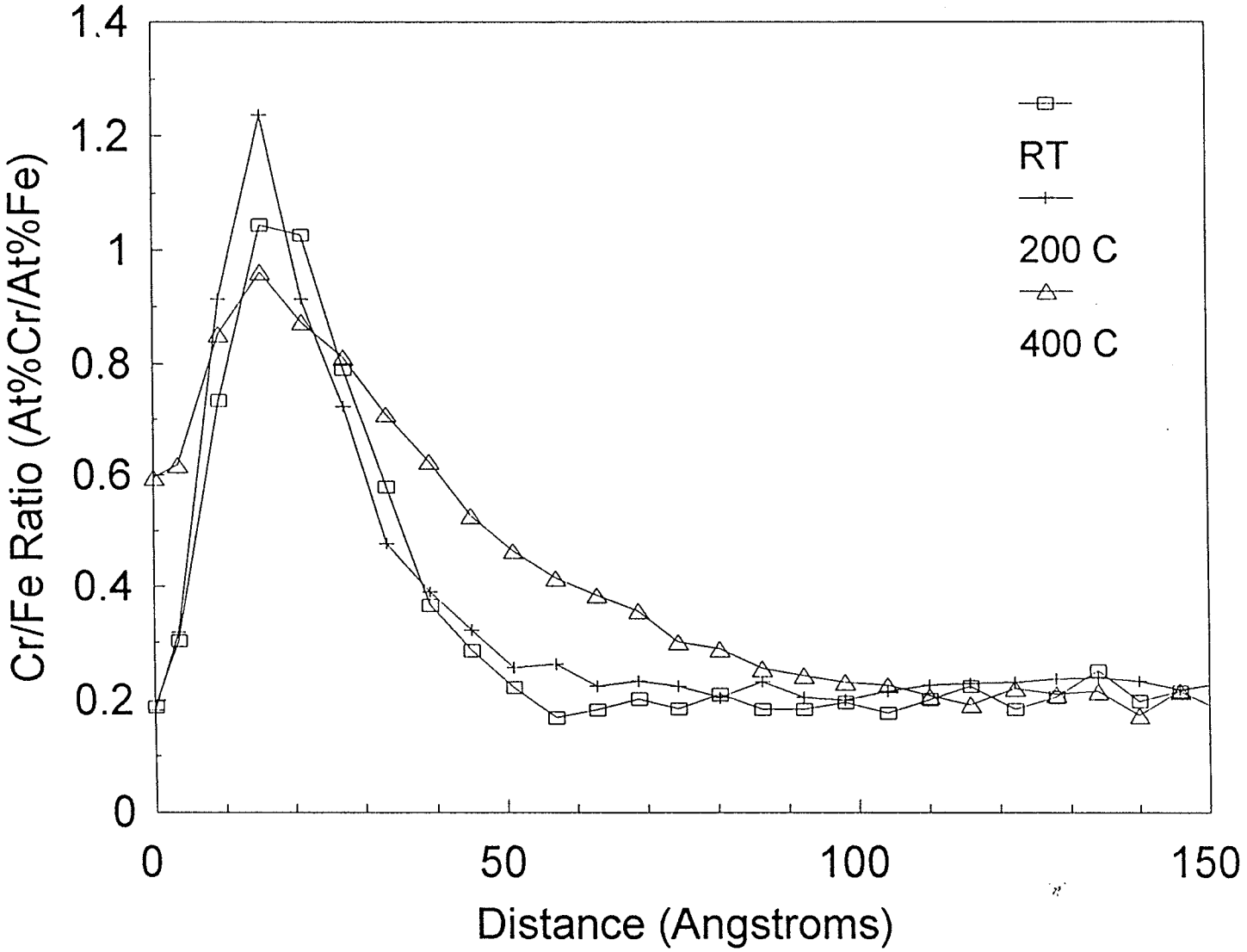

Fig. 31 The Ratio of Cr/Fe with Distance from the Metal Surface

A.1.7 The Cr/Fe Ratio

Kerber and Tverberg[48] have indicated that a high Cr/Fe ratio is beneficial to the corrosion resistance of type 316L stainless steel. The Cr/Fe ratios for the specimens with the oxide film formed under different condition are shown is Fig. 31. At a distance of 20 Å from the surface, the Cr/Fe ratios for the room temperature, the 200°C and the 400°C specimens are all above or nearly equal to 1. This means that at the surface of the oxide layer, the amount of Cr_2O_3 equals or exceeds the amount of Fe_2O_3. This is beneficial to the corrosion resistance of the materials. For the 400°C specimens, the elevated Cr/Fe ratio curves extends further into the materials than that for the room temperature and the 200°C specimens.

Since the free energies of formation of Cr_2O_3 and Fe_2O_3 are -250.0 and -176.8 kcal/mole respectively, Cr_2O_3 is more stable than Fe_2O_3. Therefore, the selective oxidation of chromium will be favored by a higher diving forces than the oxidation of iron and the chromium surface enrichment should be further promoted of oxidation occurs in a vacuum at low oxygen concentrations. At low temperature (at or below 200 °C), the oxide film comprises a mixture of chromium and iron oxides with the amount of chromium oxide exceeding that of iron oxide. This is beneficial to the corrosion resistance of the oxide film. However, as the temperature increases to 400°C, the diffusion rate of iron in the oxide layer increases. Therefore, more iron diffuses from the bulk to the surface of the oxide layer to form iron oxide, thus reducing the amount of chromium oxide and this could reduce the corrosion resistance of the oxide layer.

A.1.8 Summary of the Effect of Different Oxidation Treatments

The Cr/O ratio given in Fig. 28 shows that a stoichiometric oxide forms on all the specimens. The room temperature and 200°C specimens are very similar with the stoichiometric oxide having a thickness of 20 Å. The 400°C specimen exhibits an oxide about 50 Å in thickness. The oxide layers for the room temperature and 200°C specimens are very similar suggesting that little additional diffusion occurs at 200°C compared to room temperature. The 400°C specimen exhibits larger diffusion gradients of all the elements as would be expected because of the increased diffusion rate at elevated temperatures.

Vacuum annealing at elevated temperature resulted in the formation of an oxide film on type 316L stainless steel which contains stoichiometric Cr_2O_3 and no stoichiometric Fe_2O_3. This should result in improved corrosion resistance for the stainless steel. However, the existence of stoichiometric SiO_2 in the oxide film may reduce corrosion protection for the underlying stainless steel.

B. Electrochemical Polarization Test Results

B.1 Effect of Surface Preparation on the Electrochemical Behavior of the Oxide Film Formed on 316L Stainless Steels

Electrochemical polarization studies are most often performed on specimens sanded to 600 grit. However, surface analysis using SIMS is best performed on polished specimens. Therefore, tests were conducted to determine the effect of surface finish on the electrochemical behavior. Polarization curves for the two different surface finishes are compared in Fig. 32. It is shown that the critical potential, E_c, of the mechanically polished specimen is nearly 200 mv higher than that of the sanded specimens. Electrode potential denotes the energy barrier that must be overcome when an atom transforms into an anion or vice-versa. Critical potential is defined as the potential above which pits will nucleate and develop in the material. A higher critical potential means that a higher energy barrier must be overcome before pits occur, and therefore the material has increased pitting resistance. Since mechanically polished specimens have higher critical potentials than sanded specimens, mechanical polishing can improve the pitting resistance of materials.

The protection potential or repassivation potentials for both the polished and sanded specimens are lower than their respective corrosion potentials which means that the repairing abilities of the oxide films formed on these specimens are not sufficiently good to automatically repair the oxide film in the areas where pits form. Therefore, once pits initiate they will continue to grow.

Often, pits nucleate from inclusions (sulfides, oxides, carbides, etc.) that break the continuity of the surface oxide film of the specimens. In addition, some local breakdowns

of the oxide film are responsible for the onset of the localized corrosion attack. Mechanical polishing smoothes the surface of the specimens to a greater degree than sanding and therefore promotes the formation of an integral oxide film on the surface which improves the pitting resistance of the specimens.

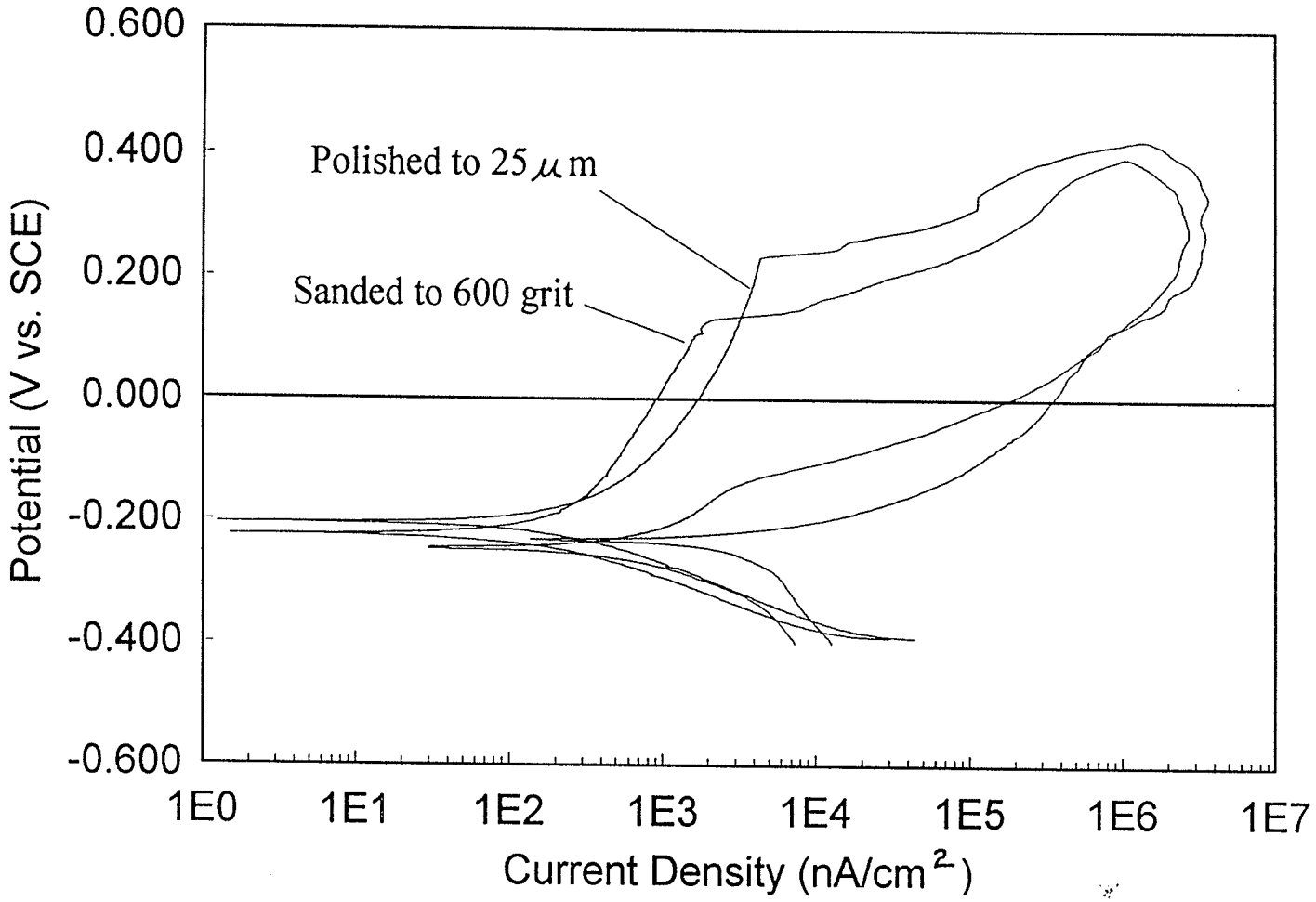

Fig. 32 Electrochemical Polarization curves for type 316L stainless steel after different surface finishes

B.2 Effect of Oxide Formation Temperature on Electrochemical Behavior of 316L Stainless Steel

Fig. 33 shows the polarization curves for specimens with oxide films formed at room temperature and vacuum annealing at 200°C for 90 min. To determine if annealing at 200°C had any effect on the electrochemical behavior, specimens were annealed at 200°C for 90 minutes, then sanded and polished at room temperature. Therefore, for these specimens the oxide film was formed at room temperature. The polarization curves in Fig. 33 are "composite" curves which contain average values of E_c, E_p and E_{rest} and I_p from several tests for each type of specimen. The corrosion potential, E_{corr} is the potential for zero net current, which means that the rate of the oxidation reaction is equal to the rate of the reduction reaction. E_{corr} therefore represents an equilibrium condition.

There are two reversible reactions occurring on the surface of the specimen when corrosion is occurring. One is metal/alloy dissolution, and the other is metal/alloy oxide formation. If the rate of dissolution is greater than that of oxide formation, the metal will dissolve and pits will form. If the oxide formation rate is greater than the dissolution rate, the oxide film will thicken and previously formed pits will be repassivated with the oxide film. Hence, these exists a potential called the protection potential or repassive potential, E_p. At potentials where $E_p<E<E_c$, previously nucleated pits will grow; on the other hand, at potentials where $E<E_p$ pits can not nucleate and pits previously nucleated will be repaired automatically. Therefore, the more positive the value of E_p, the higher the repairing ability of the oxide film.

In general, the difference between the critical potential and the protection potential is the factor used to evaluate the crevice corrosion resistance of the material. The smaller

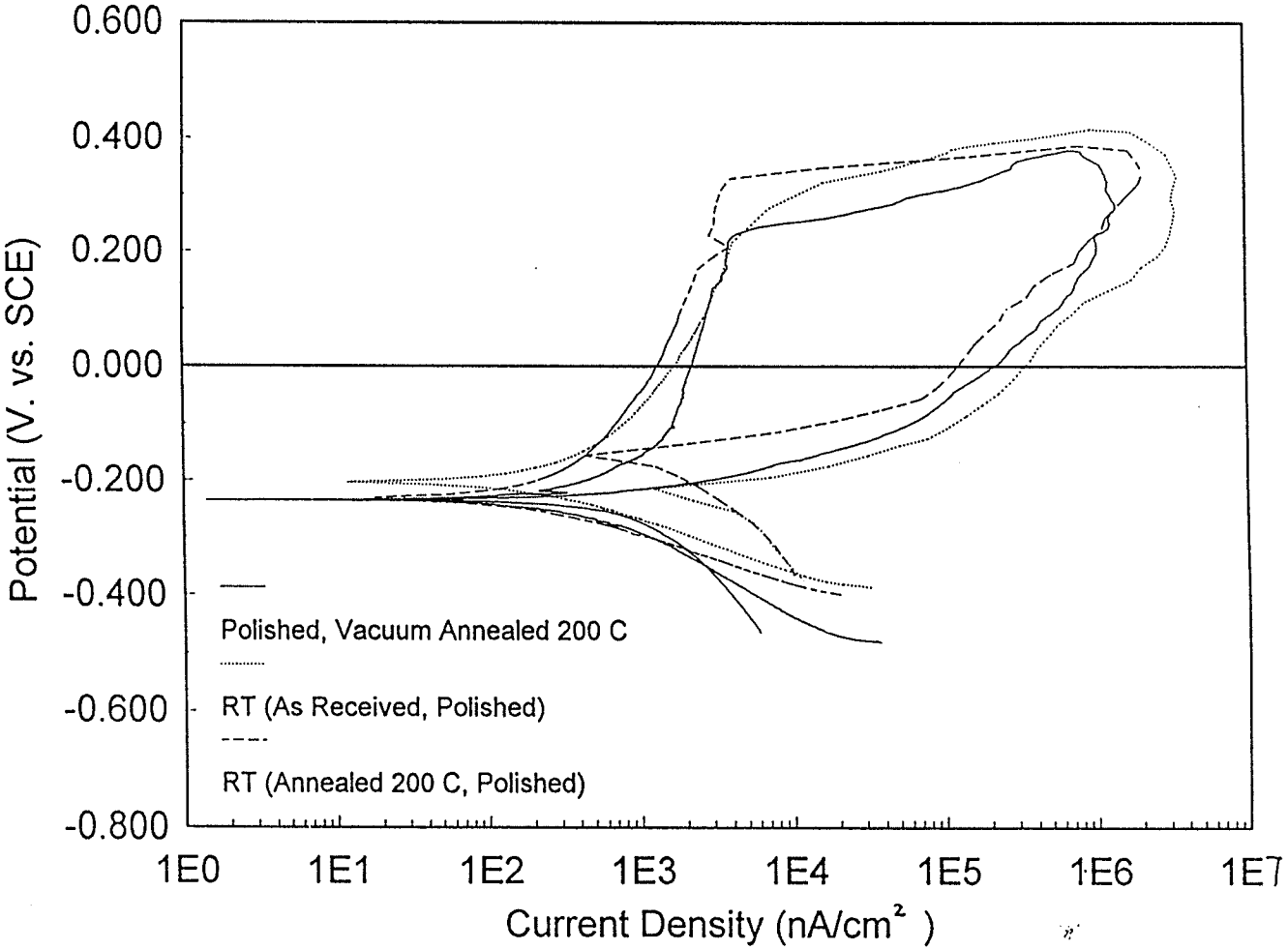

Fig 33 Electrochemical Polarization Curves for Specimens with Oxide Films Formed at Room Temperature and Vacuum Annealing at 200°C for 90 min.

the difference of these two potentials, the higher the crevice corrosion resistance of the material.

Fig. 33 shows that the electrochemical polarization curves for specimens with oxide films formed at 200°C and room temperature are nearly identical. They all have a passivation region with passive current densities of about 1000nA/cm^2. Moreover, their protection potentials are slightly higher than or equal to their rest potentials, which indicates that the oxide films have a modest ability for automatic repassivation and perhaps some crevice corrosion resistance.

The electrochemical polarization curves for 316L stainless steels with oxide films formed during vacuum annealing at temperatures from 300°C to 600°C are shown in Fig. 34. The polarization curves for specimens annealed at 500°C and above have no passivation range, which indicates that the oxide layers formed above 500°C have no protection for 316L stainless steel. The specimens with oxide layers formed at 300°C and 400°C exhibit a passivation range in the anodic polarization curve. Though the 400°C specimen has a slightly higher critical potential than the 300°C specimen, its oxide film tends to breaks down intermittently in the passivation region. Therefore, the oxide film formed at 400°C has no greater pitting corrosion resistance than that formed at 300°C. Further, the protection potentials of the alloys vacuumed annealed at 300°C and 400°C are also almost the same and are below the corrosion potentials. Therefore, the oxide layers formed at 300°C and 400°C have little crevice corrosion resistance.

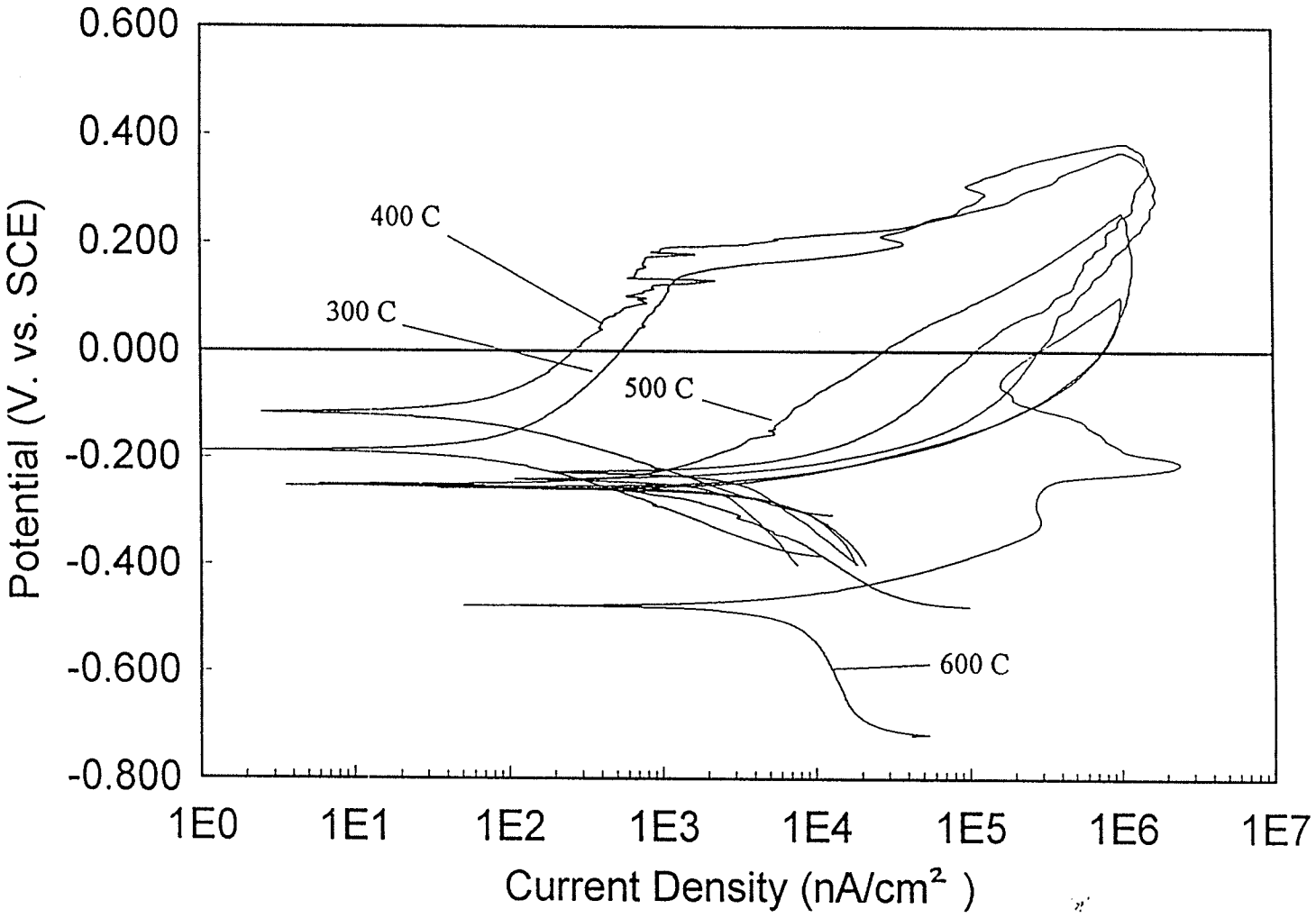

Fig. 34 Electrochemical Polarization Curves for Specimens with Oxide Films Formed During Vacuum Annealing at Temperature from 300°C to 600°C.

Comparing Fig. 33 with Fig. 34, as the oxidation temperature is increased from 200°C to 600°C, the crevice corrosion resistance is decreased. This conclusion is supported by the SIMS analyses. As the temperature of oxide formation was increased from room temperature to 200°C to 400°C, the silicon content (Fig. 23) and the Si/O ratio (Fig. 29) in the first 50 Å of the oxide layer increased while the Cr/O ratio (Fig. 28) decreased. For the 400°C specimen, a higher silicon content (Fig. 23) and lower Cr/O ratio (Fig. 28) exists in the first 80 Å of the oxide layer.

The corrosion current for a metal sample having a surface oxide layer is given by

$$I = \frac{E}{R + P_C + P_A} \cdots\cdots (49)$$

where

E is the potential,

I is the current passing through the oxide film,

R is the ohmic resistance of the oxide film,

P_C and P_A are the cathodic and anodic polarization resistances respectively.

For 316L stainless steel, chromium and iron are the two main elements which participate in oxidation. From the standpoint of electrical resistance, Cr_2O_3 is 10 Ω-cm, while Fe_2O_3 is 10^{-2} Ω-cm. Thus, Cr_2O_3 offers more corrosion resistance than Fe_2O_3 since the higher electrical resistance results in a higher corrosion resistance according to Equation (49). In addition, Cr_2O_3 forms early in most solutions, and therefore it is important for 316L stainless steel to possess high chromium contents. As a result, the corrosion resistance of stainless steel is primarily determined by its own chromium content and by the chemical composition of the oxide film formed on the alloys.

The ionic radius of Cr^{3+} is 0.65 Å while that of Fe^{3+} is 0.75 Å. This facilitates a preferential movement of Cr^{3+} ions into the surface of the alloy during oxidation and consequently a preferential formation of Cr_2O_3. In addition, the smaller radius of Cr^{3+} leads to the formation of an oxide with relatively smaller lattice parameters than ferric ions, which results in a high resistance to the diffusion of corrosive ions through its lattice. Hence, Cr_2O_3 has a higher corrosion resistance than does Fe_2O_3.

From the viewpoint of selective oxidation, the oxidation of chromium is driven by a higher energy than that of iron, since the free energies of formation of Cr_2O_3 are higher than that of Fe_2O_3, and thus Cr_2O_3 is more stable than Fe_2O_3. As a result, the oxide film of Cr_2O_3 plays an important role in protecting 316L stainless steels from corrosion. Therefore, a low Cr/O ratio in the oxide film is detrimental to the corrosion resistance of the specimen. Moreover, silicon existing on the surface of the oxide layer will damage the continuity of the oxide layer, so that detrimental chemical substances (eg. Cl^-) may diffuse through these discontinuities pits to the bulk of the materials and react with elements there to cause corrosion of the materials.

From equation (8a), the potentials symbolize the change of Gibbs free energy, which represents the tendency to transform in the equation. However, it is impossible to accurately predict the velocity of a reaction by considering only the change in free energy. In order to obtain information about the velocity of reactions, current intensity must be considered. In general, the corrosion rate can be deduced from the electrochemical polarization curves by extending the Tafel region of the cathodic curve to the corrosion potential. The current density at that intersection is the corrosion rate of that

specimen since the reduction rate (cathodic reaction rate) is equal to the oxidation rate (corrosion rate) at the corrosion potential.

Fig. 35 compares the effects of temperature of oxide formation and surface preparation on the corrosion rates of 316L stainless steel. The corrosion rates for specimens with oxide films formed above 500°C are much higher than for other treatments. The corrosion rate for 500°C is 0.4 mils per year (MPY*) and that of 600°C is more than 0.9 MPY. The corrosion rates for other treatments are very similar, in the range 0.04 to 0.2MPY. Therefore, if the temperature of formation of the oxide film is below 500°C, the corrosion rate of the specimen is independent of the temperature of oxide film formation. Also, the corrosion rates for sanded specimens and polished specimens are nearly the same which suggests that the surface preparation has little effect on the corrosion rate of the specimen.

The electrochemical polarization parameters for the specimens with different thermal annealing treatments are presented in Table 5 and the values of corrosion potential, E_{corr}, critical potential, E_c, and passivating potential, E_p, in Figs. 36 ~ 38. The time of thermal anneal was 90 min for each of these specimens. The bars in Fig. 36 ~ 38 indicate the range of values observed.

---

* 1 MPY = 0.001" per year corrosion rate

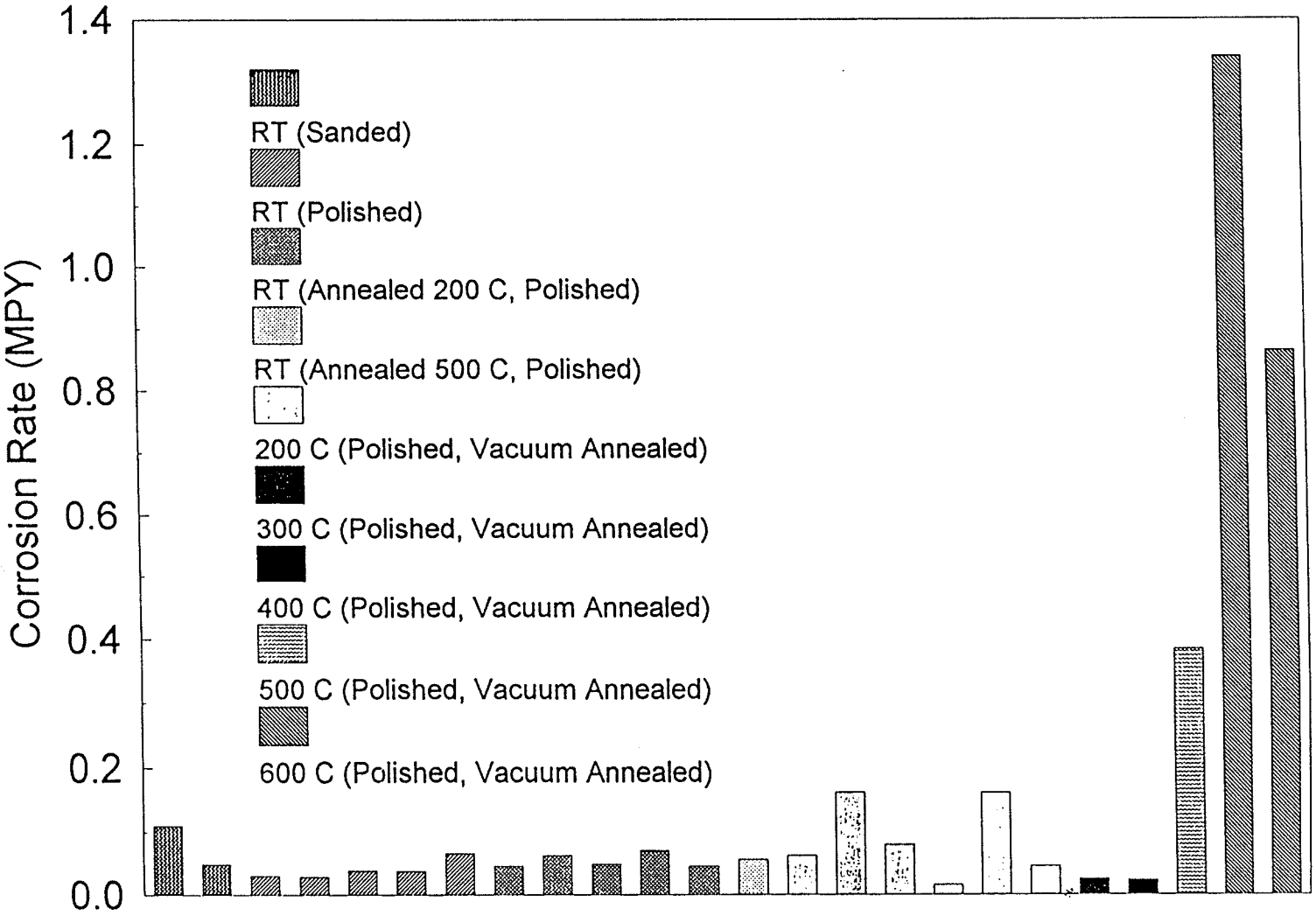

Fig. 35 Effects of Temperature of Oxide Formation and Surface Preparation on the Corrosion Rates of 316L Stainless Steel

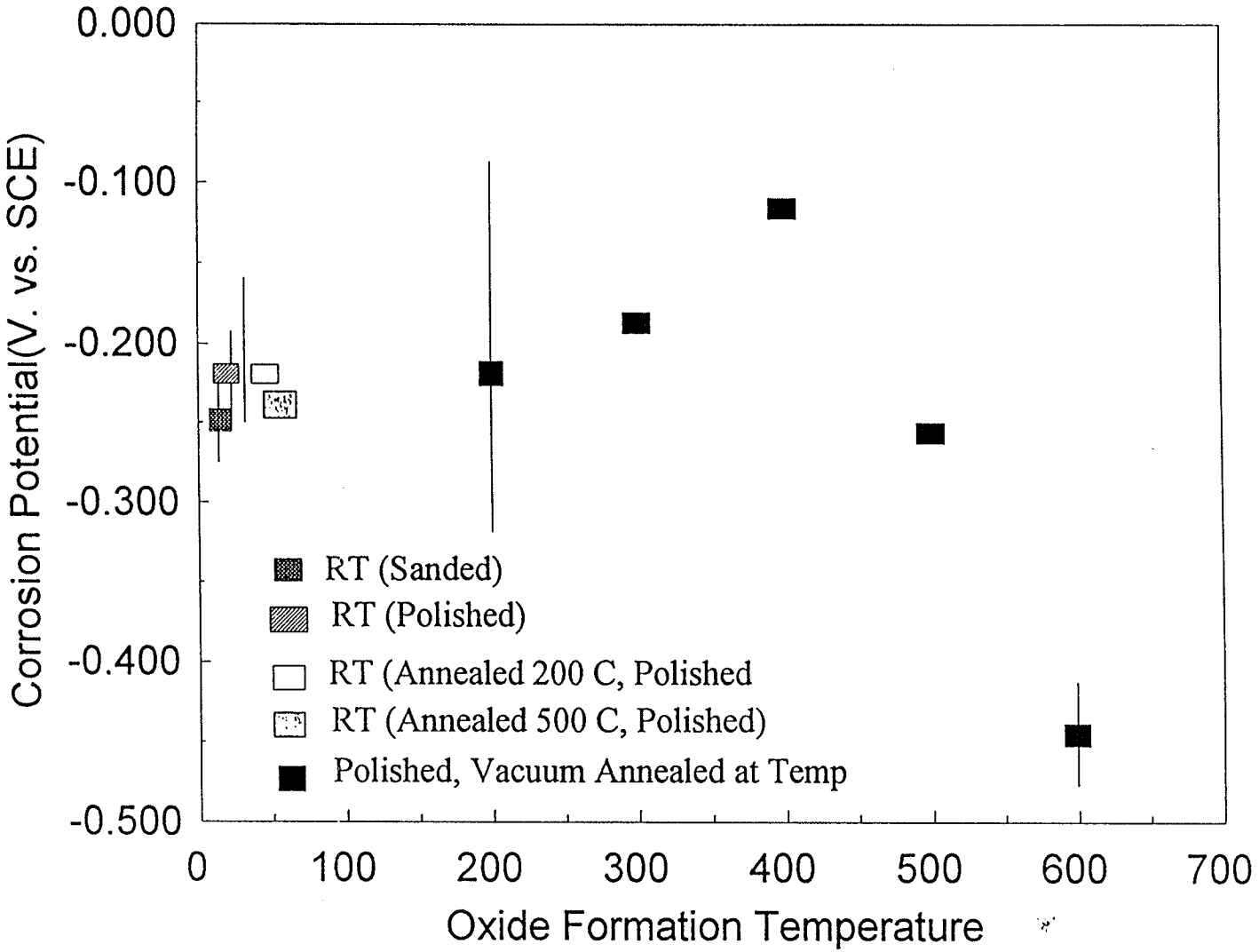

Fig. 36 Effects of Temperature of Oxide Formation and Surface Preparation on the Corrosion Potential, E_{corr}, of 316L Stainless Steel

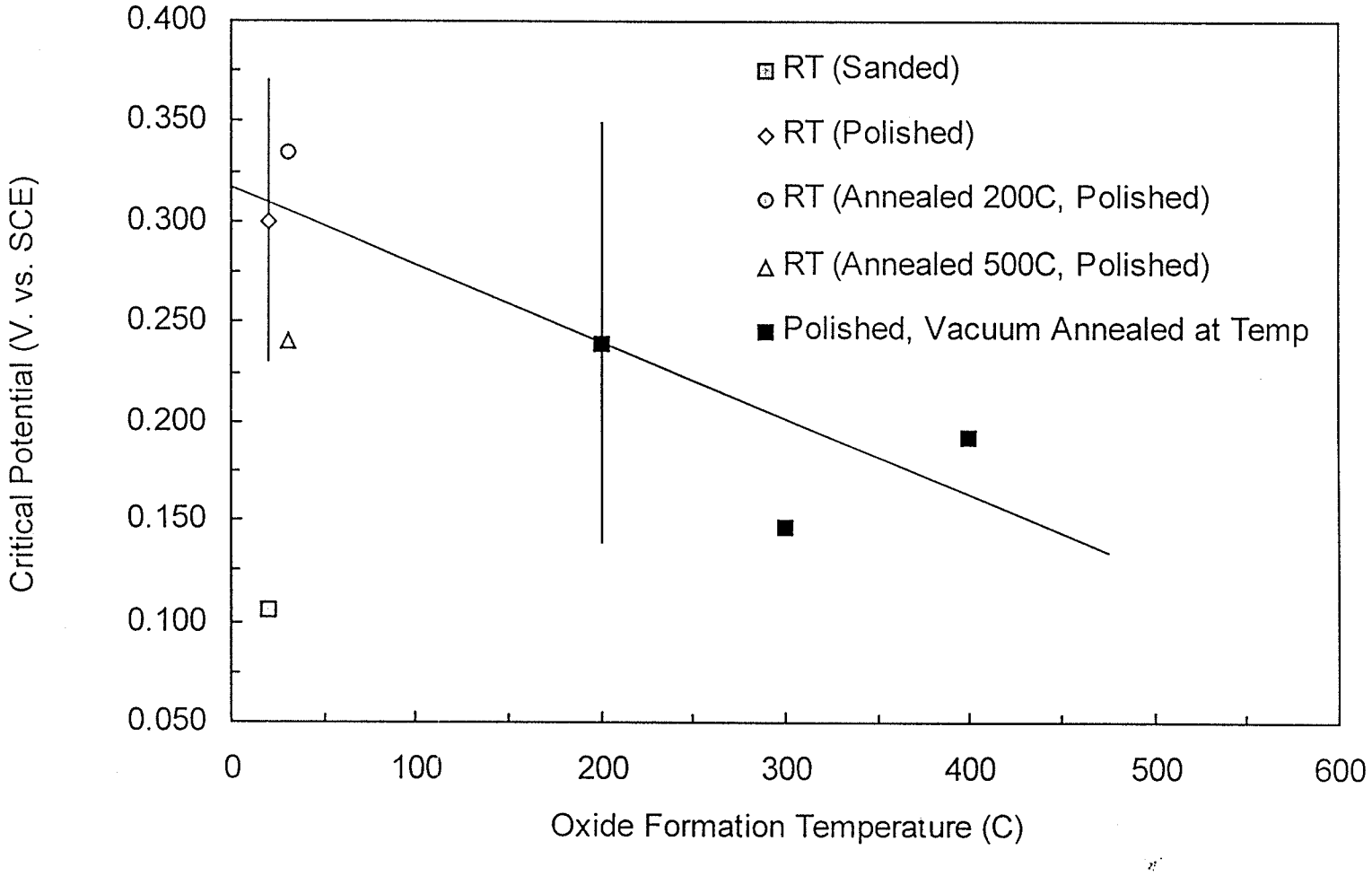

Fig 37 Effect of Temperature of Oxide Formation and Surface Preparation on the Critical Potentials, E_{cr}, of Type 316L Stainless Steel

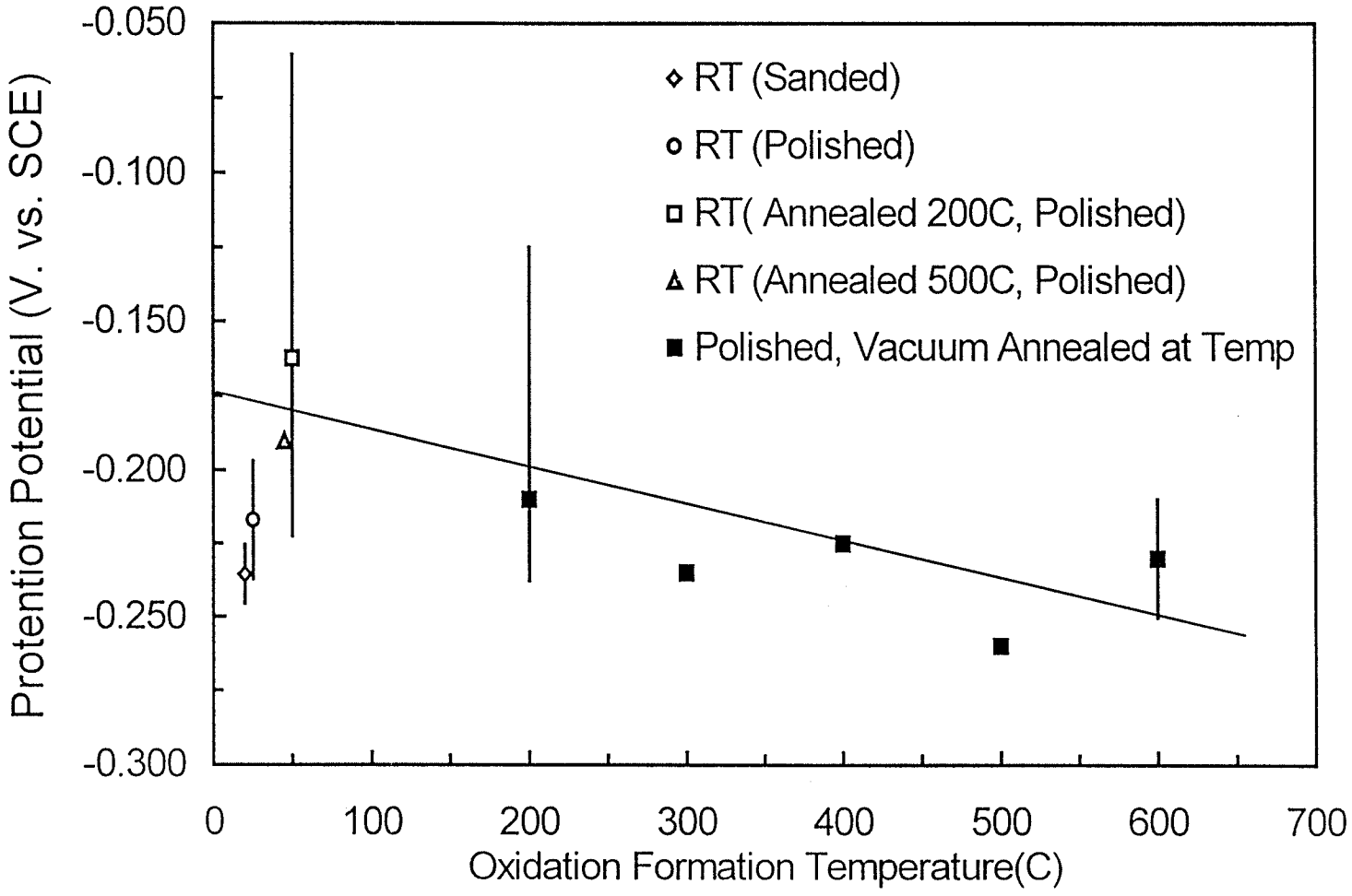

Fig. 38 Effects of Temperature of Oxide Formation and Surface Preparation on the Protection Potential, E_p, of 316L Stainless Steel

Table 5 Electrochemcial Testing Results for Oxide Films Formed in Vacuum System

Conditions	E_{rest}(V)	E_c(V)	E_p(V)	I_p(nA/Cm^2)
As Received (Sanded 600 grit)	-0.271	0.079	-0.221	1.365E3
	-0.221	0.133	-0.250	1.545E3
As received mechanical polishing (0.25μm)	-0.204	0.238	-0.225	1.452E3
	-0.192	0.342	-0.230	3.090E3
	-0.217	0.342	-0.196	1.922E3
200°C, 30 min, 7.8×10^{-6} Torr	-0.235	0.083	-0.235	6.88E2
200°C, 90 min, sanded 600 grit	-0.254	0.142	-0.231	2.534E3
200°C, 90 min, 8.3×10^{-6} Torr	-0.088	0.288	-0.225	4.45E2
	-0.169	0.242	-0.292	3.262E3
	-0.217	0.188	-0.113	1.452E3
200°C, 90 min, 8.3×10^{-6} Torr then polished	-0.230	0.335	-0.170	1.202E3
300°C, 90 min, 7.9×10^{-6} Torr	-0.188	0.146	-0.235	5.37E2
400°C, 30 min, 1.0×10^{-5} Torr	-0.192	0.208	-0.221	1.064E3
400°C, 90 min, 6.3×10^{-6} Torr	-0.115	0.192	-0.225	5.89E2
400°C, 150 min, 8.1×10^{-6} Torr	-0.183	0.317	-0.200	1.3650E4
500°C, 90 min, 4.5×10^{-6} Torr	-0.257			

Fig. 36 shows that as the temperature of oxide formation increases from room temperature to 500°C, the corrosion potentials change very little. In addition, the corrosion potentials for sanded specimens are nearly the same as for polished specimens. Therefore, oxide formation temperatures below 500°C and surface preparation have little effect on the corrosion potential of the specimen.

Fig. 37 shows the effect of oxide formation temperature and surface preparation on the critical potential of the oxide film. As the temperature of oxide formation increases, critical potentials decrease, which means that the pitting resistance of the specimens decreased with increasing temperature of oxide formation. Sanded specimens oxidized at room temperature have the lowest critical potentials in Fig. 37 with values of about 0.100 V vs SCE whereas the polished specimens oxidized at room temperature have critical potentials of about 0.300 V vs SCE. Therefore, polishing significantly improves the pitting resistance of 316L specimens.

The effect of oxidation temperature on the protection potentials is nearly identical to that on the critical potential as shown in Fig. 38. As the oxidation temperature is increased, the protection potential is decreased. And the protection potential of the sanded specimen has little difference from that of polished specimen, which suggests that surface treatment has little effect on the protection potential. Protection potential represents the repairing ability of the oxide film formed on the surface of the specimen, therefore, as the temperature increased, the repairing abilities of the oxide films decreased.

The pitting corrosion resistance of a material is actually dependent upon the difference between its critical and corrosion potentials. The effect of temperature of oxide formation on the difference between the critical potential and corrosion potential is

shown in Fig. 39. As the temperature of oxide formation is increased to 400°C, the difference of the two potentials is decreased and thus the resistance to pitting corrosion is decreased. The specimens with oxide films formed at 500°C and 600°C exhibited active behavior, not passive behavior and therefore these specimens exhibited no critical pitting potential. It is interesting to note that potential differences for polished specimens are much higher than those for sanded specimens. Therefore, polishing improves the pitting resistance of specimens and increasing temperature of oxide formation decreases the pitting resistance of the specimens.

Crevice corrosion resistance of a material can be represented by the difference between the critical potential and the protection potential. Fig. 40 shows the effect of surface preparation and temperature of oxide formation on the crevice corrosion resistance of the specimen. The sanded specimen exhibits the lowest value of E_c-E_{pp}, about 0.325 V, while all the polished specimens exhibit values of 0.400 to 0.525 V for E_c-E_{pp} with the temperature of oxide formation having little influence on these values. However, the electrochemical polarization curves for all the specimens, Fig. 32, 33, 34, shows that the protection potential is below, or at best equal to the corrosion potential and therefore none of the surface treatments add significant resistance to crevice corrosion. To have good resistance to pitting and crevice corrosion, a material should have a high value of E_c-E_{corr}, a low value of E_c-E_{pp} , and E_{pp} should be greater (more noble) than E_{corr}.

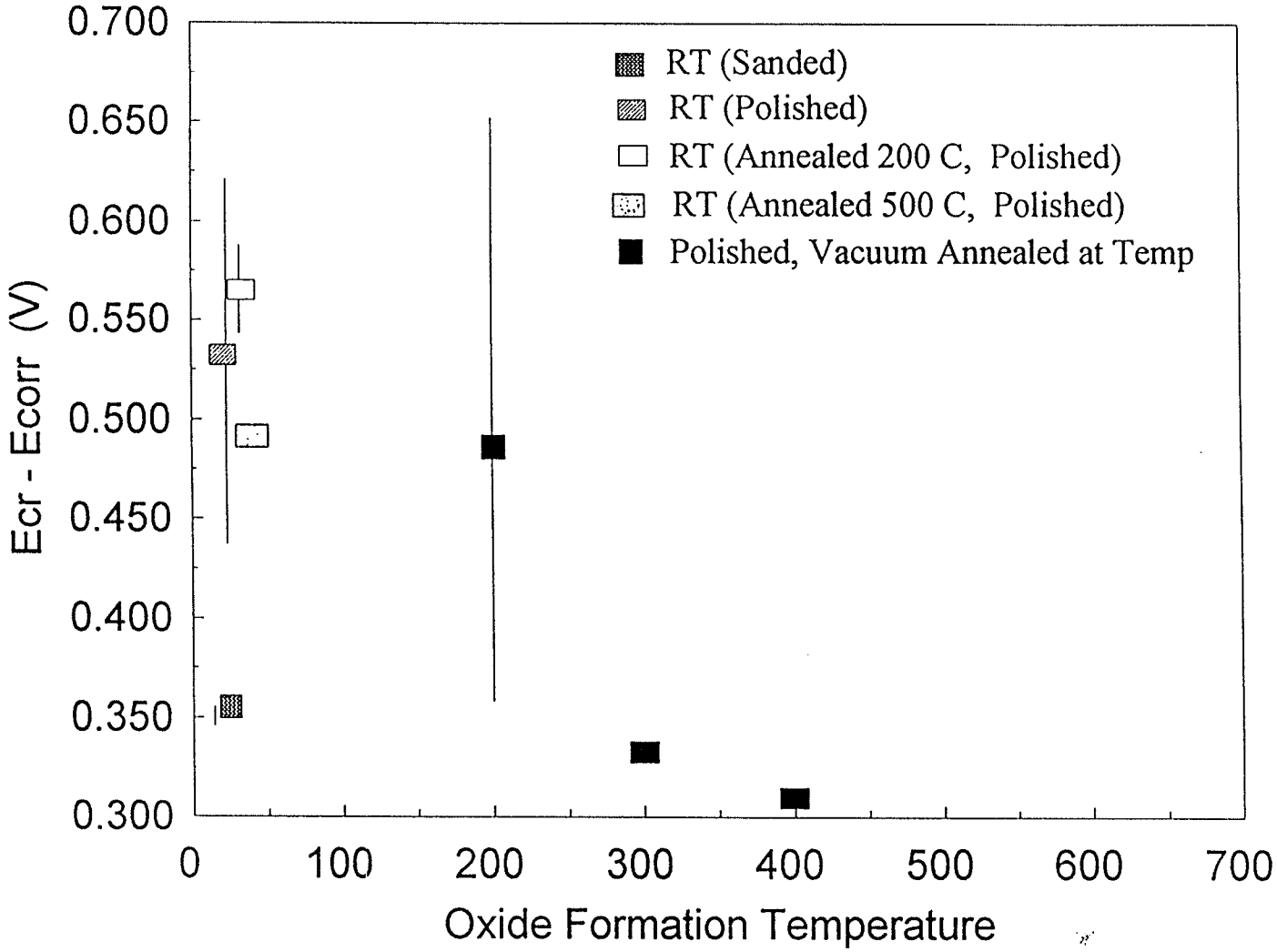

Fig. 39 Effect of Temperature of Oxide Formation on the Difference Between the Critical Potential and Corrosion Potential, Ecr-Ecorr, of 316L Stainless Steel

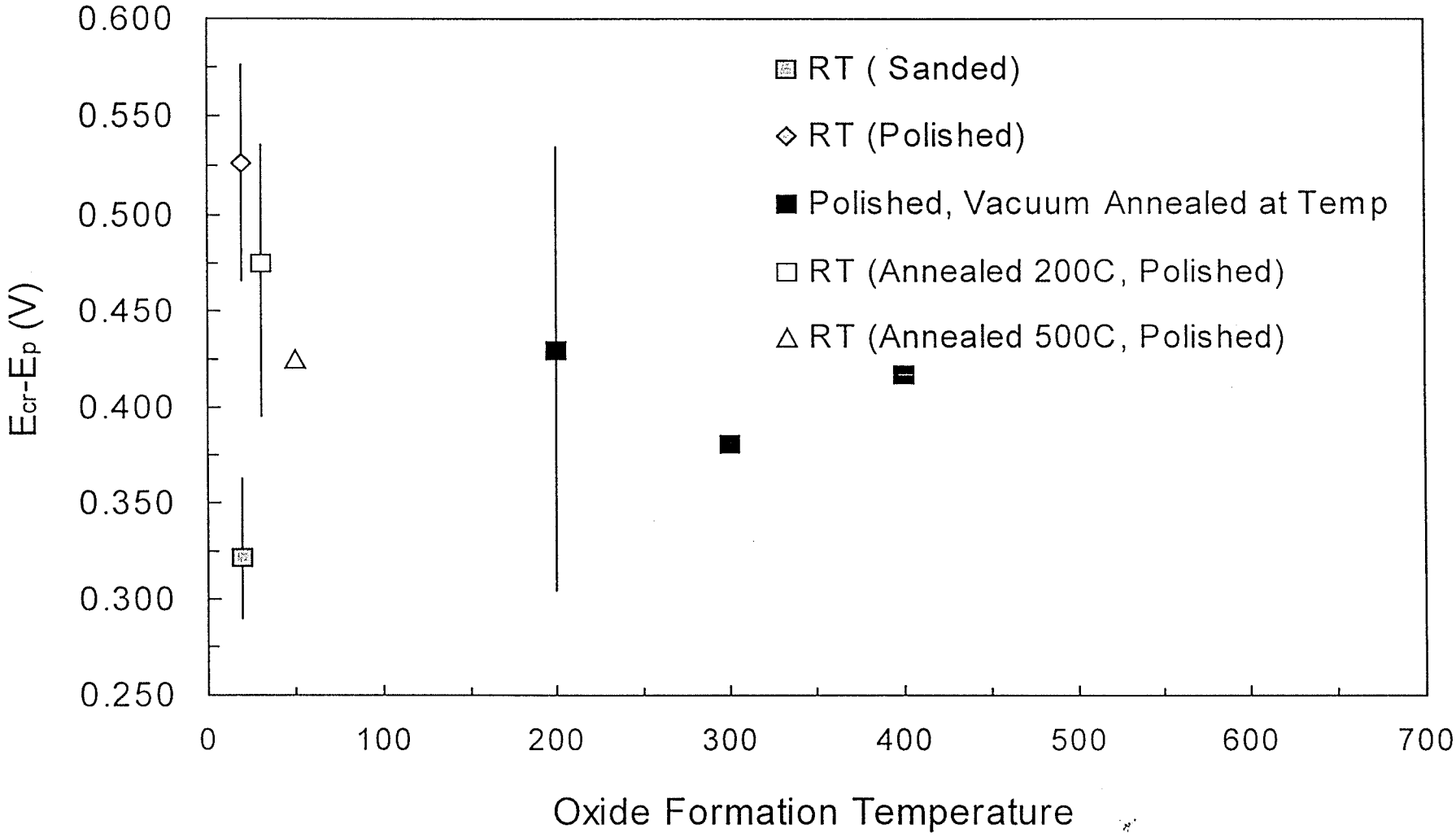

Fig. 40 The Effect of Surface Preparation and Temperature of Oxide Formation on the Difference Between the Critical Potential and the Protection Potential, E_{cr}-E_p, of Type 316L Stainless Steel

B.3 Effect of Vacuum Annealing Time at 400°C on the Electrochemical Behavior of 316L Stainless Steel

Electrochemical polarization curves and the corrosion rate of specimens with oxide films formed for different times are shown in Fig. 41 and Fig. 42 respectively. All the specimens were vacuum annealed at 400°C. While the specimen treated for 150 min has the highest critical potential, its corrosion rate is also the highest, 0.2 MPY. For the 30 min and 90 min specimens, the critical potential, protection potential and corrosion rate are nearly the same, 0.2V vs SCE, -0.200V vs SCE and ≈ 0.03 MPY respectively. Hence, oxide formation times at 400°C in excess of 90 minutes are detrimental to corrosion resistance.

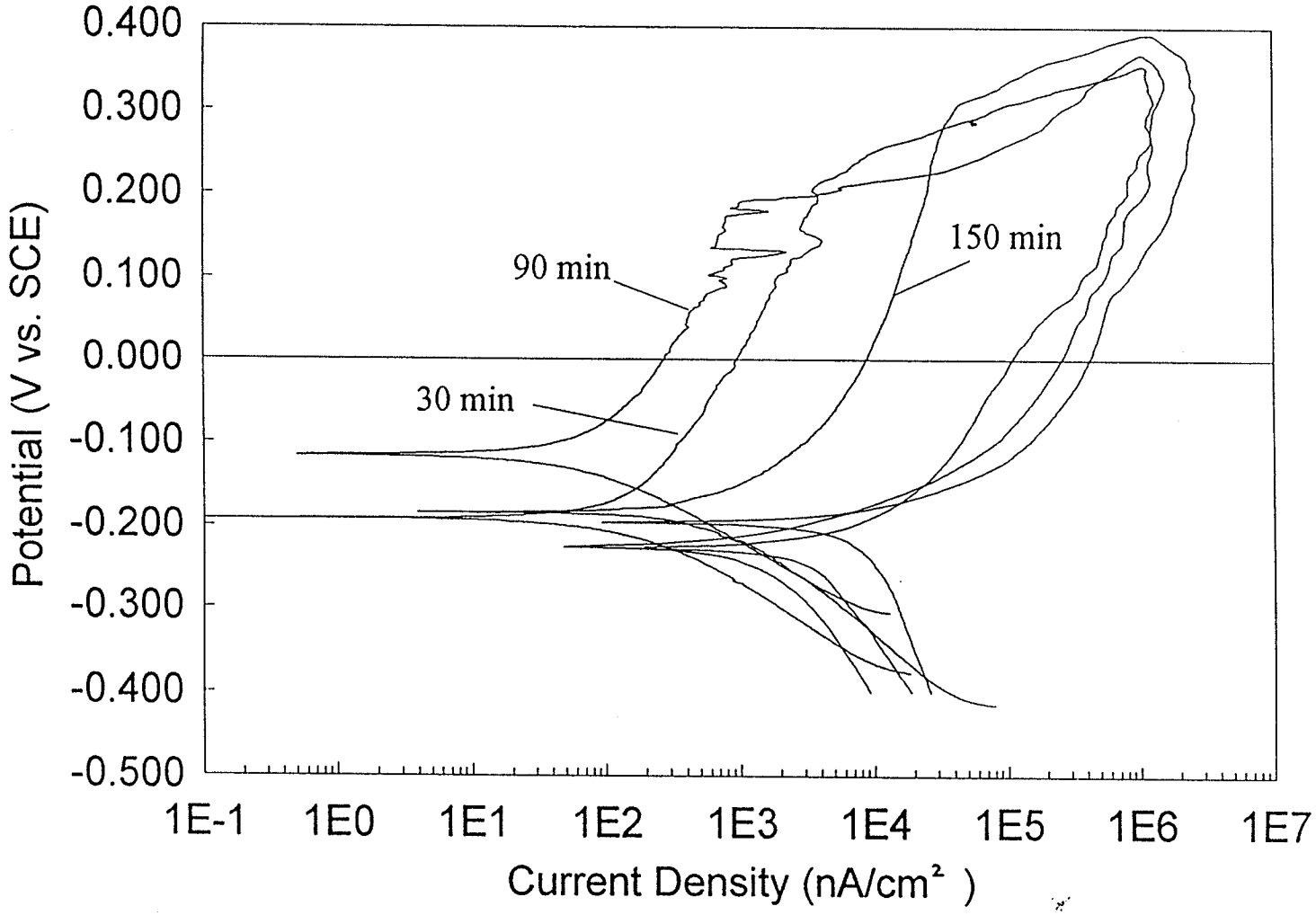

Fig. 41 Electrochemical Polarization Curves of 316L Stainless Steel with Oxide Films Formed for Different Times During Vacuum Annealing at Temperature at 400°C

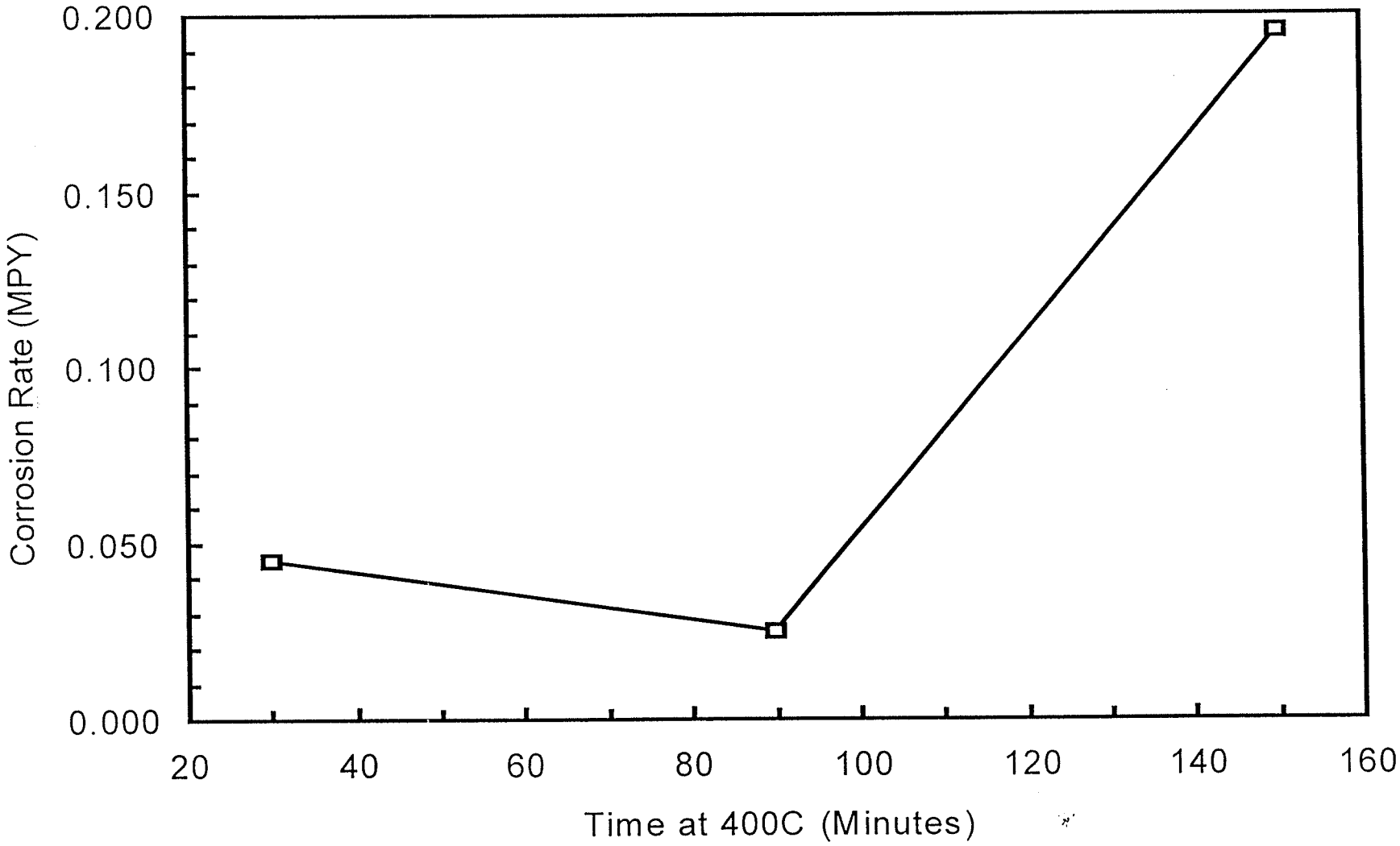

Fig. 42 Effect of Time on the Corrosion Rate of Specimens with Oxide Layers Formed During Vacuum Annealing at Temperature at 400°C

V. SUMMARY CONCLUSIONS & RECOMMENDATIONS

The objective of our experiments was to cease the corrosion of type 316L stainless steel by artificially thickening oxide film on its surface, which can be obtained by using vacuum annealing treatment. Surface treatment, temperature and time were three factors to effect the corrosion resistance of the oxide film. By investigating seven types of specimens at different surface treatment, temperature and time, some conclusions can be obtained:

1. Oxide films formed in a vacuum of 5×10^{-6} torr at 200°C and 400°C showed increased Cr contents and decreased Fe contents in the oxide film compared to the bulk material.
2. A region of essentially constant Cr/O ratio in the oxide films formed at 200°C and 400°C was attained. This indicates the presence of a stoichiometeric chromium oxide. The presence of chromium oxide should enhance the corrosion resistance of the stainless steel.
3. No region of constant Fe/O ratio was observed. This indicates the absence of a stoicheometric iron oxide which should also improve the corrosion resistance of the stainless steel.
4. A region of essentially constant Si/O ratio in the oxide film was observed. This may detract from the corrosion resistance of the stainless steel.
5. Polishing the surface of the specimens to 0.25 μm increased the critical pitting potential by about 0.2 v compared to sanding the surface to 600 grit paper. This increase in pitting potential indicates that the polished specimens have much improved resistance to pitting corrosion.

6. An oxide film formed in a vacuum of 5×10^{-6} torr at 200°C was very similar to the film formed in air at room temperature. This similarity was reflected by similar electrochemcial porperties.
7. The oxide film formed at 400°C was over twice as thick as those formed at 200°C or room temperature. However, the electrochemical properties of specimens having such films were slightly inferior to specimens with oxide films formed at lower temperature.
8. Films formed in vacuum at 500°C and 600°C offered no corrosion resistance to the stainless steel. Electrochemical studies showed that these specimens exhibited active corrosion rather than passive behavior.
9. To obtain an oxide film with good corrosion resistance, the annealing time should not excess 90 min.

By vacuum annealing treatment, an oxide film is formed on the surface of type 316L stainless steel. As the temperature increased, the thickness of the oxide film increased. However, the results of electrochemical corrosion tests showed that as the temperature increased the corrosion resistance of the oxide film decreased. Films formed in vacuum at 500°C and 600°C offered little corrosion resistance to the stainless steel. In addition, mechanical polishing significantly improved the pitting resistance compared to the sanded treatment.

Therefore, in order to improve the corrosion resistance of the oxide film, mechanical polishing or electrochemical polishing should be used to prepare the surface of the surface of the specimen. Moreover, the reason of the silicon concentration on the surface of the oxide film should be investigated and the silicon should be avoided enriching on

the surface of the oxide film. The experiments proved that the annealing temperature should be lower than 500°C and time should be 90 min.

Since the atmospheric pressure and oxygen pressure are important factors effectively the performance of the oxide film, lower vacuum pressures than 5×10^{-6} torr to should be tried to determine if an oxide film having further resistance to crevice corrosion can be obtained.

Furthermore, the corrosion resistance of type 316L stainless steel passviated in 20% HNO_3 solution at 50 ~ 60°C also has been investigated. Limited results indicate that passivation in 20% HNO_3 solution significantly improves the corrosion resistance of type 316L stainless steel by decreasing the corrosion current density from $10^3 nA/cm^2$ to 10^2 nA/cm^2 and increasing the pitting potential. An investigation concerning the corrosion resistance of 316L stainless steel passivated in 20% HNO_3 followed by a high temperature vacuum oxidation treatment may prove interesting.

REFERENCES

1. George S. Brady, Henry R. Clauser, John A. Vaccari, Materials Handbook, Fourteen Edition, McGraw-Hill, New York, 1997.
2. Metals Handbook, Tenth Edition, Vol.1, ASM International, Materials Park, OH, U.S.A, 1990.
3. Saricimen H., Jarrah N. R., Allam I. M., NACE International, p17, 1994, NACE International, Houston, Texas, U.S.A.
4. Kumada M., Boshoku Gijutsu (Corrosion Engineering), Vol.30, No.6, 344-348, 1981.
5. Sivakumar M., Rajeswari S., Journal of Materials Science Letters(UK), Vol.11, No.15, 1039-1042, 1992.
6. Magrini M., Giordano L. Ramous E., Advances in Fracture Research (Fracture 84), Proceedings of the 6th International Conference on Fracture(ICD6). 1984 Sponsored by Int Congress on Fracture, Sendai, Jpn; Natl Aeronautial Lab, Bangalore, India; Defence Metallurgical Research Lab, Hyderabad, India Pergamon press, p3931-3935.
7. Sivakumar M., Kamachi Mudali U., Rajeswara S., Journal of Materials Science Letters, Vol.14, No.2, 148-151, 1995.
8. Burstein G.T., U.K. Corrosion'85: Corrosion Science, Corrosion Protection, Bacterial Corrosion. Harrogate, UK, 4-6 Nov. 1985. Inst of Corrosion Science & Technology, p83-94.
9. Fantana Mars Guy, Corrosion Engineering, McGraw-Hill, New York, 1986.
10. David Talbot, James Talbot, Corrosion Science and Technology, CRC, N. W. Boca Raton, Florida, 1998.

11. R. Baboian, Electrochemical Techniques for Corrosion Engineering, National Association of corrosion Engineers, Houston, Texas, 1986.

12. D. L. Piron, The Electrochemistry of Corrosion, NACE, Houston, TX, U.S.A, 1991.

13. Evans Ulick Richardson, The Corrosion and Oxidation of Metals: Scientific Principles and Practical Applications, Arnold, London, 1960, First Supplementary Volume, Arnold, London.

14. L. L. Shreir, Corrosion, Volume 1, George Newnes Ltd, Second edition, 1976.

15. Z. Szklarska-Smialowska, Pitting Corrosion of Metals, National Association of Corrosion Engineers, 1986.

16. M. A. Streicher, J.Electrochem.Soc. 103, 375,1965.

17. N.D. Green, M.G. Fontana, Corrosion, Vol.15, No.1, 14, 1959.

18. Ya M. Kolotyrkin, Corrosion, Vol. 19, No.8, 261, 1963.

19. W. Scwenk, Corrosion, Vol.20, No.4, 129, 1964.

20. Z. Szklarska-Smialowska, M. Janik-Czachor, Brit, Corros. J. Vol.4, 138,1969.

21. R. Steigerwald, Corrosion, Vol.22, No.4, 107, 1966.

22. W. D. France, Jr., N. D. Greene, Corrosion, Vol.26, No.1, 1, 1970.

23. E. A. Lizlovs, A. P. Bond, J. Electrochem. Soc. Vol. 116, 574, 1969.

24. Pickering H.W. and Frankenthal R. P., J. Electrochem. Soc. 112, 761, 1965.

25. M. A. Streicher, J. Electrochem. Soc. Vol.103, 375, 1956.

26. Smialowski M., Szklarska-Smialowska Z., Rychcik M., Szummer A., Corrosion Science, Vol. 9, 123, 1969.

27. Kim T. K., Kim K. Y., Journal of the Corrosion Science of Korea, 28, 355-367, 1999.

28. Azuma S., Hirata H., Tashiro Y., Teranishi H., Institute of Environmental Sciences-Proceedings, Annual Technical Meeting, May 12-16, 1996, 1996 Inst. Of Environmental Sciences, 49-54.

29. Jackson EMLEM, Paton R., ISIJ Int (Japan), Vol. 35, 557-563, 1995.

30. Wit JHWD, Janse EFM, Jacobs LC, Passivation of Metals and Semiconductors, Clausthal, Germany, 21-26, Aug. 1994, Materials Science Forum (Switzerland), Vol. 185-188, 975-984, 1995.

31. R. Kiessling, C. Westman, J. Iron Steel Inst., Vol. 204, 377, 1966.

32. L. Backer, Rolin M., Messager C., Mem. Sci. Rev. Met., Vol. 63, No. 4, 319, 1966.

33. Stricher M. A., Corrosion, 30, 77, 1974.

34. R. Nishimura, K. Kudo, Corros. 44, 29-35, 1988.

35. Bhattacharyya A., Steel India, Vol.14, No.1, 10-17, 1991.

36. Hodgkiess T., Habilomatis P. Ramsay R., Corrosion'84, New Orleans La, U.S.A, 2-6 Apr. 1984, P18.

37. Oldfield John W., Todd Brian, Desalination, 124, No. 1-3, 75-84, 1999.

38. A. J. Sedriks, Corros. 45, 510, 1989.

39. De Schiapparelli E. R., Caceres S. P., Journal of Materials Science, Vol. 26, 1454-1458, 1991.

40. S. Brennert, J. Iron Steel Inst, Vol. 135, 101, 1936; Met. Prog., Vol. 31, 641, 1937.

41. M. Pourbaix, L. Klimzach-Mathieu, Corros. Sci. Vol. 3, 239, 1963.

42. Z. Szklarska-Sialowska, Corros. Sci. Vol. 11, 901, 1971.

43. A. Broli, H. Holtan, Corros. Sci. Vol. 17, 59, 1977.

44. M. Pourbaix, Corrosion, Vol. 26, No. 10, 431, 1970.

45. J. Horvath, H.H. Uhlig, J. Electrochem. Soc. Vol.115,791,1968.

46. K. Sugimoto, Y. Sawada, Corros.Sci. Vol.17, 425, 1977.

47. E. A. Lizlovs, A. P. Bond, J. Electrochem.Soc. Vol.116, 574,1969.

48. Susan J. Kerber, John Tverberg, Advanced Materials & Processes, Vol. 158, No.5, 33-36, 2000.

49. J. B. Lumsden, R.W. Staehle, Scripta, Metall., Vol. 6 (12), 1205,1972.

50. A. E. Yaniv, J. B. Lumsden, R. W. Staehle, J. Electrochem. Soc., Vol. 124, 490, 1977.

51. H. Ogawa, H. Omata, H. Itoh, H. Okada, Corrosion, Vol.34, No.2 53,1978.

52. J. R. Cahoon, R. Bandy, Corrosion, Vol.38, No.6, 299, 1982.

53. D. A. Stout, J. B. Lumsden, R. W. Staehle, Corrosion, Vol.35, No.4, 141,1979.

54. Beddoes J., Bucci K., Journal of Materials Science: Materials in Medicine (UK), Vol. 10, 389-394, 1999.

55. Mudali U. K., Ningshen S., Dayal R. K., Tyagi A. K., High Nitrogen Steels'98: 5th International conference on High Nitrogen Steels. Espoo, Stockholm, Finland, Sweden, May 24-26, 1998; May 27-28, 1998, Materials Science Forum (Switzerland), Vol. 318-320, 495-502, 1999.

56. Malik A. U., Kutty P. C. M., Sidiqi N. A., Andijani I. N., Ahmed S., Corrosion Science (UK), Vol. 33, No. 11, 1809-1827, 1992.

57. Chaudhary Z., Dissertation Abstracts International (USA), Vol. 52, No. 11, 336, 1992.

58. Hong Y. K., Diss. Abstr. Int. Vol. 42, No. 9,168, 1982.

59. Skinner W., Schwartz W. A., Corros. Coatings, Vol. 9, No. 1, 7-11, 13, 19, 1982.

60. Abd El Meguid E. A., Gouda, V. K., Mahmoud N. A., Materials Transactions JIM, Vol. 35, No. 10, 699-702, 1994.

61. Marshall P. I., Burstein G. T., International Congress on Metallic Corrosion, Vol. 2, Toronto, Canada, 3-7, June, 1984, National Research Council of Canada, 121-128, 1984.

62. Holt D., Cottis R. A., International Congress on Metallic Corrosion, 1984. Vol. 3, Toronto, Canada, 3-7 June, 1984, National Research Council of Canada, 614-617, 1984.

63. Salvago G., Fumagalli G., Corrosion Science (UK), Vol. 33. 985-995, 1992.

64. V. Vignal, J.M. Olive, D. Desjardins, Corros. Sci. (USA) 41, 869-884, 1999.

65. L. E. Price and G. J. Thomas, J. Ins. Met. 63, 21, 1938.

66. J. Moreau and J. Bénard, J. Ins. Met., 83, 87, 1954-1955.

67. R. P. Abendroth, Trans, Metall. Soc. AIME, 230, 763, 1964.

68. G. C. Wood and D. P. Whittle, Corros. Sci. 7, , 763,1967.

69. I. Olefjord, Corros. Sci, 687-696, 1975.

70. C . Leygraf, G. SchÖn and S.E kelund, Scand. J. Metall. 2, 313, 1973.

71. R. K. Wild, Corros. Sci. 14, 575, 1974.

72. K. Asami, K. Hashimoto, S. Shimodaira, Corros. Sci., 18, 125, 1978.

73. G. Hultquist and C. Leygraf, Material Science and Engineering, 42, No. 1-2, 199-206, 1980.

74. C. Leygraf, G. Hultquist and S. Ekelund, Surf. Sci. Vol. 51, No.2, 409, 1975.

75. Haupt S., Strehblow H., Corros. Sci. (USA), Vol. 29, 163-182, 1989.

76. Wagner, C., Z. Phys. Chem. B., 21, 25(1933).

77. S. P. Trasatti, E. Camona, F. Mazza, E. Sivieri, Journal of Applied Electrochemistry, Vol. 28, No. 12, 1333-1341, 1998.

78. I. Olefjord, Metal Science, 9, 263, 1975.

79. A. F. Smith, Corros. Sci. 22, 857-865, 1982.

80. M. G. S. Ferreira, N. E. Hakiki, M. F. Montemor, Da Cunha Belo M., Corros. Sci. 42, 687-702, 2000.

81. Setoh H., Tomari H. Satoh F., Kobe Research and Development , Vol. 39, No.1, 54-57, 1989.

82. Kosaka T., Suzuki S., Inoue H., Saito M., Waseda Y., Matsubara E., Applied Surface Science (Netherlands), Vol. 103, 55-61, 1996

83. F. S. Shieu, M. J. Deng, S. H. Lin, Corros. Sci. 40, 1267-279, 1998.

84. M. F. Montemor, A. M. P. Simões, M. G. S. Ferreira, Da Cunha Belo M., Corros. Sci. 41, 17-34, 1999.

85. Tan M. W., Akiyama E., Kawashima A., Asami K., Hashimoto K., Corros. Sci. 37, 1289, 1995.

86. Habazaki H., Kawashima A., Asami K., Hashimoto K. Corros. Sci. (UK), Vol. 33, No. 2, 225, 1992.

87. H. J. Mathieu, D. Landolt, Corros. Sci. 26, 547, 1986.

88. Wagner C., Z. Phys. Chem. B., 32, 47 (1936).

89. J. A. Yoakam, J. C. Schumacher, High Rate Metal Dissolution Processes, Chicago, Illinois, U.S.A. 11-12, Oct. 1995, Electrochemical Society. Inc., 290-301, 1996.

90. I. Olefjord, Scand. J. Metallurgy, 3, 129, 1974.

91. Doychak J., Smialek J. and Mitchell T.E., Metall. Trans. A. 20, 499, 1989.

92. Habazaki H., Shimizu K., Skeldon P., Thompson G.E., Wood G.C., Zhou X., Corros. Sci. 39, 731, 1997.

93. Yamanaka K. Matsuda Y. Boshoku Gijutsu (Corros. Eng.), Vol. 39, 254-262, 1990.

94. Yashiro T., Netsu Shori, Journal of the Japan Society for Heat Treatment (Japan), Vol. 31, No. 4, 205-211, 1991.

95. Yen S. K., Tsai Y.C., Journal of the Electrochemical Society, 143, 2493-2497, 1996.

96. J. F. Grubb, Proceedings of the International Conference on Stainless Steels, Iron and Steel Institute of Japan, (Tokyo, Japan, 1991), 944.

97. C. Leygraf, G. Hultquist, Surf. Sci. 61, 69, 1976.

98. G. Hultquist, C. Leygraf, Corros. Sci. 22, 331-346, 1982.

99. G. Hultquist, C. Leygraf, Corros. Sci. 21, 401, 1981.

100. C. J. Greyling, J. P. Roux, Corros. Sci. 24, 675-690, 1984.

101. K. Kuroda, P. A. Labun, Welsch G., Mitchell T. E., Oxidation of Metals, 19, 117-127, 1983.

102. Hulquist G., Leygraf C., Journal of Vacuum Science and Technology, 17, 85-88, 1979.

103. Smith A. F. Corros. Sci., Vol. 21, 517-529, 1981.

104. Konno Hidetaka, Zairyo to Kankyo/ Corrosion Engineering, 44, 30-36, 1995.

105. W.R. Whitney, J. Amer. Chem. Soc., Vol. 25, No. 4, 394, 1903.

106. MacDowell L. G., Ontiveros C., Technology 2000, Vol. II, Washington, D.C. USA, 27-28 Nov. 1990, NASA Conference Publication, 210-217, 1991.

107. Forsen O., Aromaa J., Tavi M., Electrochemical Methods in Corrosion Research V.I., Sesimbra, Portugal, 5-8, Sep. 1994, Materials Science Forum (Switzerland), Vol. 192-194. No. 1, 41-52, 1995.

108. Tennese, Wayne Wylie, Corrosion of Type 316 Stainless Steel Orthopedic Implants, University of Manitoba, Master Thesis, 1976.

109. Malik Aness U., Al Fozen Saleh, Desalination, Vol. 97, No. 1-3, 199-212, Elsevier Science Publishers B. V., 1994.

110. J.M. West, Electrodeposition and Corrosion Processes, D. Van Nostrand Company Limited, London, p.13-15, 1965.